Pressure drop over a packed bed of coke particle mixtures

R Horn

orcid.org/0000-0003-1374-9793

Dissertation accepted in fulfilment of the requirements for the degree Master of Engineering Chemical Engineering at the North-West University

Supervisor: Dr FH Conradie

Co-supervisor: Mr AF van der Merwe

Graduation: August 2023

Student number: 28441540

PREFACE

I want to thank every person directly and indirectly involved with the project who supported me and encouraged me to keep going. I would like to thank the following people personally:

- My supervisor, Dr. Frikkie Conradie; thank you for guiding me through the years and giving me your insight and recommendations when needed.

- My co-supervisor, Mr. Frikkie van der Merwe; thank you for attending the weekly meeting to share your knowledge and for suggesting alternative options.

- Thank you, North-West University Potchefstroom, for allowing me to use your facilities and equipment to conduct my experimental procedure.

- My colleague and friend, Mr. Hennie Honiball; thank you for working alongside me and for your continuing support.

- My undergraduate students, Ms. Marizaan Lindeque and Mr. Rohan Botha for sample preparation and data generation.

ABSTRACT

Coke particles are a solid fuel used in blast furnaces, and the packing of these particles inside the enclosed vessel is a typical example of a packed bed reactor. The type of coke used in a blast furnace impacts the packing and bed voidage of the blast furnace. When gas is injected into the blast furnace to reduce the iron oxide to liquid iron, with the help of the carbon in the coke, this characteristic packing is critical in understanding and improving the reaction behaviour of this complex multiphase reactor. The injected gas would experience a pressure drop while passing through the packed bed of coke particles, impacting the overall process and the blast furnace's efficiency.

Many factors influence the packing of particles in a reactor or blast furnace, for example, how the particles are handled, the characteristics of the reactor geometry and the attributes of the particle. The particle itself is the most unpredictable due to various parameters that can affect the packing density. The factors include the particle shape and size, roughness, the particle size distribution used in the reactor and the particle coefficient of restitution. Particles form a packing structure when inserted into a reactor and depend on particle characteristics and how individual particles are stacked upon each other. Non-spherical particles form a random packing structure when forming a packed bed. The three main effects particles have on each other during packing are the wedging, wall and loosening effects. The packing structure leads to forming bed voidage, a critical parameter that is used to estimate the pressure drop in a packed bed.

Flow through a packed bed has been investigated before and is classified into two categories, the discrete particle model and the pipe flow analogy. The pipe flow analogy models can be used for spherical particles, with the capillary tube model being the most used pipe flow analogy model. The capillary model defines the flow through the packed bed as a pack of straight capillaries which are equally sized. The discrete particle model is used for non-spherical particles and defines the flow through the packed bed as individual particles with their boundary layers.

The study focused on predicting the effect of non-spherical particle characteristics on fixed bed morphology to model the pressure drop based on a fundamental approach. This can be done by determining the particle characteristics that influence packed bed voidage of arbitrary-shaped coke particle mixtures and evaluating the effect of particle and packing characteristics of mixtures based on the measured and modelled pressure drop in a fixed bed.

It was found that present bed voidage models that rely only on the pipe diameter to particle diameter or particle diameter to particle diameter are insufficient to model the packing; the model can be improved by including mono-size batch voids as a parameter. The main parameter that influences bed voidage is the average particle diameter of the bed. The modified Kwan model was the best-fitting models for binary mixtures and the regressed D-optimal Design model was the best-fitting models for ternary mixtures of coke particles but were regressed from models found in literature to fit the coke particle characteristics.

Most pressure drop models are developed from the basis of the friction factor but were inefficient in predicting pressure drop for the size range and mixtures of coke particles. Statistical models were created due to no existing model being able to accurately predict the pressure drop for coke particles. It was found that the standard polynomial statistical method was the most accurate for predicting pressure drop across a packed bed of coke particles.

Comparing the mostly used literature pressure drop model to the statistical models it was found that the pressure drop to fluid velocity correlation for the Ergun model is given as $\Delta P \propto U^2$ compared to the correlation for the statistical models given as $\Delta P \propto U^{1.441}$. From using statistical models to predict pressure drop it would be beneficial to integrate particle parameters to the model like sphericity, voidage and average particle diameter. Particle size distribution was seen to have the most significant influence on pressure drop in mixtures compared to sphericity and bed voidage.

Keywords: Ergun equation, bed voidage, packing model, packed bed.

TABLE OF CONTENTS

LIST OF TABLES

List of Figures

Nomenclature

Symbol	Definition	Unit
A	Longest calliper value	m
A_b	Packed bed/ reactor area	m^2
A_E	Ergun viscus energy loss constant	-
a_{LE}, a_{KM}, a_{WK}	Loosening effect parameter	-
A_p	Area particle	m^2
a_s	Surface area to volume ratio of particle	m^{-1}
A_w	Function of pipe diameter to particle diameter constant	-
B	Medium calliper value	-
B_E	Ergun kinetic energy loss constant	-
b_{EH}, b_{TM}, b_{KM}, b_{WK}	Wall effect parameter	-
B_w	Function pipe diameter to particle diameter constant	-
C	Shortest calliper value	m
c_{KM}, c_{WK}	Wedging effect parameter	-
D	Diameter pipe/ reactor	m
D_{50}	Average particle sieve diameter	m
d_a	Sieve diameter	m
d_{ep}	Equivalent diameter	m
d_i	Ring inner diameter	m
d_{MA}	Martin diameter	m
d_o	Ring outer diameter	m
d_{pAve}	Average particle diameter	m
d_{pm}	Particle diameter of mixture	m
dp_{SM}	Sauter mean particle diameter	m
$d{p}_i^I$	Particle diameter	m
d_s	Surface diameter	m
d_{st}	Stokes diameter	m
d_{sv}	Surface-volume diameter	m
d_v	Volume diameter	m
d_y	Cylinder diameter	m
f	Friction factor	-
g	Gravitational acceleration constant	m/s^2
G	Yu coefficient based on particle diameter ratio	-
H_0	Initial fluid height	m
H_1	Final fluid height	m
h_1, h_2, z_1, z_2	Reference points in packed bed height	m
h_p	Particle height	m
J	Subramanian constant	-

K, K'	Darcy constant	-
k_d	Toufar diameter ratio constant	-
L	Packed bed/reactor height	m
l_y	Cylinder length	m
M_w	Mass water	kg
Q	Volume fluid moving through the packed bed	m^3
R	Toufar constant based on voidage and volume fraction	-
Re	Reynolds number	-
Re_m	Modified Reynolds number	-
s	Particle diameter ratio, small divided by large	-
S_p	Surface area of particle	m
t	Time to drain fluid	s
U	Superficial velocity	m/s
V_c	Volume pipe/reactor	m^3
V_i	Specific volume of small particles	m^3
V_j	Specific volume of large particles	m^3
V_m	Specific volume of mixture	m^3
V_p	Volume particle	m^3
V_w	Volume water	m^3
x_i	Volume fraction small particle	-
x_j	Volume fraction large particle	-
x_i^I	Volume fraction of individual size range	-
β, θ	Model constants calculated or regressed	-
ΔP	Pressure drop across the packed bed	Pa
$\Delta P_1, \Delta P_2$	Pressure drop across reference points	Pa
ε_c	Core bed voidage	-
ε_i	Small particle bed voidage	-
ε_j	Large particle bed voidage	-
ε_m	Bed voidage	-
ε_T	Middle point of reference for bed voidage	-
ε_w	Wall bed voidage	-
ε_{m1}^*	Bed voidage when loosening effect is dominant	-
ε_{m2}^*	Bed voidage when wall effect is dominant	-
ε_{m3}^*	Bed voidage when wedge effect is dominant	-
μ	Kinematic viscosity	Pa.s
π	Pie	-
ρ_ϵ	Density of packing	kg/m^3
ρ_g	Fluid density	kg/m^3
ρ_p	Particle density	kg/m^3
ρ_W	Water density	kg/m^3
τ	Tortuosity	-
φ	Sphericity	-
φ_c	Circularity, roundness	-

Basic polynomial function -

CHAPTER 1 BACKGROUND AND RATIONALE

Packed bed reactors are fed with coal or coke in order to gasify these solid materials to produce an energy-rich product (Gräbner, 2014; Jia *et al.*, 2009). A common material used as solid feedstock in a packed bed reactor in South Africa is: (1) coal when fed to fixed bed gasifiers which react with hydrogen or carbon monoxide to produce liquid fuels, gaseous fuels and electricity (Gräbner, 2014; Peacey & Davenport, 2016), or similar gasification reactions found for coke in typical coke-fed blast furnaces for iron production. ArcelorMittal in South Africa is a large steel producing company, with operational coke ovens in Newcastle, Vanderbijlpark, Vereeniging, Saldanha and Pretoria. The company uses coke oven batteries, a sinter plant and blast furnaces for iron and steel production (Coetzee, 1971; Geyer & Halifa, 2014; Johns, 2010). Over time there have been three generations of coke gasification processes utilised, including the use of fluidised bed and fixed bed processes. The newest generation focuses on the improvement from the previous by using different energy sources like lower grade coke and reducing the production of CO_2 (Gräbner, 2014). Coal and coke gasification reactors operate by feeding coke to a reactor to form a packed bed, injecting the reaction gas at the reactor's bottom to pass through the coke bed, and adding heat so that the gasification reaction can take place(Gräbner, 2014; Peacey & Davenport, 2016). The full workings of a blast furnace to produce iron as described above is depicted in Figure 1-1.

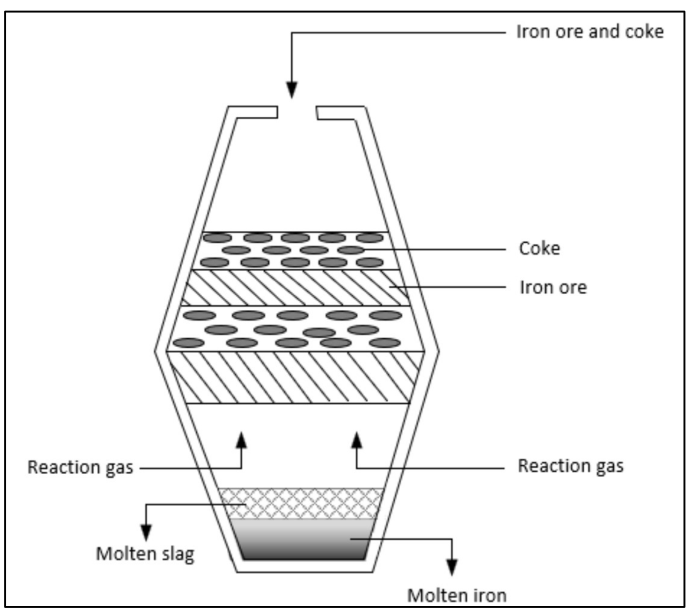

Figure 1-1 : Blast furnace adapted from Wang (2016)

The main chemical reaction taking place in a blast furnace to produce molten iron from iron ore and coke particles are given below (Wang 2016).

$$Fe_2O_3\ (s) + 3CO(g) \rightarrow 2Fe(l) + 3CO_2(g)$$
$$Fe_2O_3(s) + 3H_2(g) \rightarrow 2Fe(l) + 3H_2O(g)$$

In any reactor, the feedstock type influences the quality of the product; thus, the type of coke influences the gasification efficiency in a packed bed reactor. South African steel and ferro-alloy industries produce coke by heating coal in the absence of air (Johns, 2010; Nhiwatiwa & Cromarty, 2022). Coal is placed in the coke oven chambers at a temperature between 1200 ˚C and 1 300°C for approximately 19 hours of baking. If the centre of the coal has reached 1100°C it is converted to coke and most of the volatile matter and moisture is removed (Johns, 2010). Two different types of coke are used in the steel and ferro-alloy industries as reducing agents and an energy source (Johns, 2010; Nhiwatiwa & Cromarty, 2022; Van Niekerk & Dippenaar, 1991). Metallurgical coke is used in blast furnaces which is a harder and more stable compared to ferro-alloy coke which is used in the ferro-alloy industry. The ferro-alloy coke is more reactive compared to metallurgical coke (Johns, 2010; Jones *et al.*). Coke is a dark grey, hard and slightly porous material that has desirable characteristics to be used in a blast furnace (Johns, 2010). Coke has certain criteria set out by the British Iron and Steel Research Association to be able to be used for feedstock for blast furnace operation. The desired characteristic is that the ash content be lower than 10%, it should contain less than 1% sulphur and the moisture content should be lower than 2% (Morgan & La Grange, 1951). The properties of the specific coke feedstock that influences the reactor's efficiency most are the moisture and ash content (Gräbner, 2014; Kuang *et al.*, 2018). These coke properties influence the coke's fragmentation, corrosion, and fouling during the operation of the packed bed reactor. The physical properties of the coke influence the efficiency, pressure drop and fluidisation inside the reactor. These properties include the coke size, shape and packing behaviour of the coke in bulk (Gräbner, 2014).

Gas would be injected into the blast furnace or reactor and a pressure drop would occur when passing through the packed bed of particles. The pressure drop that occurs during the blast furnace or reactor operation impacts the efficiency of product formation. This is because an increase in pressure drop can lower the reaction rate and conversion of the coke. An increase in pressure drop leads to more injecting gas flow needed to keep the blast furnace or reactor efficient and increases the operating cost (Fogler & Gürmen, 1999). The gas that flows through the packed bed of the reactor from the bottom is assumed to be a one-dimensional flow to simplify the modelling of the pressure drop that occurs (Gräbner, 2014; Nemec & Levec, 2005).

A common equation used to estimate the pressure drop that occurs over the height of the packed bed in the reactor is the Ergun equation (Amiri *et al.*, 2019; Gräbner, 2014; Nemec & Levec, 2005). The Ergun equation is versatile because it can be used for different particle shapes and sizes as well as a variety of inlet gas flow rates (Jia *et al.*, 2009; Nemec & Levec, 2005). The Ergun equation has been adapted to include different aspects of the feedstock and reactor design. The properties of the feedstock that have been considered include (i) if the particle shape is spherical or non-spherical, (ii) the type of material, (iii) the particle diameter and (iv) the particle size distribution used in the reactor (Amiri *et al.*, 2019; Brunner *et al.*, 2015; Du Plessis, 1994; Jia *et al.*, 2009; Koekemoer & Luckos, 2015). If the wrong particle size is selected the reactor can become inefficient due to the channelling effect which can cause bypass flow patterns resulting in uneven gas distribution (Duffy & Eaton, 2013; Yang *et al.*, 2001). As research progressed, the reactor properties that have been adapted or included in the Ergun equation are the wall friction and the shape of the reactor (Ozahi *et al.*, 2008).

As mentioned, the bulk packing and mixing of the feedstock also affect the operation of the gasification reactor because this influences the spaces formed around the particles known as bed voidage (Yu *et al.*, 1996). Bed voidage influences the pressure drop across the bed and is included in the Ergun equation (Amiri et al., 2019; Nemec & Levec, 2005). Packing models have been modelled to predict the bed voidage using the particle size, volume and mass as input (Yu *et al.*, 1996). The culmination of the factors presented in the previous paragraphs forms the basis for the research problem that will be investigated in this study.

1.1 Research problem

Accurately measuring and predicting the voidage of packed beds presents a complex and challenging research problem. The bed voidage is influenced by various factors such as the size, shape, and packing density of the particles, which interact in complex ways, making it difficult to develop universally applicable models for predicting the voidage of packed beds. The current methods for measuring voidage can be time-consuming and costly, leading to inaccurate and unreliable measurements under especially when different particle sizes are mixed. Packed bed voidage models typically rely on simplified assumptions, such as uniform particle size and homogeneous packing density, which may not accurately reflect the complex nature of packed bed morphology. Furthermore, these models can have limited accuracy and high sensitivity to particle properties like size, shape, and packing density that can vary significantly across different particle types, leading to significant errors in the predicted voidage. The lack of experimental data on packed bed voidage, particularly for mixtures of different particle sizes, further compounds this issue. To address this problem, this study will focus on improving the accuracy and reliability of packed bed voidage measurements and developing more robust models for predicting the voidage of binary and ternary mixtures of coke particles in packed beds. It is worth noting that packed bed voidage models are not universally applicable for all types of particles and that is why this study will focus on coke particle packing.

The problem with models that predict pressure drop in packed beds is similar to that of bed voidage models, in that it is a complex task and affected by factors such as particle size, shape, and packing density, and additionally the flow rate and fluid properties. Existing models for predicting pressure drop, such as empirical correlations and computational fluid dynamics (CFD) simulations, are not universally applicable due to the variations in physical and chemical properties of different packed bed systems. Empirical correlations based on experimental data may be limited to specific operating conditions and particle geometries and may not account for the interactions between different factors affecting pressure drop. CFD simulations can provide a detailed understanding of flow behavior but are computationally expensive and require accurate input data, which can be difficult to obtain experimentally. Moreover, limited experimental data are available for particle mixtures with different-sized particles and varying mixing ratios, whether they be binary or ternary mixtures. To be useful, pressure drop models should be applicable to different packed bed systems and require a thorough understanding of the physical structure of packed beds. Therefore, this study aims to examine more applicable models for predicting pressure drop in packed beds that account for mixtures of coke particle sizes.

1.2 Research aim

The aim of this study is to predict the effect of non-spherical particle characteristics on fixed bed morphology and subsequently to model the pressure drop based on the fundamental particle attributes. This is done to better understand the pipe flow analogies found in a blast furnace during the iron making process and how particle characteristics have an influence. To be able to predict the pressure drop across a packed bed of particles in a blast furnace will enable the operation to be more efficient.

1.3 Objectives

- Determine the extent to which particle characteristics influence packed bed voidage of arbitrary-shaped coke particles mixtures.

- Evaluate the effect of particle and packing characteristics of mixtures based on the measured and modelled pressure drop in a fixed bed.

1.4 Outline of dissertation

The dissertation consists of five chapters: introduction, literature review, research methodology, results and discussion, conclusion and recommendations. The introductory chapter provides the necessary background and motivation for the study. The literature review chapter provides background information regarding particle characteristics, packing models, and pressure drop models. The literature review chapter also includes statistical equations that will be used later in the study. The methodology chapter entails the materials used, sample preparation applied, and the experimental setup used for the study. The results and discussion chapter includes the results from using the materials, experimental setup, and models for voidage and pressure drop modelling across a packed bed of coke particles. Lastly, the conclusion and recommendation chapter provides the conclusions made from the results of the study aswell as recommendations for future study.

CHAPTER 2 LITERATURE REVIEW

Chapter 2 provides background information regarding particle characteristics, packing models, and pressure drop models. The literature review chapter also includes statistical equations that will be used later in the study.

2.1 Characterisation of multiparticle systems

2.1.1 Variation in particle diameter

Different methods are used to define irregular and non-spherical particle diameters to be used in research or modelling. The non-spherical particles used are characterised by equivalent diameters based on their geometric parameters (Wang & Fan, 2013). Feret and Martin's diameter are statistical models used in optical imaging as they are based on the particles' projection (Wang & Fan, 2013). The Sauter diameter is mostly used in pressure drop studies using non-spherical particles, as reported by Trahan (2014), Koekemoer & Luckos (2015), and Luckos & Bunt (2011), for the Ergun model correlation. Table 2-1 gives various diameter characterizations found in the literature to define the diameters of irregular particle shapes (Deng *et al.*, 2021; Yang, 2003).

Table 2-1: Variation in particle diameter characterization

Diameter characterization	Definition	Equation	
Volume diameter	The diameter of the particle is the same as an equal-volume sphere.	$d_v = \left({6V_p}/{\pi}\right)^{1/3}$	Equation 2-1
Surface diameter	The diameter of a sphere with a surface area equal to that of the particle.	$d_s = \left({S_p}/{\pi}\right)^{1/2}$	Equation 2-2
Surface-Volume diameter (Sauter diameter)	The diameter of a sphere with a surface area-to-volume ratio equal to that of the particle.	$d_{sv} = {6V_p}/{S_p}$	Equation 2-3
Sieve diameter	Width of the minimum square aperture in a sieving screen.	-	
Stokes diameter	The diameter of an equal dens, free-falling velocity sphere as the particle in a fluid of equal density and viscosity in the Stokes law region.	$d_{st} = \sqrt{{18\mu U}/{g(\rho_p - \rho_g)}}$	Equation 2-4
Perimeter diameter	The diameter of a circle with a perimeter equal to that of the particle's	-	

	projection perpendicular to the sphere.		
Projected area diameter	The diameter of a sphere with an area equal to that of the particle's projection perpendicular to the sphere.	-	
Feret diameter	The statistical diameter of which the mean length from two furthest points of the particle.	-	
Martin diameter	The statistical diameter of which the mean chord length of the particle bisects the projected area of the particle.	$d_{MA} = {}^{4}/_{(\rho_{\epsilon} a_s)}$	Equation 2-5

2.1.2 Average particle diameter

A mechanical method that is used to separate particles based on their diameter is through a sieve analysis (Carter & Gregorich, 2007). Sieve analysis is useful when handling a large sample size of particles and is a relatively cheap method to separate particles (Wills & Finch, 2015). Sieve analysis is done by sifting particles through a metal sieve (also known as a mesh) with decreasing aperture sizes (Carter & Gregorich, 2007; Wills & Finch, 2015). The particles are easily passed through the metal mesh by swirling, vibrating or shaking the tower of sieves (Carter & Gregorich, 2007). Particles with a diameter larger than the sieve aperture don't pass through and remain on the sieve. Each sieve's number of particles is weighed to calculate the percentage of particles retained on each sieve. The cumulative weight percentage of the particles is plotted against particle diameter to form a particle size distribution graph, as indicated in Figure 2-1 (Wills & Finch, 2015). The average particle diameter D_{50} is the particle size where half of the particles will pass through the sieves or the mean particle size of the sample batch (Wills & Finch, 2015). Sieve Analysis is one of the most widely used of all developed particle size analysis techniques. Other methods include imaging, gravity and centrifugal sedimentation, characterisation by elutriation, cascade impaction technique, resistivity and optical zone sensing techniques (Yang, 2003).

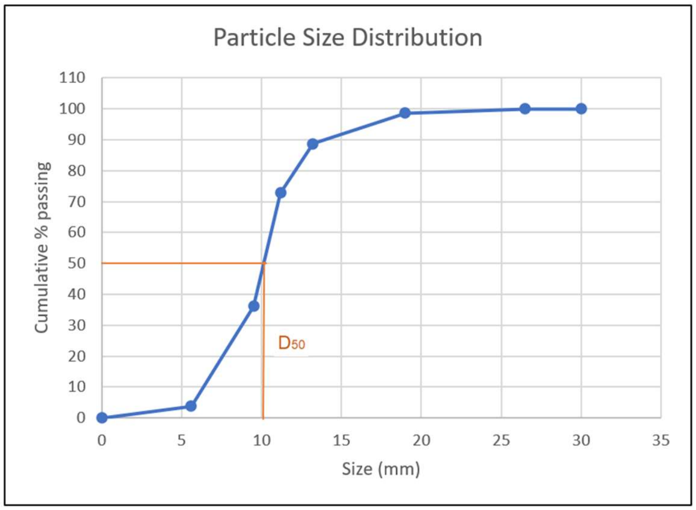

Figure 2-1: Particle size distribution graph

2.1.3 Sauter Mean particle diameter

Another method to describe the average particle diameter is through the Sauter mean diameter, which is also referred to as the surface-volume mean. The Sauter mean diameter is used in applications with bubbles, droplets and particles; thus, any polydisperse matter (Kowalczuk & Drzymala, 2016). The Sauter mean diameter is shown in Equation 2-6, where x_i is the volume fraction, d_{pi} the particle diameter and *i* the size interval. The Sauter mean diameter can be used to approximate a packed bed's average particle diameter (Koekemoer & Luckos, 2015). In the case of sieve analysis, x_i denotes the mass fraction of particles in the size interval *i*. If the particle size diameter is determined using a laser scattering technique, then x_i denotes the volume fraction.

$$d_{p_{SM}} = \frac{1}{\sum \frac{x_i^I}{d_{p_i}^I}} \qquad \text{Equation 2-6}$$

2.1.4 Particle sphericity

Sphericity is defined as the ratio of the surface with equal volume to the particle and the surface of the particle and is calculated using Equation 2-7 (Trahan *et al.*, 2014; Wang & Fan, 2013).

$$\varphi = \frac{\pi^{1/3}(6V_p)^{2/3}}{A_p}$$ Equation 2-7

The sphericity factor can be experimentally obtained using the Subramanian method and described as the water drain method. The technique uses a burette with the stopper cut off or a cylinder, filling the burette with the particles. After the particles are added, a fluid with known properties is added and engulfs the particles to a height of H_0 of the burette; the fluid is then drained to the bottom of the burette at a height H_1. The time to drain the fluid from height H_0 to H_1 is denoted as t, with μ the kinematic viscosity. The sphericity can be calculated using the Subramanian method with Equation 2-8 (Subramanian & Arunachalam, 1980). The constant J used in Equation 2-8 is calculated in Equation 2-9 and refers to the time for the fluid to drain between the two reference points.

$$\varphi = \sqrt{\frac{\left(\frac{150 \cdot L \cdot J \cdot \mu \cdot (1-\varepsilon_m)^2}{dp_m{}^2 \varepsilon_m{}^3 g}\right)}{\left(1-\frac{L}{H_1}\right)}}$$ Equation 2-8

$$J = \frac{lnH_0 - lnH_1}{t}$$ Equation 2-9

2.1.5 Particle shape

Particles come in various shapes, from spherical particles to cylindrical and irregular or non-spherical shapes. A baseline, equivalent particle diameter exists to compare the effects of various particle shapes based on a comparison with one another. Different particle shapes and their respective equivalent diameters are expressed in Table 2-2 (Rase, 2013; Yang, 2003). The Sauter mean diameter is mostly used in pressure drop studies using a mixture of non-spherical particles, as seen in Koekemoer & Luckos (2015), and Luckos & Bunt (2011), for the Ergun model correlation (Koekemoer & Luckos, 2015; Luckos & Bunt, 2011).

Table 2-2: Particle shape characterisation and equivalent particle diameter

Particle shape	Definition	Equivalent particle diameter	
Sphere	Sphericity of 1	$d_{ep} = 6/a_s$	Equation 2-10
Cylinder	• Equal length to diameter cylinder	$d_{ep} = d_y$	Equation 2-11
	• Length not equal to diameter cylinder	$d_{ep} = 6d_y/(4 + 2\,d_y/l_y)$	Equation 2-12
Ring	Circular shape with an inner and outer diameter	$d_{ep} = 1.5(d_o - d_i)$	Equation 2-13

Non-spherical	Sphericity of 0.5 to 0.7	$d_{ep} = \varphi d_a$	Equation 2-14
Mixed sizes	Mixture of different size particles	$d_{ep} = \frac{1}{\sum \frac{x_i}{d_{p_i}}}$	Equation 2-15

2.1.6 Image analysis

Particle characteristics such as shape, size and sphericity can be determined using photos taken by cameras; this is known as photogrammetry and is used for image analysis of particles.

2.1.6.1 ImageJ

The National Institute of Health developed ImageJ a public domain image processing program that was written using Java was developed as a cost effective method for medical researchers for bacterial analysis (Helmy & Abdel Azim, 2012). The program captures objects and determines their perimeter and area in the given unit. Circularity or roundness is then calculated using Equation 2-16 (Helmy & Abdel Azim, 2012; Takashimizu & Iiyoshi, 2016). ImageJ has been mainly used in the medical field but has been extended into particle characterisation by converting the captured image to a binary image (Đuriš *et al.*, 2016).

$$\varphi_C = 4\pi(A \cdot perimeter^2) \quad \text{Equation 2-16}$$

An object with a circularity of 1 is a perfect circle and a 0 is an elongated polygon. The image processing technology becomes less accurate the smaller the object is (Helmy & Abdel Azim, 2012). The area and perimeter of the object are directly proportional to the circularity of the object (Takashimizu & Iiyoshi, 2016).

2.1.6.2 RhoVol

The RhoVol analyser is the equipment used for density and image analysis on an individual particle basis,; the machine consists of a conveyor belt, mass scale, cameras and ten collection buckets (Botlhoko *et al.*, 2021; DeBeers, 2013). The machine can process between 800 and 1200 particles an hour and be programmed to sort the particles into various collection buckets based on the particle parameters such as size, shape, etc. (Botlhoko *et al.*, 2021). The particle falls into a chamber where cameras are distributed around the falling particle; through numerous simultaneous photos, a 3D model is crated of the particle, and the calliper values are measured (Botlhoko *et al.*, 2021; DeBeers, 2013). There are currently three models derived from the RhoVol machine that measure particles of different size ranges: -3 mm to +1 mm model, the -8 mm to +3 mm model, and the -25 mm to +8 mm model (DeBeers, 2013).

The particle parameters the RhoVol analyser can output are listed below (Botlhoko *et al.*, 2021; DeBeers, 2013):

- Weight
- Volume
- Density
- Square sieve size
- Round sieve size
- Flatness
- Elongation
- Compactness (Sphericity factor)
- Roller gap size

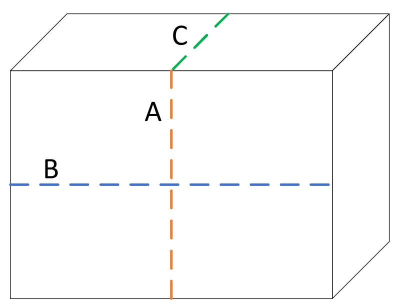

Figure 2-2: Capiller values displayed on a cube adapted from DeBeers (2013)

Some particle parameters are obtained from calliper values, which are based on the indicated dimensions in Figure 2-2, where the particle would fit into a rectangular parallelepiped and the values are obtained from measuring the face dimensions. Calliper values are three orthogonal lengths (mm) where *A* is the longest calliper and descending until *C* being the shortest calliper (DeBeers, 2013). Flatness is defined as the ratio *B:C*; a sphere's flatness is equal to 1. Elongation is defined as the ratio *A:B*; the elongation of a sphere and a cube is equal to 1. Compactness is defined as shown in Equation 2-17; a sphere and a cube's compactness equals 1 (DeBeers, 2013).

$$Compactness = \left(\frac{B \cdot C}{A^2}\right)^{\frac{1}{3}} \qquad \text{Equation 2-17}$$

2.2 Packing characteristics of non-spherical particles packing

Packing characteristics (how the particles stack upon each other and in the vessel) influence how liquids and gases flow through the packed bed of particles and the bed's permeability (Wong & Kwan, 2014). Packing characteristics depend on the particles' geometry (shape and size), which conversely relies on the geometry of the voids between the particles. Bed voidage is the most common packing characteristic for spherical and non-spherical particles (Yang, 2003). Bed voidage is defined as the void volume in the packed bed divided by the total volume of the packed bed (Dullien, 1997). Specific surface is the second packing characteristic to consider and is defined as the internal surface of packing divided by the total volume of solids in the packed bed (Yang, 2003). Specific surface is independent of bed voidage and type of packing; however, it is dependent on the particle shape and size. Packing density is another packing characteristic and is defined as the ratio between the number of particles to the bulk volume and is influenced by the packing structure and effects of particles relative to each other (Wong & Kwan, 2014).

2.2.1 Factors affecting packing density and bed voidage

When particles are handled and are charged into a reactor to form a packed bed, certain factors affect the packing density and bed voidage, including the deposition intensity and method applied (Yang, 2003). The reactor shape, size and material can affect bed voidage and packing density. The particle itself is the most unpredictable due to various parameters that can affect the packing density (Sohn & Moreland, 1968; Yang, 2003). The factors include the particle shape, and size, if it is porous or smooth, the particle size distribution used in the reactor and the particle coefficient of restitution. Other factors that can affect the bed voidage and packing density is if the particles are vibrated into place or if pressure is applied on top of the particle bed (Yang, 2003).

Particles form a packing structure when they are inserted into a reactor. The packing structure depends on the particle size, shape and how individual particles are stacked upon each other (Dullien, 1997; Yang, 2003). Regular packing structure is found in spherical and equal-sized particles in parallel rows. A common packing structure is the cubic packing structure, where one layer of spherical particles is stacked upon the second layer with particle centres placed upon the other particle centres (Yang, 2003). Variations of the packing structure are found when the centre of one layer is placed at different positions in the additional layer of particles (Dullien, 1997). Non-spherical particles form a random packing structure when forming a packed bed. In a random packing structure, the position of one particle relative to the previous layer of particles cannot be given with accuracy (Dullien, 1997; Yang, 2003). There are three main effects particles have on each other: the wedging, wall and loosening effects, as seen in Figure 2-3; the effects are related to the ratio of the particle sizes being mixed (Liu *et al.*, 2020; Wong & Kwan, 2014). The wedging effect occurs when particles form voids between them, mainly when larger particles lock in smaller particles. An increase in bed voidage occurs when the voids formed around the particles are smaller than the small particles. This leads to the smaller particles being unable to fill the voids and are wedged between the larger particles (Liu *et al.*, 2020; Wong & Kwan, 2014). The wall effect occurs when smaller particles are enveloped around larger particles forming small voids in the packed bed. The loosening effect occurs when larger particles are enveloped around smaller particles forming voids in the packed bed (Liu *et al.*, 2020). All three effects increase the total bed voidage. Some packing correlations consider the effects mentioned above when being developed (Liu *et al.*, 2020; Wong & Kwan, 2014).

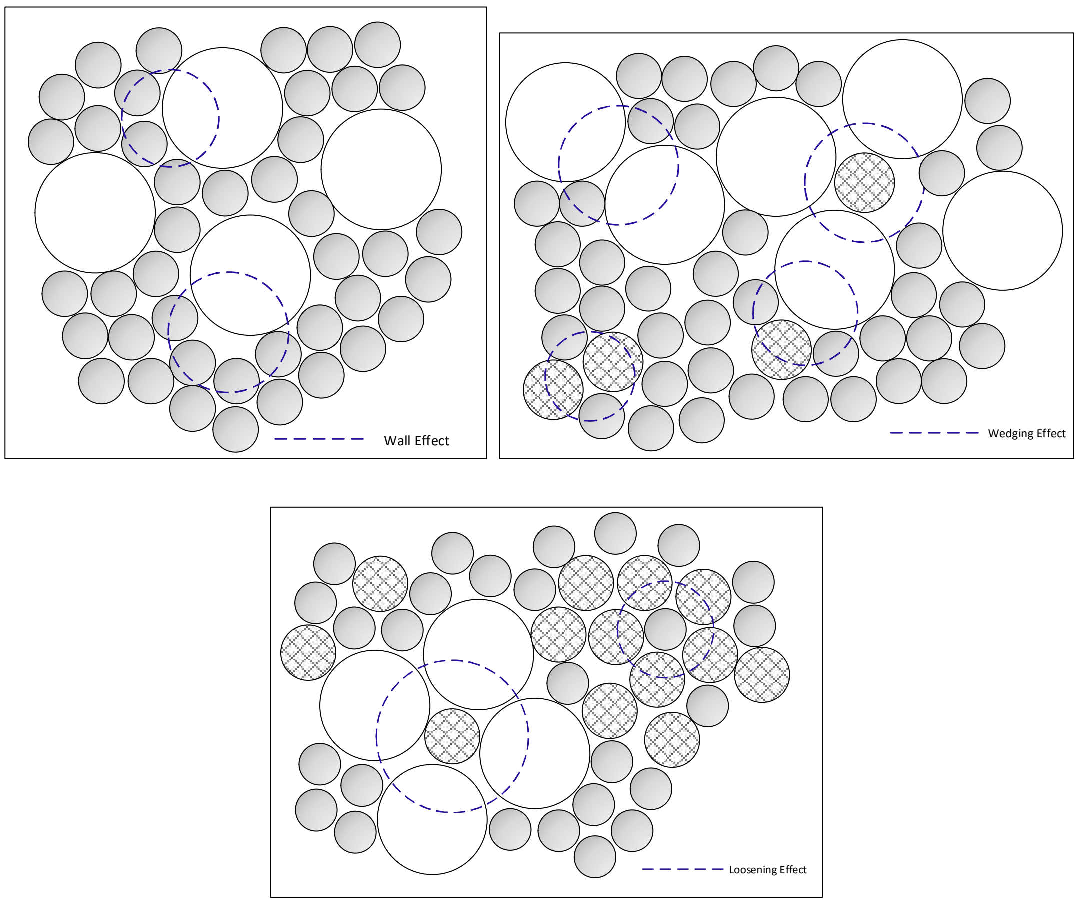

Figure 2-3: Wall, wedging and loosening effect of particle packing adapted from Liu *et al.* (2020)

2.2.2 Correlations for fixed bed bulk voidage

Bed voidage is a critical parameter that is used to estimate the pressure drop in a packed bed. The water displacement technique is the experimental method to determine the bed voidage (Yang, 2003). Bed voidage can also be obtained using x-ray microtomography by taking multiple projections to capture the gas in a packed bed and inserting the projections into software to calculate the bed voidage (Zhou *et al.*, 2017). A comprehensive list of considered correlations for predicting bed bulk voidage is summarised in Table 2-3.

Table 2-3: Voidage models found in the literature

Model equation		Limitations
Furnas		
$\varepsilon_w = \left[1 + 0.6\left(\frac{d_{p_m}}{D}\right)\right]\varepsilon_m - 0.6\left(\frac{d_{p_m}}{D}\right)$	Equation 2-18	• 0.77 < φ < 1 • 1.0503 cm < d_p < 2.401 cm • 0.380 < ε_m < 0.651
$\varepsilon_c = [\varepsilon_m + 0.3(1-\varepsilon_m)]\left[1 + 0.6\left(\frac{d_{p_m}}{D}\right)\right] - 0.6\left(\frac{d_{p_m}}{D}\right)$	Equation 2-19	
$\varepsilon_m = \frac{void\ volume\ in\ packed\ bed}{total\ packed\ bed\ volume}$	Equation 2-20	
Abbas		
$\varepsilon_m = 0.375 + 0.34\left(\frac{d_{pSM}}{D}\right)^1$	Equation 2-21	• Mono size particles • Spherical particles
$\varepsilon_m = i_1 + i_2\left(\frac{d_{p_m}}{D}\right)^{i_3}$	Equation 2-22	
$\varepsilon_m = 0.36 + 0.08\left(\frac{d_{p_m}}{D}\right)^{0.5}$	Equation 2-23	
Haughey and Beveridge		
$\varepsilon_m = \left[1 + 0.6\left(\frac{d_{p_m}}{D}\right)\right] - 0.6\left(\frac{d_{p_m}}{D}\right)^2$ with $\frac{d_{p_m}}{D} \le 0.5$	Equation 2-24	• Spherical particles
$\varepsilon_m = 0.528 + 2.464\left(\frac{d_{p_m}}{D} - 0.5\right)$ with $0.5 \le \frac{d_{p_m}}{D} \le 0.536$	Equation 2-25	
$\varepsilon_m = 1.0 - 0.667\left(\frac{d_{p_m}}{D}\right)^3\left[2\left(\frac{d_{p_m}}{D}\right) - 1\right]^{-0.5}$ with $\frac{d_{p_m}}{D} \ge 0.536$	Equation 2-26	
Hartman		
$\varepsilon_m = 1.0 - 0.8648\varphi + 0.2745\varphi^2$	Equation 2-27	• 0.14 mm < d_p < 0.72 mm • 0.4 < ε_m < 1

Westman		
$\left(\frac{V_m - V_j x_j}{V_i}\right)^2 + 2 \cdot G \cdot \left(\frac{V_m - V_j x_j}{V_i}\right)\left(\frac{V_m - x_j - V_i x_i}{V_j - 1}\right) + \left(\frac{V_m - x_j - V_i x_i}{V_j - 1}\right)^2 = 1$	Equation 2-28	• Spherical particles
$V_m = \frac{1}{1 - \varepsilon_m}$	Equation 2-29	
$V_i = \frac{1}{1 - \varepsilon_i}$	Equation 2-30	
$V_j = \frac{1}{1 - \varepsilon_j}$	Equation 2-31	
$G = [1.355(s)^{1.566}]^{-1};\ 0 < s \leq 0.824$ $G = 1;\ 0.824 < s \leq 1$	Equation 2-32	
$s = \frac{d_{p_i}}{d_{p_j}};\ i < j$	Equation 2-33	
El-Husseiny		
$\frac{1}{1 - \varepsilon_{m1}^*} = \left(\frac{x_i}{1 - \varepsilon_i} + \frac{x_j}{1 - \varepsilon_j}\right) - (1 - aEH) \cdot \left(\frac{x_i}{1 - \varepsilon_i}\right)$	Equation 2-34	• Irregular particles • Non-spherical particles • d_p =8.0mm
$\frac{1}{1 - \varepsilon_{m2}^*} = \left(\frac{x_i}{1 - \varepsilon_i} + \frac{x_j}{1 - \varepsilon_j}\right) - (1 - bEH) \cdot \varepsilon_j \cdot \left(\frac{x_j}{1 - \varepsilon_j}\right)$	Equation 2-35	
$aEH = 1 - (1 - s)^{3.3} - 2.8 \cdot s \cdot (1 - s)^{2.7}$	Equation 2-36	
$bEH = 1 - (1 - s)^{2.0} - 0.4 \cdot s \cdot (1 - s)^{3.7}$	Equation 2-37	
$\varepsilon_m = \max\{\varepsilon_{m1}^*, \varepsilon_{m2}^*\}$	Equation 2-38	
$s = \frac{d_{p_i}}{d_{p_j}};\ i < j$		
Toufar		
$\varepsilon_m = (1 + \varepsilon_i) \cdot x_i + (1 + \varepsilon_j) \cdot x_j - k_d b_{TM} \varepsilon_j x_j - 1$	Equation 2-39	• Spherical particles
$k_d = \frac{d_{p_j} - d_{p_i}}{d_{p_j} - d_{p_i}}$	Equation 2-40	
$b_{TM} = 1 - \frac{1 + 4z}{(1 + z)^4}$	Equation 2-41	
$z = \frac{(1 + \varepsilon_i) \cdot x_i}{\varepsilon_j \cdot x_j};\ i < j$	Equation 2-42	

Kwan		
$\frac{1}{\varepsilon_{m1}^{*}} = \left(\frac{x_i}{\varepsilon_i} + \frac{x_j}{\varepsilon_j}\right) - (1 - a_{KM}) \cdot \frac{x_i}{\varepsilon_i} \cdot (1 - c_{KM}[3.8^{x_i} - 1])$	Equation 2-43	• Granite particles
$\frac{1}{\varepsilon_{m2}^{*}} = \left(\frac{x_i}{\varepsilon_i} + \frac{x_j}{\varepsilon_j}\right) - (1 - b_{KM}) \cdot (1 - \varepsilon_j) \cdot \frac{x_j}{\varepsilon_j} \cdot (1 - c_{KM}[2.6^{x_j} - 1])$		
	Equation 2-44	
$\varepsilon_m = \min\{\varepsilon_{m1}^{*}, \varepsilon_{m2}^{*}\}$		
$a_{KM} = 1 - (1 - s)^{5.0} - 1.9 \cdot s \cdot (1 - s)^{3.6}$	Equation 2-45	
	Equation 2-46	
$b_{KM} = 1 - (1 - s)^{1.9} - 2.1 \cdot s \cdot (1 - s)^{10.5} - 0.2 \cdot (1 - s)^{7.6}$		
$c_{KM} = 0.335 \cdot \tanh{(26.9 \cdot s)}$	Equation 2-47	
	Equation 2-48	
$s = \frac{d_{p_i}}{d_{p_j}};\ i < j$	Equation 2-49	
$\varepsilon_{m1}^{*} = (1 + \varepsilon_i) \cdot x_i + (1 + \varepsilon_j) \cdot x_j - (1 - a_{KM})(1 + \varepsilon_i) \cdot x_i \cdot (1 - c_{KM}[3.8^{x_i} - 1]) - 1$	Equation 2-50	
$\varepsilon_{m2}^{*} = (1 + \varepsilon_i) \cdot x_i + (1 + \varepsilon_j) \cdot x_j - (1 - b_{KM}) \cdot \varepsilon_j \cdot x_j \cdot (1 - c_{KM}[2.6^{x_j} - 1]) - 1$	Equation 2-51	
$\varepsilon_m = \max\{\varepsilon_{m1}^{*}, \varepsilon_{m2}^{*}\}$		
Simple Centroid Design		
$\varepsilon_m = \sum_{i=1}^{3} \beta_{i\_SC} X_i + \sum_{1 \le i < j \le 3} \beta_{ij\_SC} X_i X_j + \beta_{123\_SC} X_1 X_2 X_3$	Equation 2-52	• Nonuniform particles • Uniform particles • Spherical particles • Defined geometric unit • Coke particles
$\beta_{i\_SC} = \varepsilon_i$	Equation 2-53	
$\beta_{ij\_SC} = 4\varepsilon_{ij} - 2(\varepsilon_i + \varepsilon_j)$	Equation 2-54	
$\beta_{123\_SC} = 27\varepsilon_{123} - 12(\varepsilon_{12} + \varepsilon_{13} + \varepsilon_{23}) + 3(\varepsilon_1 + \varepsilon_2 + \varepsilon_3)$	Equation 2-55	
$i, j = 1, 2, 3;\ i < j$		
D-optimal Design		
$\varepsilon_m = \sum_{i=1}^{3} \beta_{i\_DO} X_i + \sum_{i<j} \beta_{ij\_DO} X_i X_j + \sum_{i<j} \nu_{ij\_DO} X_i X_j (X_i - X_j) + \beta_{123\_DO} X_1 X_2 X_3$	Equation 2-56	• Nonuniform particles • Uniform particles • Spherical particles • Defined geometric unit • Coke particles
$\beta_{i\_DO} = \varepsilon_i$	Equation 2-57	
$\beta_{ij\_DO} = \frac{\varepsilon_{ij} + \varepsilon_{ji} - (\varepsilon_i + \varepsilon_j)}{0.4032}$	Equation 2-58	
$\nu_{ij\_DO} = \frac{\varepsilon_{ij} - \varepsilon_{ji} - 0.44(\varepsilon_i - \varepsilon_j)}{0.177408}$	Equation 2-59	
$\beta_{123\_DO} = 27\varepsilon_{123} - \frac{3}{0.4032}(\varepsilon_{12} + \varepsilon_{13} + \varepsilon_{23} + \varepsilon_{21} + \varepsilon_{31} + \varepsilon_{32} - 2[\varepsilon_1 + \varepsilon_2 + \varepsilon_3]) - 9(\varepsilon_1 + \varepsilon_2 + \varepsilon_3)$	Equation 2-60	
$i, j = 1, 2, 3;\ i < j$		

Wong & Kwan		
$$\frac{1}{\varepsilon_{m1}^{*}} = \frac{1}{\varepsilon_T} - (1-b_{12})(1-\varepsilon_2)\left(\frac{x_2}{\varepsilon_2}\right)\left(1-c_{12}[2.6^{(x_2+x_3)}-1]\right) - (1-b_{13})(1-\varepsilon_3)\left(\frac{x_3}{\varepsilon_3}\right)\left(1-c_{13}[2.6^{(x_2+x_3)}-1]\right)$$	Equation 2-61	• Spherical • Non-cohesive coarse • Refined for non-spherical • Glass beads • 1.43 mm < d_p <15.73 mm
$$\frac{1}{\varepsilon_{m2}^{*}} = \frac{1}{\varepsilon_T} - (1-a_{12})\left(\frac{x_1}{\varepsilon_1}\right)\left(1-c_{12}[3.8^{x_1}-1]\right) - (1-b_{23})(1-\varepsilon_3)\left(\frac{x_3}{\varepsilon_3}\right)\left(1-c_{23}[2.6^{x_3}-1]\right)$$	Equation 2-62	
	Equation 2-63	
$$\frac{1}{\varepsilon_{m3}^{*}} = \frac{1}{\varepsilon_T} - (1-a_{13})\left(\frac{x_1}{\varepsilon_1}\right)\left(1-c_{13}[3.8^{x_1}-1]\right) - (1-a_{23})\left(\frac{x_2}{\varepsilon_2}\right)\left(1-c_{23}[3.8^{x_2}-1]\right)$$	Equation 2-64	
$$\varepsilon_m = \min\{\varepsilon_{m1}^{*}, \varepsilon_{m2}^{*}, \varepsilon_{m3}^{*}\}$$	Equation 2-65	
$$a_{WK} = 1-(1-s)^{3.3} - 2.6\cdot s\cdot(1-s)^{3.6}$$	Equation 2-66	
$$b_{WK} = 1-(1-s)^{1.9} - 2\cdot s\cdot(1-s)^{6}$$	Equation 2-67	
$$c_{WK} = 0.322\cdot\tanh(11.9\cdot s)$$	Equation 2-68	
$$\frac{1}{\varepsilon_T} = \frac{x_1}{\varepsilon_1} + \frac{x_2}{\varepsilon_2} + \frac{x_3}{\varepsilon_3};\ for\ mono-size\ particles$$		
$$s = \frac{d_{p_i}}{d_{p_j}};\ i<j$$		

2.2.2.1 Furnas (1929)

Furnas proposed two equations for bed voidage, an equation to calculate bed voidage close to the wall of the reactor and an equation to calculate bed voidage at the core of the packed bed, which is shown in Equation 2 18 and Equation 2 19, respectively (Furnas, 1929). With d_p being the particle diameter, *D* the diameter of the tube or reactor and ε_m the average bed voidage as described by Equation 2-20 (Yang, 2003).

2.2.2.2 Abbas (2011)

Abbas took Furnas' (1931) findings, shown in Equation 2-21, further and constructed an empirical formula based on it to develop Equation 2-22. Using mono-sized spherical particles for their study, Abbas regressed his own constants to formulate Equation 2-23 (Abbas, 2011; Furnas, 1931).

2.2.2.3 Haughey and Beveridge (1969)

Haughey and Beveridge formulated the bed voidage for spherical particles in classes of the ratio of particle diameter to tube diameter, as shown in Equation 2-24 to Equation 2-26 (Haughey & Beveridge, 1969).

2.2.2.4 Hartman *et al.* (2000)

Hartman *et al.* formulated the bed voidage described by Equation 2-27 using sphericity and regressed constants. The Hartman correlation was developed for a bed voidage range of 0.4 to 1.0 (Hartman et al., 2000).

2.2.2.5 Westman (1936)

Westman developed a Simple Empirical Equation, Equation 2-28, to calculate voidage for binary mixtures of two-size particles that are approximately spherical (Li *et al.*, 2005; Westman, 1936). The equation was aimed to be constructed by only using one parameter to calculate bed voidage (Westman, 1936). V_m is the specific volume of the mixture, V_i is the specific volume of the small particle, and V_j is the specific volume larger particle. *G* is a coefficient based on diameter ratio *s* and was developed by Yu (Yu *et al.*, 1993).

2.2.2.6 El-Husseiny et al. (2019)

El-Husseiny *et al.* developed a packing model, Equation 2-34 and Equation 2-35 for binary mixtures made up of irregular, non-spherical particles. The model was based on experimental results using calcite aggregate and was developed to include the loosening effect, Equation 2-36 and the wall effect, Equation 2-37. El-Husseiny *et al.* found that when the larger particles were more dominant, the greater the loosening effect (El-Husseiny *et al.*, 2019). Where aEH is defined as the correction function for the loosening effect and is a function of diameter ratio s, *and* bEH is defined as the correction function for the wall effect and is a function of diameter ratio s.

2.2.2.7 Toufar (Liu *et al.*, 2020)

Toufar developed a packing model based on binary mixtures using spherical particles, Equation 2-39, but the model included only the wall effect parameter (b_{TM}), Equation 2-40 and diameter ratio constant (k_d), Equation 2-41. The wall effect parameter (b_{TM}) is a function of a constant z, Equation 2-42 which is a function of voidage (ε_i) and volumetric ratio (x_i). Toufar found that using small amounts of the small particles gave large deviation in the model (Liu *et al.*, 2020).

2.2.2.8 Kwan et al. (2013)

Kwan *et al*. developed a 3-parameter model based on granite particle mixing by creating binary mixtures via mixing different particle sizes. Kwan *et al*. introduced the wedging effect as the third parameter for a binary packing model (Kwan *et al.*, 2013). The loosening, wall and wedging effect parameters are based on the diameter ratio. Wong and Kwan did further research on spherical glass beads with sizes 1.43 mm < d_p < 15.73 mm with voidage of 0.586 < ε_m < 0.605 (Wong & Kwan, 2014). Based on the experimental values of the loosening effect (a_{KM}), wall effect (b_{KM}) and wedging effect (c_{KM}) obtained , best-fit curves were derived by regression analysis to generate Equation 2-43 to Equation 2-44 (Wong & Kwan, 2014)

Liu *et al.* developed empirical models Equation 2-50 and Equation 2-51 based on the Kwan *et al.* model using the same parameters in Equation 2-46 and Equation 2-47 regressed by Kwan *et al.* (Liu *et al.*, 2020).

2.2.2.9 Standish and Yu (1987)

Standish and Yu developed ternary packing models for nonuniform and uniform particles that are spherical or a defined geometric unit; coke particles were tested in their research to develop the packing models (Standish & Yu, 1987a). Standish and Yu developed two models, the Simple Centroid Design and the D-optimal Design; each was developed to include different reference points (Table 2-4 and Table 2-5) to develop the models, with the Simple Centroid Design using the minimal reference points (Standish & Yu, 1987a; Standish & Yu, 1987b). The models consist of parameters *β* and *v*, which are functions of the references and are regressed for each model.

2.2.2.9.1 Simple Centroid Design

The Simple Centroid Design uses references as shown in Table 2-4 to construct parameters in Equation 2-53 to Equation 2-55 and used in Equation 2-52.

Table 2-4: Simple Centroid Design reference points

x_1	x_2	x_3	Voidage
1	0	0	ε_1
0	1	0	ε_2
0	0	1	ε_3
1/2	1/2	0	ε_{12}
1/2	0	1/2	ε_{13}
0	1/2	1/2	ε_{23}
1/3	1/3	1/3	ε_{123}

2.2.2.9.2 D-optimal Design

Like the Simple Centroid Design, the D-optimal Design uses references as shown in Table 2-5 to construct parameters from Equation 2-57 into Equation 2-60, to be used in Equation 2-56. The difference is that the D-optimal design uses more parameters and reference points requiring more experimental work and data points to construct a valid model.

Table 2-5: D-optimal Design reference points

x_1	x_2	x_3	Voidage
1	0	0	ε_1
0	1	0	ε_2
0	0	1	ε_3
0.72	0.28	0	ε_{12}
0.72	0	0.28	ε_{13}
0	0.72	0.28	ε_{23}
0.28	0.72	0	ε_{21}
0.28	0	0.72	ε_{31}
0	0.28	0.72	ε_{32}
1/3	1/3	1/3	ε_{123}

2.2.2.10 Wong & Kwan (2014)

Wong and Kwan developed a ternary packing model, Equation 2-61 to Equation 2-63, for mono-sized spherical and non-cohesive coarse particles, which was further refined to be used for non-spherical particles. (Liu *et al.*, 2020) The 3-parameter model is based on their binary packing model also for spherical glass beads with sizes 1.43 mm < d_p < 15.73 mm with voidage of 0.586 < ε_m < 0.605 (Wong & Kwan, 2014). The ternary model also includes the loosening effect (a_{WK}), wall effect (b_{WK}) and wedging effect (c_{WK}) which were obtained through regression analysis to generate Equation 2-65 to Equation 2-67. (Wong & Kwan, 2014).

2.3 Fluid flow and pressure drop through packed beds

Consider as an example, coke particles that are used as a solid fuel for blast furnaces in the ironmaking industry (Matsuhashi *et al.*, 2012). The coke rate needed to operate a blast furnace can be as high as 300kg/t, kilograms of coke consumed per ton of hot metal produced. (Matsuhashi *et al.*, 2012). Modern industry has a lower coke rate and high gas injection rate due to the coke quality (Babich *et al.*, 2009). The quality of coke impacts the packing in the blast furnace. Gas would be injected to start the melting process and generate a pressure drop when passing through the packed bed of coke particles. The pressure drop that occurs during the blast furnace operation impacts the blast furnace's efficiency (Fogler & Gürmen, 1999). This is because an increase in pressure drop can lower the reaction rate and conversion of the coke (Fogler & Gürmen, 1999). An increase in pressure drop leads to more injecting gas flow needed to keep the blast furnace efficient and increases the operating cost (Fogler & Gürmen, 1999).

Flow through a packed bed has been investigated before and is classified into two categories, the discrete particle model and the pipe flow analogy. The pipe flow analogy models can be used for spherical particles to measure pressure drop across the packed bed but fail to predict the pressure drop for non-spherical particles (Yang, 2003). The capillary tube model, also known as the channel model, is the most used pipe flow analogy model for spherical particles with sphericity larger than 0.6. The capillary model defines the flow through the packed bed as a pack of straight capillaries which are equally sized (Yang, 2003). The capillary model was further investigated and perfected to be redefined as the constricted tube model. The constricted tube model defines the flow through a packed bed as circuitous channels with differentiating dimensions like cross-section and pore curvatures (Yang, 2003). The discrete particle model is used for particles with sphericity less than 0.6, also known as non-spherical particles. The discrete particle model defines the flow through the packed bed as individual particles with their boundary layers (Yang, 2003).

As a fluid flows through a packed bed, it passes particles, creating a flow pattern. The Reynolds number is a dimensionless parameter to describe this pattern. The Reynolds number for a single particle, Equation 2-69, was used as a basis for flow models and for the original literature Ergun model (Rhodes, 2008).

$$Re = \frac{d_p U \rho_g}{\mu} \qquad \text{Equation 2-69}$$

The Reynolds number for the flow through a packed bed also known as the modified Reynolds number, is described by Equation 2-70 and was introduced by Blake's correlation (Rhodes, 2008; Yang, 2003). The laminar flow regime is for Re_m less than 10, and the turbulent flow regime is for Re_m greater than 2000 (Rhodes, 2008).

$$Re_m = \frac{U d_p p_f}{\mu(1-\varepsilon)} \qquad \text{Equation 2-70}$$

Pressure drop across a packed bed can be challenging to estimate due to different particle shapes and sizes causing different flow analogies. Table 2-6 indicates models found in the literature on how to calculate pressure drop across a packed bed.

Table 2-6: Pressure drop models found in the literature

Model equation	Limitations
Darcy's Law	

$$Q = -\frac{KA_b\,(h_2-h_1)}{L}$$	Equation 2-71	• Porous particles • High velocity liquid • Low and high velocity gasses
$$Q = -\frac{K'A\,(P_2-P_1+p_g gL)}{L}$$	Equation 2-72	
$$P_1 = p_g g(h_1-z_1)$$	Equation 2-73	
$$P_2 = p_g g(h_2-z_2)$$	Equation 2-74	
Blake's Correlation		
$$f = \frac{\Delta P}{L}\frac{d_{p_m}}{U^2 g p_g(1-\varepsilon_m)}\frac{{\varepsilon_m}^3}{(1-\varepsilon_m)}$$	Equation 2-75	• $0.3 < \varepsilon_m < 0.7$
Reichelt		
$$\frac{\Delta P}{L} = \left(\frac{(1-\varepsilon_m)^2}{\varepsilon_m^3}\right)\left(\frac{\mu U}{{d_p}^2}\right)\left(\frac{154A_w^2\mu(1-\varepsilon_m)}{\rho_g U d_p}+\frac{A_w}{B_w}\right)$$	Equation 2-76	• $0.01 < Re < 17635$ • 9.71 cm $< d_p < 24.05$ cm • $3.32 < D/d_p < 14.32$ • $0.366 < \varepsilon_m < 0.485$
$$A_w = 1+\left(\frac{2}{3\frac{D}{d_p}(1-\varepsilon_m)}+1\right)^2$$	Equation 2-77	
$$B_w = \left(1.15\left(\frac{D}{d_p}\right)^2+0.87\right)$$	Equation 2-78	
Wu		
$$\frac{\Delta P}{L} = 72\tau\left(\frac{(1-\varepsilon_m)^2}{\varepsilon_m^3}\right)\left(\frac{\mu U}{{d_p}^2}\right)+\frac{3}{4}\tau\left(\frac{(1-\varepsilon_m)}{\varepsilon_m^3}\right)\left(\frac{\mu U^2}{d_p}\right)\left(\frac{3}{2}+\frac{1}{\beta_{Wu}^4}+\frac{5}{2\beta_{Wu}^2}\right)$$	Equation 2-79	• $0 < Re_m < 4000$ • $d_p = 100$mm • $\varepsilon_m = 0.42$
$$\beta_{Wu} = \frac{1}{1-\sqrt{1-\varepsilon_m}}$$	Equation 2-80	
$$\tau = \frac{1}{2}\left[1+\frac{1}{2}\sqrt{1-\varepsilon_m}+\sqrt{1-\varepsilon_m}\,\frac{\sqrt{\left(\frac{1}{\sqrt{1-\varepsilon_m}}-1\right)^2+\frac{1}{4}}}{1-\sqrt{1-\varepsilon_m}}\right]$$	Equation 2-81	
KTA		
$$\frac{\Delta P}{L} = \left(\frac{320}{Re/(1-\varepsilon_m)}+\frac{6}{Re/(1-\varepsilon_m)^{0.1}}\right)\left(\frac{(1-\varepsilon_m)}{\varepsilon_m^3}\right)\left(\frac{\mu U^2}{d_p}\right)\left(\frac{1}{2\rho_g}\right)$$	Equation 2-82	• $10 < Re_m < 10^5$ • $0.36 < \varepsilon_m < 0.42$
Montillet		
$$\frac{\Delta P}{L} = \left(\frac{1410}{Re}+16+\frac{45}{Re^{0.45}}\right)\left(\frac{\rho_g U^2}{d_p}\right)$$ $$Re = \frac{d_p U\rho_g}{\mu}$$	Equation 2-83	• $30 < Re < 1500$ • $d_p = 49.2$mm • $D/d_p = 12.2$ • $\varepsilon_m = 0.367$
Ergun		
$$\frac{\Delta P}{L} = 150\frac{(1-\varepsilon_m)^2}{\varepsilon_m^3}\frac{\mu U}{(\varphi d_p)^2}+1.75\frac{(1-\varepsilon_m)}{\varepsilon_m^3}\frac{\rho_g U^2}{\varphi d_p}$$	Equation 2-84	• $1 < Re < 10^3$
$$\frac{\Delta P}{L} = A_E\frac{\mu U}{(\varphi d_{p_m})^2}\frac{(1-\varepsilon_m)^2}{{\varepsilon_m}^3}+B_E\frac{U^2 p_g}{\varphi d_{p_m}}\frac{(1-\varepsilon_m)}{{\varepsilon_m}^3}$$	Equation 2-85	

2.3.1 Darcy's Law

Darcy's Law focuses on the flow through a packed bed with homogeneous particles containing pores. Newtonian fluids with low Reynolds numbers follow Darcy's Law. Darcy's Law is represented by Equation 2-71 (Yang, 2003). With *Q*, the volume of fluid moving through the packed bed, *K* constant dependant on fluid and particle properties, A_b is the bed area, and *L* is the bed height. The negative sign in the equation shows that the fluid flow is in the opposite direction of the height.

Darcy's Law can be modified to include pressure and fluid density shown in Equation 2-72 (Yang, 2003). The parameter *K'* is defined as the specific permeability divided by the liquid kinematic viscosity, μ and *g* the gravitational acceleration constant. A visual representation of Darcy's experiment is shown in Figure 2-4.

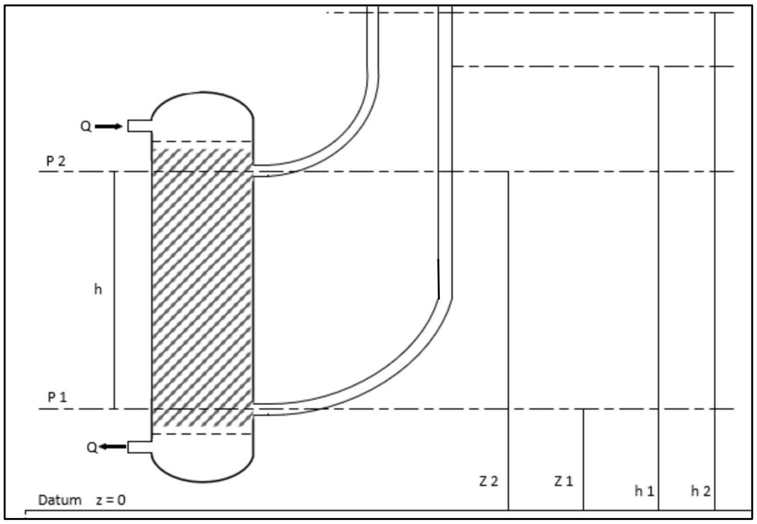

Figure 2-4: Darcy's experimental setup adapted from Yang (2003)

2.3.2 Blake's Correlation

Blake's Correlation was the first to include bed voidage ε in the equations. Blake suggested that the modified Reynolds number (Re_m), Equation 2-70, be used with the friction factor to be calculated using Equation 2-75 (Yang, 2003). With *U* the interstitial velocity, d_p the particle diameter and *L* the bed height. Equation 2-20 can be used to evaluate the bed voidage, and subsequently, the pressure drop across the packed bed can now be calculated.

2.3.3 Reichelt (1972)

Reichelt developed a pressure drop model, Equation 2-76, using particles with sizes 9.71 cm < d_p < 24.05 cm and pipe diameter to the particle diameter of 3.32 < D/d_p < 14.32, a Reynolds number (*Re*) of 0.01 < *Re* < 17635 and a bed voidage range of 0.366 < ε_m < 0.485. The model includes two parameters A_w, which is a function of the pipe diameter to particle diameter and bed voidage and $B_{w,}$ which is a function of the pipe diameter to particle diameter (Hassan & Kang, 2012).

2.3.4 Wu *et al.* (2008)

Wu *et al.* developed a model based on the average hydraulic radius model and the contracting–expanding channel model, Equation 2-79. The Wu *et al.* model uses Ergun's findings but removes the constants and exchanges them with functions. The Wu *et al.* model also includes the tortuosity factor (Wu *et al.*, 2008). The model was developed for particles with a size diameter of 100 mm and bed voidage of 0.42 and a Reynolds number (Re_m) range of $0 < Re_m < 4000$ (Hassan & Kang, 2012).

Tortuosity was first defined as the ratio of the average pore length to the thickness of the medium. Although easily defined, tortuosity is difficult to obtain through the experimental procedure but can be calculated using voidage and the effective diffusion coefficient or from the Kozeny coefficient (Abbas, 2011).To calculate tortuosity Equation 2-81 was used in the Wu et al. model and was defined by Bo-Ming and Jian-Hua (Bo-Ming & Jian-Hua, 2004).

2.3.5 KTA (1986)

The Nuclear Safety Standards Commission (KTA) developed a pressure drop model, Equation 2-82, through a high-temperature gas-cooled reactor with spherical particles (pebbles) with identical diameters. The model was developed for particles with the pipe diameter to particle diameter of $D/d_p > 20$, voidage range of $0.36 < \varepsilon_m < 0.42$ and a Reynolds number (Re_m) range of $10 < Re_m < 10^5$ ((KTA), 1986; Hassan & Kang, 2012).

2.3.6 Montillet (2004)

Montillet developed a pressure drop model for single phase flow through porous media, Equation 2-83, using particles with 49.2 mm and pipe diameter to the particle diameter of 12.2, a Reynolds number (Re) of $30 < Re < 1500$ and a bed voidage of 0.367 (Montillet, 2004).

2.3.7 Ergun correlation

The most used correlation to predict the flow and pressure drop of a packed bed is the Ergun correlation. The Ergun correlation can be used for irregular and non-spherical particles with a Reynolds (*Re*) number range of $1 < Re < 10^3$ and thus includes the term for sphericity; the Ergun correlation is given by Equation 2-84 (Koekemoer & Luckos, 2015).

With φ indicating the sphericity of the particles**.** Many adaptions and modifications were made to the Ergun correlation based on the researcher's data and accountability of other parameters. Parameters include the particle size distribution, the type of particles used to conduct the experiments and the packed bed shape in which the experiments are conducted (Keyser *et al.*, 2006; Koekemoer & Luckos, 2015; Ozahi *et al.*, 2008).

The Ergun equation can be rewritten as Equation 2-85. With A_E the viscous energy loss term dominates laminar flow, and B_E, the kinetic energy loss term dominates turbulent flow (Trahan *et al.*, 2014). The constants A_E and B_E can be experimentally obtained by applying a fluid across the packed bed of particles and obtaining the pressure drop across the bed. Constants A_E and B_E change with different types of particles because of the particle's physical characteristics and packing characteristics. Examples of constants A_E and B_E with different aspect ratios h_p/d_p are shown in Table 2-7 (Nemec & Levec, 2005).

Table 2-7: Ergun constants for various particle types

Particle shape	hp/dp	φ	ε_m	A_E	B_E
Cylindrical	0.37	0.757	0.418 - 0.500	280	4.60
Cylindrical	0.72	0.862	0.323 - 0.490	190	2.70
Cylindrical	0.91	0.872	0.336 – 0.588	200	2.50
Cylindrical	1.00	0.874	0.363	200	2.00
Cylindrical	1.00	0.874	0.350	180	2.00
Cylindrical	1.33	0.866	0.368 – 0.420	210	1.90
Cylindrical	1.91	0.835	0.334 – 0.682	210	2.50
Trilobe	4.33	0.630	0.466	295	4.71
Trilobe	4.33	0.630	0.511	263	4.99
Quadralobe	3.85	0.593	0.471	292	3.93
Quadralobe	3.85	0.593	0.502	294	4.19

* h_p is the height of the particle, and d_p is the particle diameter.

2.3.8 Statistical empirical pressure drop models

For further model development, statistical models were investigated. Starting with a basic model only to include only mono-sized and binary interactions as reference points which can be worked up to more complex models to include mono-size, binary, and ternary interactions.

Table 2-8: Statistical empirical pressure drop models

Model equation		Limitations
Pade polynomial		
$$\frac{\Delta P}{L} = \left(\frac{\sum \beta_i x_i^2 + \sum \beta_{ij} x_i x_j}{\sum \beta_{ii} x_i}\right) U^{\theta}$$ $$i, j = 1, 2, 3, 4, 5$$	Equation 2-86	• 2 < Re < 212 • 2.36 mm < d_p < 13.2 mm • 9.3 < D/d_p < 44.1 • 0.378 < ε_m < 0.515
Quad-K polynomial		
$$\frac{\Delta P}{L} = \left(\sum \beta_i x_i^2 + \sum \beta_{ij} x_i x_j\right) U^{\theta}$$ $$i, j = 1, 2, 3, 4, 5$$	Equation 2-87	• 2 < Re < 212 • 2.36 mm < d_p < 13.2 mm • 9.3 < D/d_p < 44.1 • 0.378 < ε_m < 0.515
Standard polynomial		
$$\frac{\Delta P}{L} = \left(\sum \beta_i x_i + \sum \beta_{ij} x_i x_j + \sum \beta_{ijk} x_i x_j x_k\right) U^{\theta}$$ $$i, j, k = 1, 2, 3, 4, 5$$	Equation 2-88	• 2 < Re < 212 • 2.36 mm < d_p < 13.2 mm • 9.3 < D/d_p < 44.1 • 0.378 < ε_m < 0.515

Observing the pressure drop (*ΔP/L*) vs fluid velocity (*U*) graphs, it is noted that all curves follow an exponential trend. It can be displayed as Equation 2-89.

$$\frac{\Delta P}{L} = \Upsilon \cdot U^{\theta} \qquad \text{Equation 2-89}$$

Using Equation 2-89 as a basis where Υ is a function of volumetric configuration between different size mixtures, Υ is written using standard polynomial functions as shown in Table 2-8. Where the constants β and θ are regressed for each polynomial function to fit the specific particles.

2.4 Error Calculations

When conducting experimental work, the result's repeatability or coefficient of variation should be tested; this is done to verify the accuracy of the applied method and is calculated using Equation 2-90 (Everitt & Skrondal, 2010).

$$Repeatability\ (\%) = \frac{Standard\ deviation}{Mean}\ x\ 100$$ Equation 2-90

The absolute percentage difference is an indication of how accurate the modelled data is compared to the experimental data and is expressed in Equation 2-92 (Gonick & Smith, 1993).

$$Percentage\ differece_{ABS} = \frac{|\ Modelled\ value - Experimental\ value\ |}{Experimental\ value}\ x\ 100$$ Equation 2-91

The study made use of the relative percentage difference to determine the upper and lower differences using Equation 2-93 and was derived from Equation 2-92.

$$Percentage\ differece_{Rel} = \frac{Modelled\ value - Experimental\ value}{Experimental\ value}\ x\ 100$$ Equation 2-92

The average percentage difference can be calculated using Equation 2-94, as shown as an example in Table 2-9. This demonstrates a typical application of this generally accepted method to show the percentage difference and to make use of it in the field of particle mixtures.

$$Ave. percentage\ differece_{ABS} = \frac{Percentage\ differece_{ABS}}{Number\ of\ data\ points}$$ Equation 2-93

Table 2-9: Percentage difference example (Wong & Kwan, 2014).

Particle 2 volumetric interval	Particle 1 volumetric interval					
	0.0	0.2	0.4	0.6	0.8	1.0
0.0	0.0	-0.1	+0.9	+0.6	-0.3	-0.1
0.2	-0.2	0.0	-1.0	0.0	+0.5	
0.4	+0.3	+1.5	+0.1	+0.8		
0.6	-0.9	-0.6	-0.6			
0.8	0.0	+0.4				
1.0	+0.1					
The average percentage difference is +0.07%						

The root mean square error (RMSE) is a measurement of how concentrated the data is around the best-fitting line between modelled and experimental data; thus a lower RMSE indicates a better fit to the model (Kenney, 1939; Liu *et al.*, 2020).

$$RMSE = \sqrt{\frac{\sum(\ Modelled\ value - Experimental\ value\ )^2}{Number\ of\ data\ points}}$$ Equation 2-94

The squared correlation or R^2 is a measurement of how well the data fits the model and can be calculated using Equation 2-96; the closer the value is to 1, the better the fit of the model to experimental values is (Gonick & Smith, 1993).

$$R^2 = 1 - \frac{\sum(\mathit{Modelled\ value} - \mathit{Experimental\ value}\ )^2}{\sum(\mathit{Experimental\ value} - \mathit{Mean\ experimental\ value})^2} \quad \textbf{Equation 2-95}$$

CHAPTER 3 RESEARCH METHODOLOGY

The methodology chapter entails the materials used, sample preparation applied, and the experimental setup used for the study.

3.1 Particle preparation

Coke particles obtained from ArcelorMittal are crushed with a jaw crusher and sieved Figure 3-1 into size ranges displayed below. As schematically shown in Figure 3-2, a Y-mixer was used to mix the binary and ternary mixtures effectively.

- -13.20 + 11.20 mm
- -11.20 + 9.50 mm
- -9.50 + 6.70 mm
- -6.70 + 4.75 mm
- -4.75 + 2.36 mm

The cone and quarter method (ISO 18283:2022) were used when collecting samples for RhoVol and ImageJ analysis.

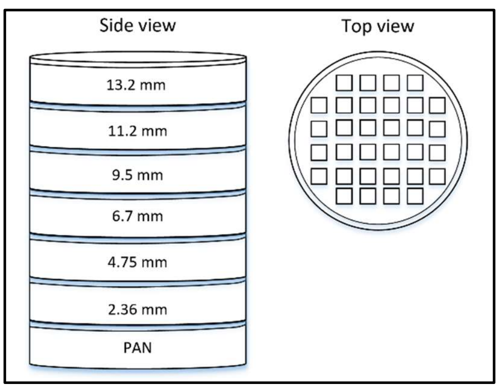

Figure 3-1: Sieves

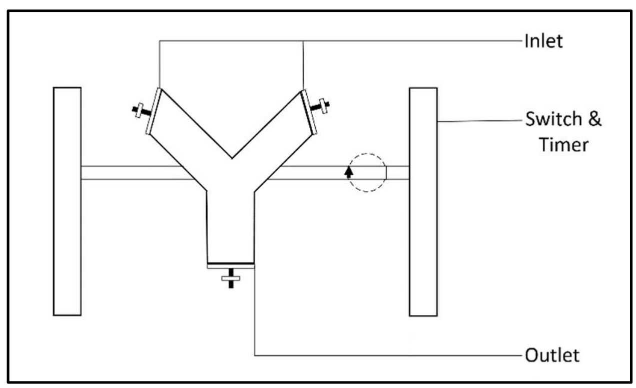

Figure 3-2: Mixer

3.1.1 Mixtures of particles used in the study

The following particle sizes were used to conduct the study:

1. -13.20 + 11.20 mm
2. -11.20 + 9.50 mm
3. -9.50 + 6.70 mm
4. -6.70 + 4.75 mm
5. -4.75 + 2.36 mm

Using the five size ranges above, mixtures were made for binary mixtures Table 3-1 and ternary mixtures Table 3-2 with 10% volume increments of each particle. Table 3-3 summarises the binary mixture compositions, and Table 3-4 the ternary mixture compositions.

Table 3-1: Binary mixture

Experiment	Size 1 (mm)	Size 2 (mm)
1	+2.36	+4.75
2	+2.36	+6.70
3	+2.36	+9.50
4	+2.36	+11.20
5	+4.75	+6.70
6	+4.75	+9.50
7	+4.75	+11.20
8	+6.70	+9.50
9	+6.70	+11.20
10	+9.50	+11.20

Table 3-2: Ternary mixtures

Experiment	Size 1(mm)	Size 2(mm)	Size 3(mm)
1	+2.36	+4.75	+6.70
2	+2.36	+4.75	+11.20
3	+2.36	+4.75	+9.50
4	+2.36	+6.70	+11.20
5	+2.36	+6.70	+9.50
6	+2.36	+9.50	+11.20
7	+4.75	+6.70	+11.20
8	+4.75	+6.70	+9.50
9	+4.75	+9.50	+11.20
10	+6.70	+9.50	+11.20

Table 3-3: Binary mixture volume composition

	x_i (%)	x_j (%)
1	100	0
2	90	10
3	80	20
4	70	30
5	60	40
6	50	50
7	40	60
8	30	70
9	20	80
10	10	90
11	0	100

Table 3-4: Ternary mixture volume composition

	x_i (%)	x_j (%)	x_k (%)
1	80	10	10
2	70	20	10
3	70	10	20
4	60	30	10
5	60	20	20
6	60	10	30
7	50	40	10
8	50	30	20
⋮	⋮	⋮	⋮
94	10	20	70
95	10	10	80

3.2 Particle characterisation

3.2.1 RhoVol data

Two on-site RhoVol photogrammetry analysis instruments were used to collect the characteristics data on the coke particles. The analysis gave data on the minimum square sieve size and compactness of the particles displayed in Table 3-5 and Table 4-1, respectively, that will be further used in data analysis; a full analysis can be found in Annexure A. The Sauter mean particle size for binary and ternary coke mixtures was calculated using Equation 2-6 and the characteristic particle data given in Table 3-5.

Table 3-5: RhoVol particle characteristic data

Particle size range	Minimum Square Sieve Size (mm)
-13.20 + 11.20 mm	11.230 ± 1
-11.20 + 9.50 mm	10.234 ± 0.7
-9.50 + 6.70 mm	7.262 ± 0.4
-6.70 + 4.75 mm	5.733 ± 0.6
-4.75 + 2.36 mm	3.579 ± 0.5

3.2.2 ImageJ data

Pictures of different coke size ranges were taken and analysed using ImageJ as shown in Figure 3-3. Using photogrammetry analysis in ImageJ the circularity could be obtained, as summarised in Table 4-1. A full analysis can be found in Annexure A.

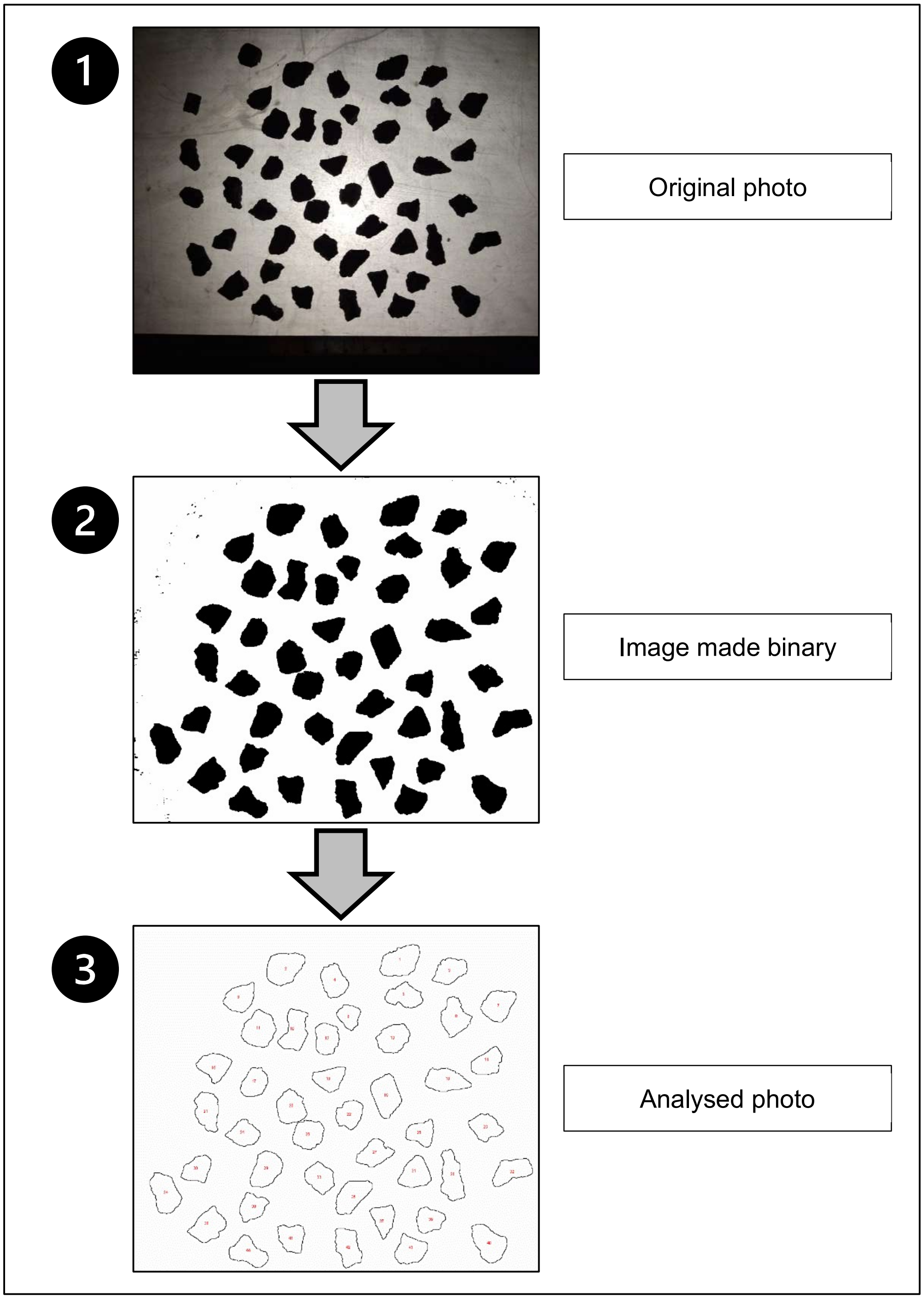

Figure 3-3: ImageJ photogrammetry analysis of -11.20 mm +9.50 mm

3.3 Bed voidage setup and operating procedure

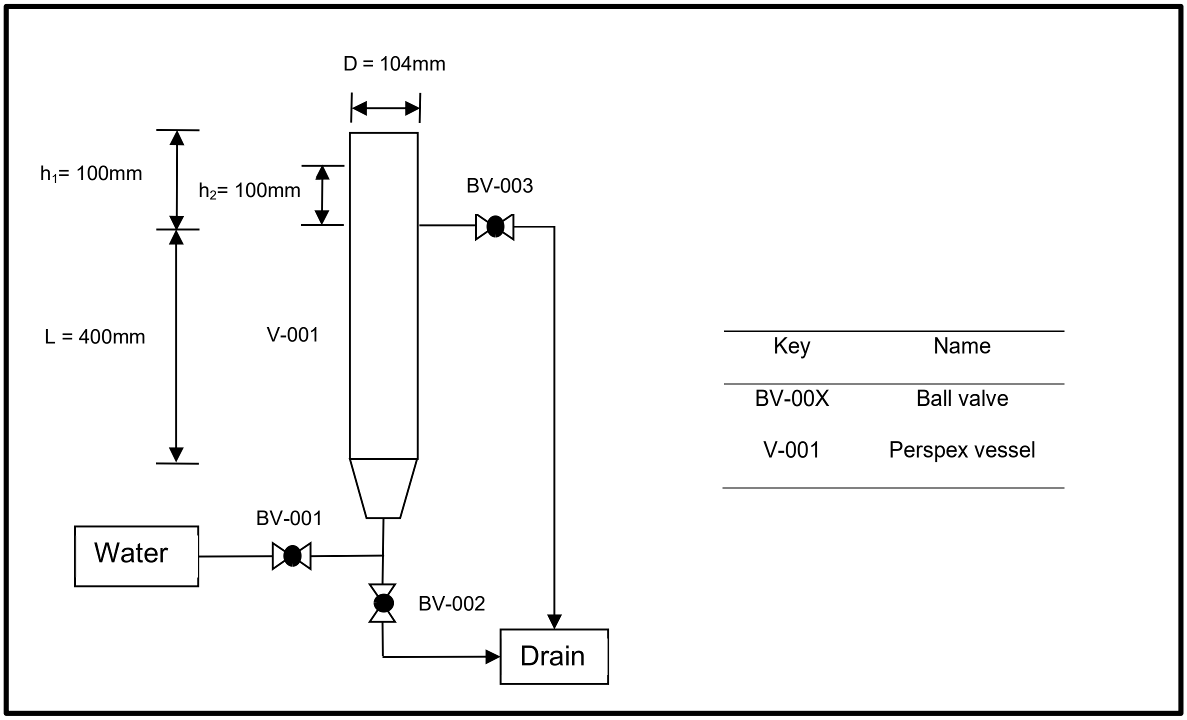

Figure 3-4: PFD of voidage setup

Water and particles are inserted into the pipe with a diameter (D) of 104mm, as seen in Figure 3-4; after 30 minutes, the particles would have absorbed the maximum amount of water, and excess water is drained until level with the particle bed height, (L = 400mm). The remaining particle bed water is emptied into a bucket and weighed using the laboratory balance. The water mass is used to calculate the bed voidage using Equation 3-1. The voidage tests are done for all the particle mixtures shown in Table 3-3 and Table 3-4.

$$\varepsilon_m = \frac{V_W}{V_C} = \frac{\left(M_W / \rho_W \right)}{\pi L \left(D/2 \right)^2} \qquad \text{Equation 3-1}$$

3.4 Pressure drop setup and operating procedure

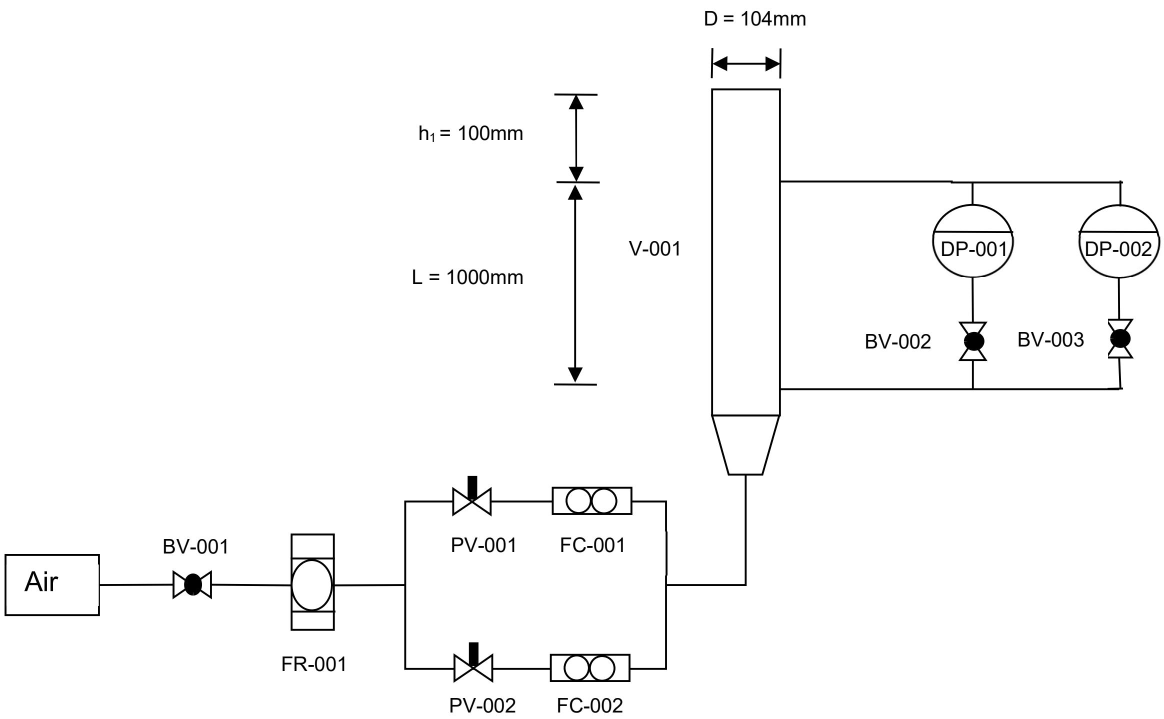

Key	Name	Description
BV-00X	Ball valve	
V-001	Perspex vessel	
FR-001	Filter regulator	40 μm Filtration size
PV-00X	Pin-needle valve	
FC-001	Flow meter	0-50 L/min
FC-002	Flow meter	0-200 L/min
DP-001	Differential pressure sensor	0-1000 Pa
DP-002	Differential pressure sensor	0-125 Pa

Figure 3-5: PFD of pressure drop setup

Compressed air flows through a ball valve (BV-001) to a filter and regulator (FR-001) to a split, as shown in Figure 3-5. The line is split and sent to two needle-pin valves, PV-001 and PV-002. The needle-pin valves are used to control the inlet flow of air; PV-001 goes to flow meter FC-001, and PV-002 goes to flow meter FC-002. The compressed air passes through the packed bed of particles with diameter D = 104 mm and bed height (L = 1000 mm). The differential pressure sensors DP-001 and DP-002 are connected to the packed bed and record the results. The compressed air is sent through at different flow rates (superficial velocities), and the differential pressure across the bed is measured. The voidage tests are done for binary particle mixtures with 20% volume increments and ternary mixtures with similar mean particle diameters and bed voids.

Following the bed voidage experiments, pressure drop experiments were conducted with the same coke mixtures as described in the bed voidage experiments. The pressure drop experiments were used to determine how the average particle size and how particle size distribution affect the pressure drop in a packed bed.

3.5 Data processing

After data collection is completed, it will be put into Excel for data regression and to be used with mathematical methods to produce results. Graphs will be constructed with the data to indicate any trends. Data will also be compared to previous studies. The focus is on the Ergun, relative pressure drop, and particle packing models. An updated model will be constructed from the data to describe better the pressure drop and voidage across a packed bed.

CHAPTER 4 RESULTS AND DISCUSSION

This chapter includes the results from using the materials, experimental setup, and models for voidage and pressure drop modelling across a packed bed of coke particles.

4.1 RhoVol vs ImageJ

Table 4-1 displays both the RhoVol and ImageJ shape factor for the coke particle size ranges. The data shows that both methods are usable and provide relatively similar trends in the results that sphericity increases as the particle size increases. The RhoVol data will subsequently be used further in the study using a 3D approach to determine sphericity.

Table 4-1: ImageJ vs RhoVol sphericity data

Particle size range	ImageJ circularity	RhoVol compactness	Relative difference (%)
-13.20 + 11.20 mm	0.712 ± 0.04	0.726 ± 0.08	1.93
-11.20 + 9.50 mm	0.724 ± 0.06	0.739 ± 0.08	2.03
-9.50 + 6.70 mm	0.723 ± 0.07	0.744 ± 0.08	2.82
-6.70 + 4.75 mm	0.707 ± 0.09	0.727 ± 0.09	2.75
-4.75 + 2.36 mm	0.686 ± 0.1	0.680 ± 0.1	0.88

4.2 Bed voidage results

4.2.1 Mono-size bed voidage result

The bed voidage for every mono-size batch (single particle size range batch) is displayed in Table 4-2; the average repeatability percentage is ±2.11%. The experimental data follows a characteristic parabolic curve when voidage is plotted against average particle diameter, as seen in the literature of Yu *et al.* (1996) and Liu & Miao (2020). The results shown in Figure 4-1 indicate that the densest packing range is for the particle size range of (-9.50 + 6.70 mm) particles with a voidage of 0.448.

Table 4-2: Mono-size batch bed voidage results

Particle size range	d_{pAve}	D/d_p	Bed voidage
-13.20 + 11.20 mm	11.23 mm	9.26	0.484 ± 0.004
-11.20 + 9.50 mm	10.23 mm	10.2	0.471 ± 0.005
-9.50 + 6.70 mm	7.26 mm	14.3	0.448 ± 0.01
-6.70 + 4.75 mm	5.73 mm	18.2	0.474 ± 0.01
-4.75 + 2.36 mm	3.58 mm	29.1	0.515 ± 0.03

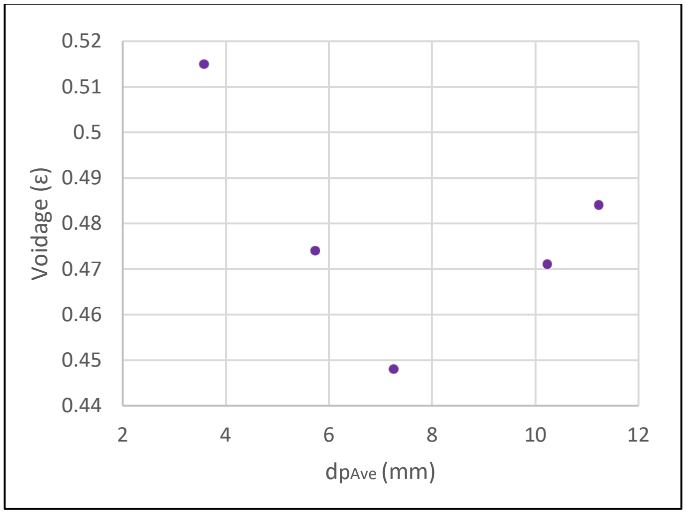

Figure 4-1: Average particle size diameter (d_{pAVE}) vs bed voidage for mono-size batches

4.2.2 Binary bed voidage result

The complete experimental analysis for binary coke mixtures, with an average repeatability percentage of ±2.11%, is displayed in Figure 4-2 to Figure 4-11, with the densest packing configuration for every binary mixture shown in Table 4-3. Not all experimental data follow the usual parabolic curve or v-curve, as in Yu *et al.* (1996) and Liu & Miao (2020). Some follow a more linear curve or an outlier breaking the v-curve. This can be due to narrow particle size distribution. The linear curve is dominant in the smaller size distributions, where the size ranges follow up on each other (sizes in the binary mixtures being similar, for example +2.36 mm and +4.75 mm) as in Figure 4-2, Figure 4-6, Figure 4-9, and Figure 4-11. When an outlier is present in the data, the overall curve follows the v-shape until the outlier disrupts this trend, as shown in Figure 4-8 and Figure 4-10.

Table 4-3 shows that the densest packing is between the largest and smallest particle sizes, also known as a large size distribution, such as the +2.36 mm and +11.20 mm binary mixture displayed in Figure 4-5. This is due to the small particles filling the voids between larger particles during packing, thereby decreasing the voids in the packed bed.

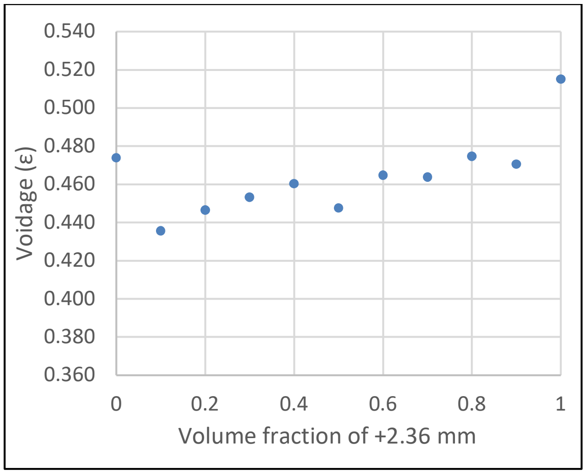

Figure 4-2: Voidage of +2.36 mm and +4.75 mm mixture

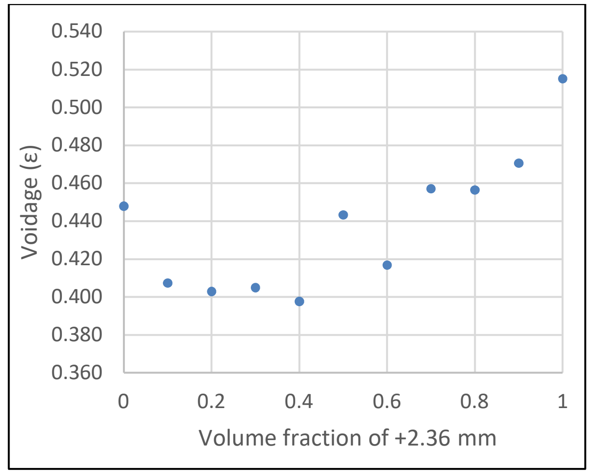

Figure 4-3: Voidage of +2.36 mm and +6.70 mm mixture

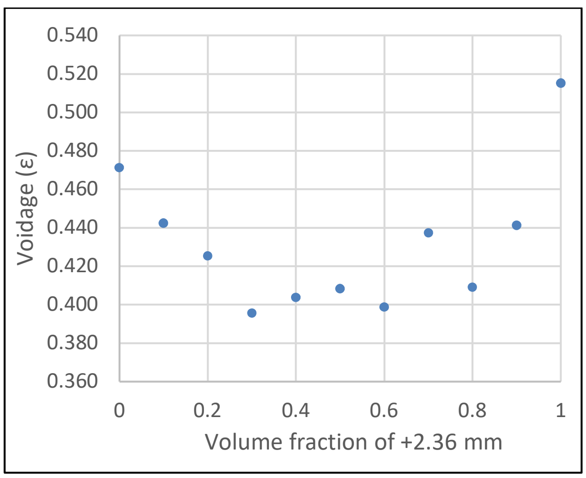

Figure 4-4: Voidage of +2.36 mm and +9.50 mm mixture

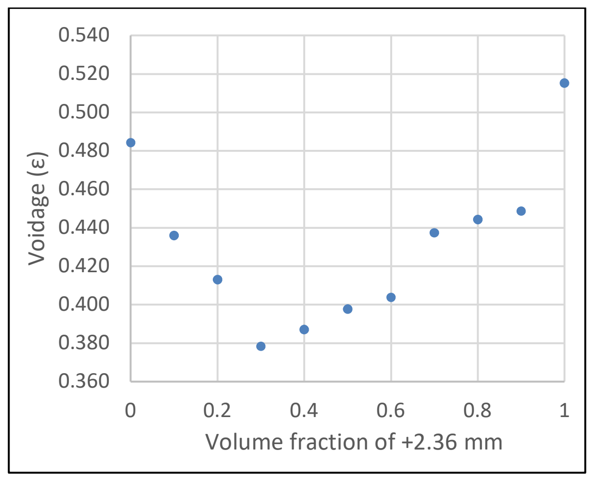

Figure 4-5: Voidage of +2.36 mm and +11.20 mm mixture

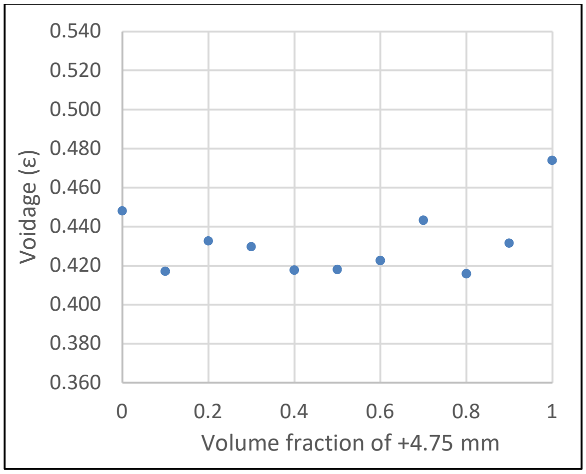

Figure 4-6: Voidage of +4.75 mm and +6.70 mm mixture

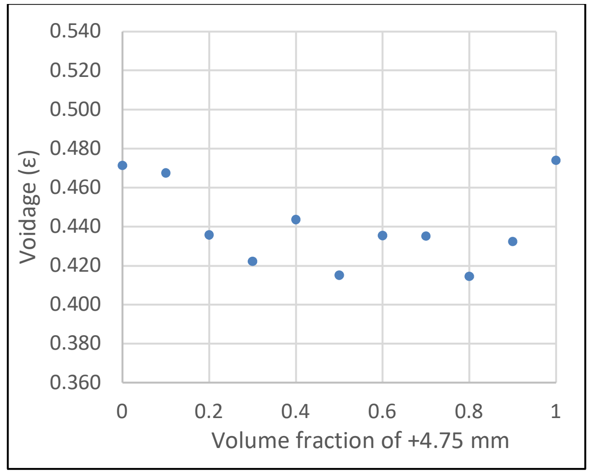

Figure 4-7: Voidage of +4.75 mm and +9.50 mm mixture

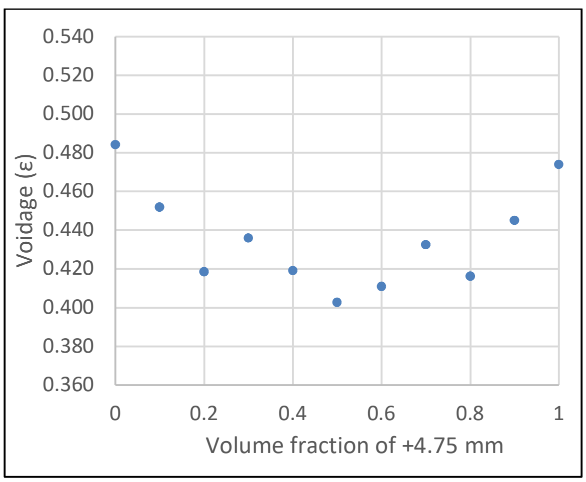

Figure 4-8: Voidage of +4.75 mm and +11.20 mm mixture

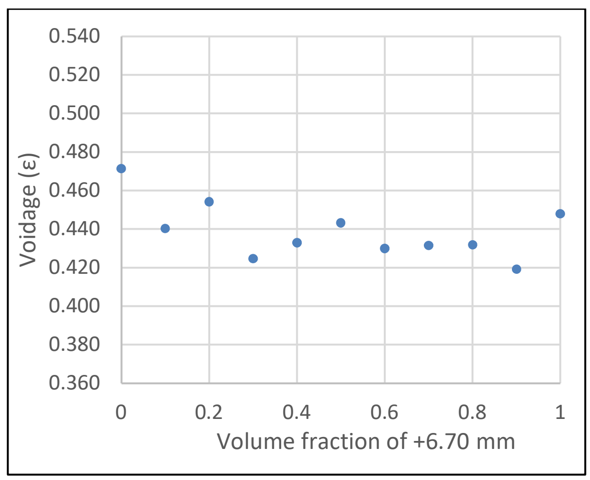

Figure 4-9: Voidage of +6.70 mm and +9.50 mm mixture

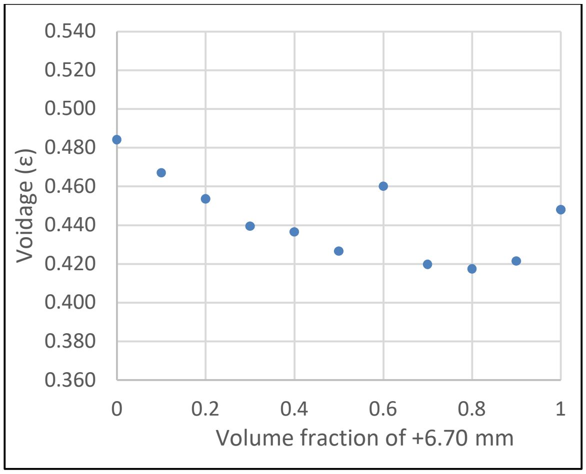

Figure 4-10: Voidage of +6.70 mm and +11.20 mm mixture

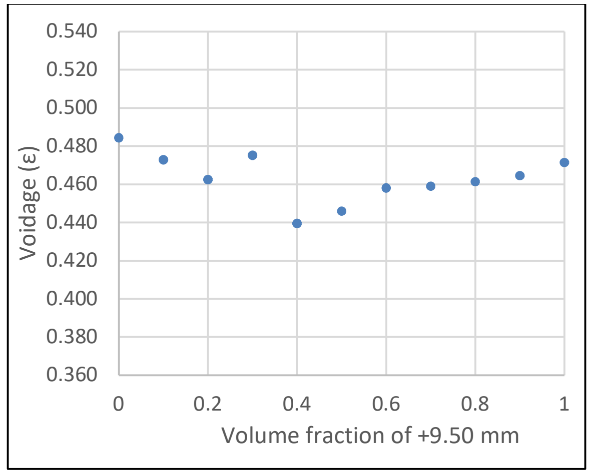

Figure 4-11: Voidage of +9.50 mm and +11.20 mm mixture

Table 4-3: Densest packing configuration for binary coke mixtures from experiments

d_i (mm)	x_i (%)	d_j (mm)	x_j (%)	Voidage (ε)
+2.36	0.1	+4.75	0.9	0.436
+2.36	0.4	+6.70	0.6	0.398
+2.36	0.3	+9.50	0.7	0.396
+2.36	0.3	+11.20	0.7	0.378
+4.75	0.8	+6.70	0.2	0.416
+4.75	0.8	+9.50	0.2	0.414
+4.75	0.5	+11.20	0.5	0.403
+6.70	0.9	+9.50	0.1	0.419
+6.70	0.8	+11.20	0.2	0.417
+9.50	0.4	+11.20	0.6	0.439

4.2.2.1 Binary bed voidage existing models

Table 4-4 displays how voidage models from literature fit the coke particles studied here. The three best-fitting models based on the lowest average percentage difference are the El-Husseiny, Westman, and Kwan models. The best-fitting model overall for the coke particles from the literature is the Kwan model, which has the largest R^2-value. However, it is not a satisfactory fit for the coke particles due to over-prediction.

Table 4-4: Binary voidage models from literature summary

Model	Model equation	Parity plot	Description	Ave. difference	Min. difference	Max. difference	R^2
Westman	Equation 2-28	Figure 4-12	Overprediction	4.9%	-3%	17%	0.694
El-Husseiny	Equation 2-34	Figure 4-13	Overprediction	5.0%	-3%	19%	0.581
Abbas	Equation 2-21	Figure 4-14	Underprediction	9.6%	-25%	5%	0.010
Toufar	Equation 2-39	Figure 4-15	Underprediction	7.6%	-26%	13%	0.413
Kwan	Equation 2-49	Figure 4-16	Overprediction	3.8%	-4%	14%	0.713

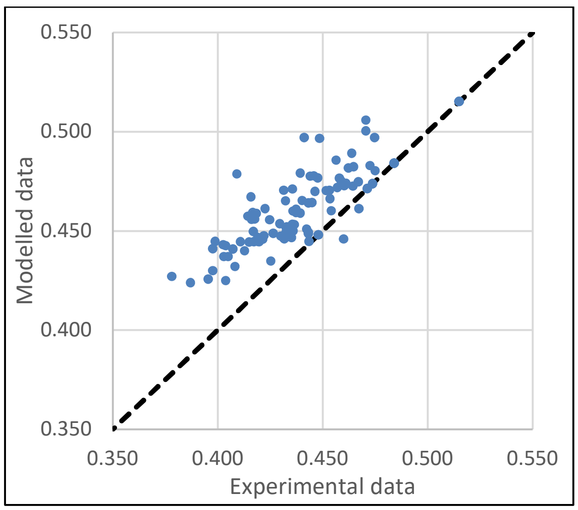

Figure 4-12: Parity plot of Westman model

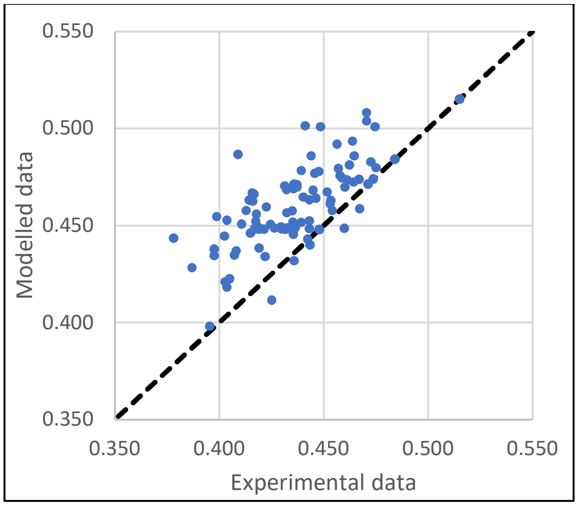

Figure 4-13: Parity plot of El-Husseiny model

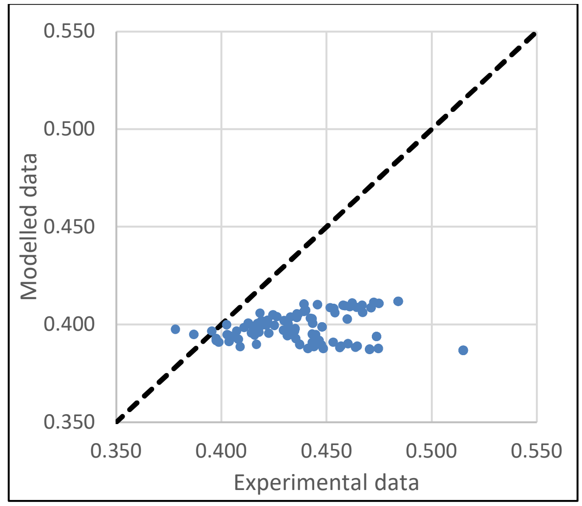

Figure 4-14: Parity plot of Abbas model

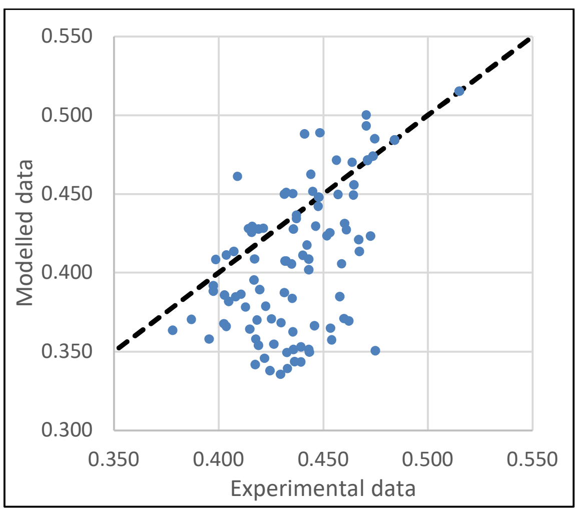

Figure 4-15: Parity plot of Toufar model

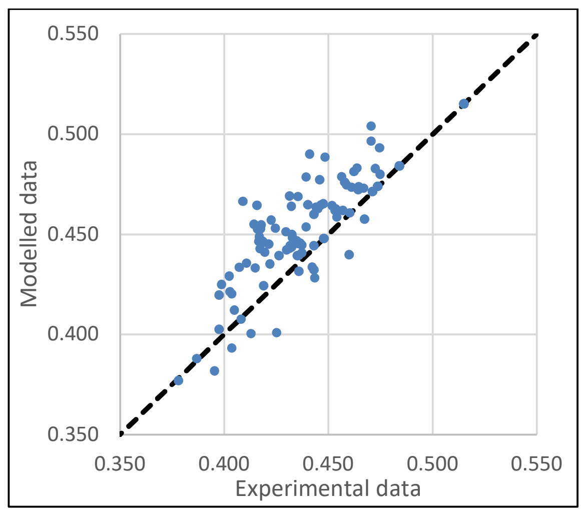

Figure 4-16: Parity plot of Kwan model

Figure 4-17 displays how the models in Table 4-4 compared to each other with a mixture of +2.36 mm and +11.20 mm coke particles. This size range was chosen on the basis that all the models predict this size range the best. It is prominent that the Kwan model is the best fitting, as discussed, compared to the other models. The bed voidage for volume fractions 0 and 1 are inputs to the models and are used as reference points for binary voidage model development as seen in the Toufar model (Equation 2-40); thus the model will predict the said volume fractions with 100% accuracy; compared to the Abbas model (Equation 2-21) not using these as inputs which leads to the low accuracy prediction.

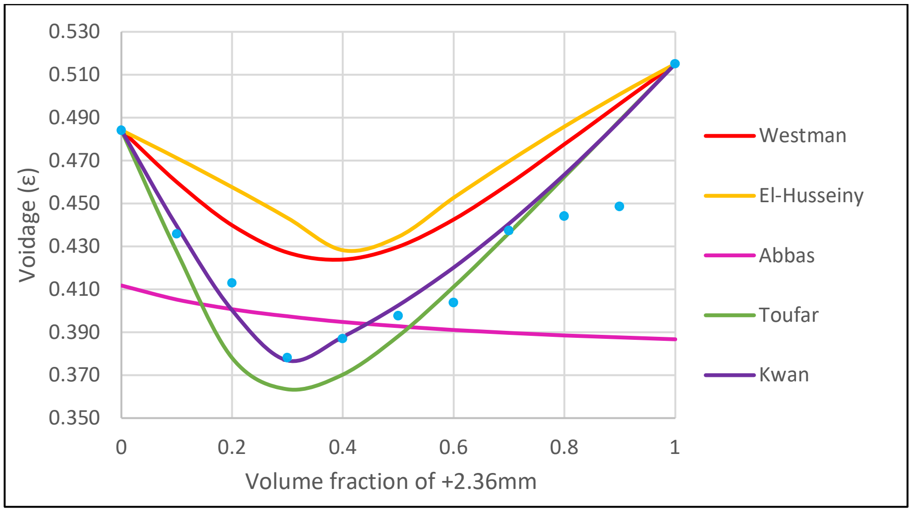

Figure 4-17: Comparing voidage models from literature for +2.36 mm and +11.20 mm mixture

4.2.2.2 Regressed binary voidage models from the literature

Table 4-5 displays the results obtained after regressing the models in Table 4-4 for the coke particles, with each model's parity plot presented in Annexure B. There is an overall improvement in all the models compared to the originals literature models, with the regressed Kwan model being the most suitable fit for the coke particles.

Table 4-5: Binary voidage regressed models summary

Model	Model equation	Parity plot	Description	Ave. difference	Min. difference	Max. difference	R^2
El-Husseiny	Equation 2-34	Figure 4-13	Mixed prediction	3.7%	-12%	17%	0.597
Abbas	Equation 2-21	Figure 4-14	Mixed prediction	5.0%	-17%	15%	0.000
Toufar	Equation 2-39	Figure 4-15	Mixed prediction	4.3%	-13%	17%	0.427
Kwan	Equation 2-49	Figure 4-16	Satisfactory	2.4%	-9%	9%	0.764

Below are the results of the original literature models compared to their regressed versions for bed voidage of binary coke mixtures with the worst-fitting binary mixture of the original literature model depicted by a graph (A) and the best-fitting binary mixture of the original literature model depicted by a graph (B).

4.2.2.2.1 El-Husseiny model

The original literature model and regressed El-Husseiny models still overpredict the worst-fitting size range, as seen in Figure 4-18 A. The regressed El-Husseiny model is an improvement over the original literature model, as seen in Figure 4-18 B.

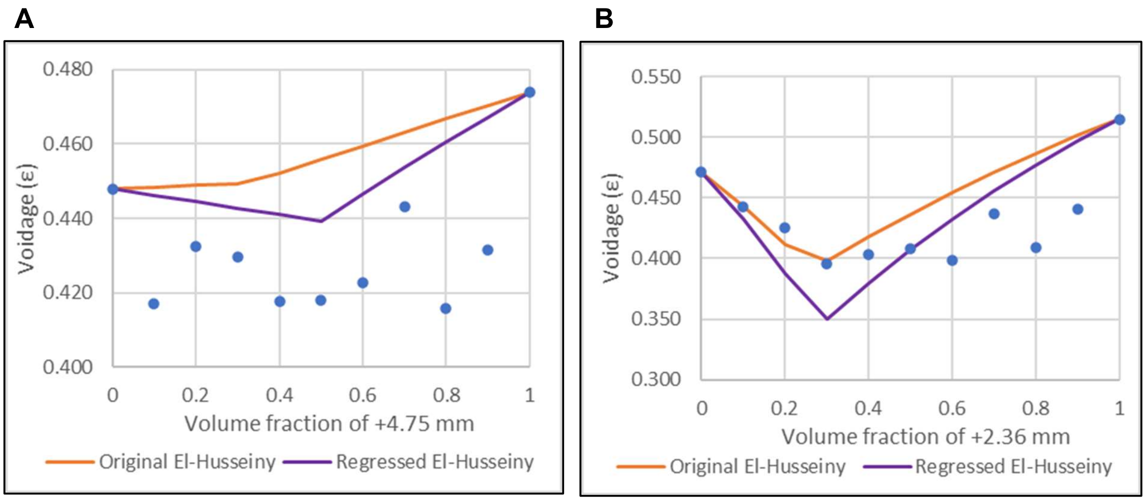

Figure 4-18: Voidage of El-Husseiny model for (A) +4.75 mm and +6.70 mm mixture, (B) +2.36 mm and +9.50 mm mixture

4.2.2.2.2 Abbas model

Both the original literature model and regressed Abbas models underpredict the coke particle binary mixtures, as seen in Figure 4-19 A and B, with the regressed Abbas model only lifting the original literature model to produce less of an underprediction.

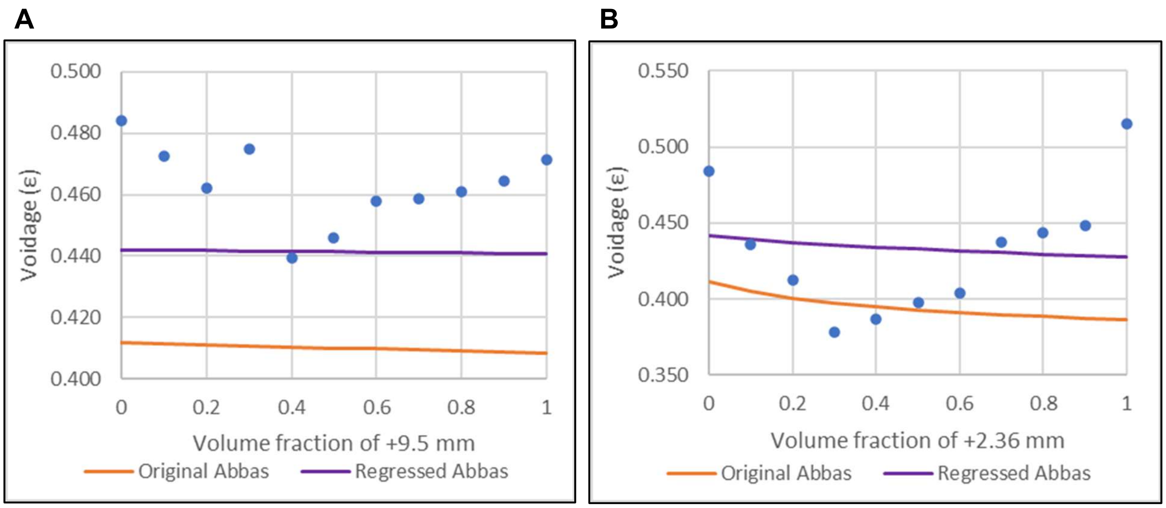

Figure 4-19: Voidage of Abbas model for (A) +9.50 mm and +11.20 mm mixture, (B) +2.36 mm and +11.20 mm mixture

4.2.2.2.3 Toufar model

The regressed Toufar model is an improvement from the original literature model in Figure 4-20 A but overpredicts in Figure 4-20 B, where the original literature Toufar model yielded a satisfactory fit for the coke particles.

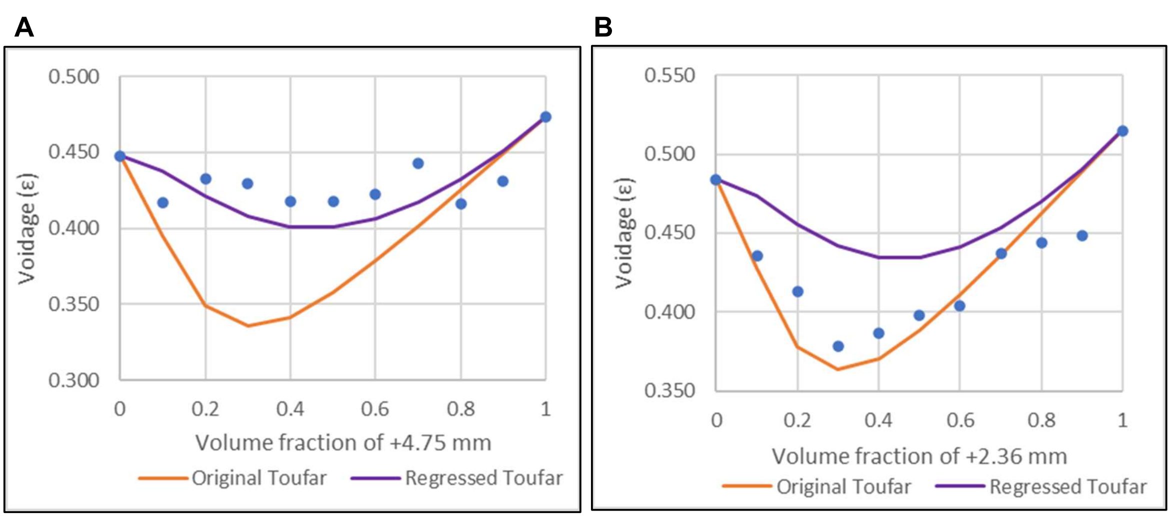

Figure 4-20: Toufar model voidage of (A) +4.75 mm and +6.70 mm mixture, (B) +2.36 mm and +11.20 mm mixture

4.2.2.2.4 Kwan model

The regressed Kwan model is a large improvement on the original literature model, as shown in Figure 4-22 A and B, representing both the best- and worst-fitting prediction of the original literature Kwan model.

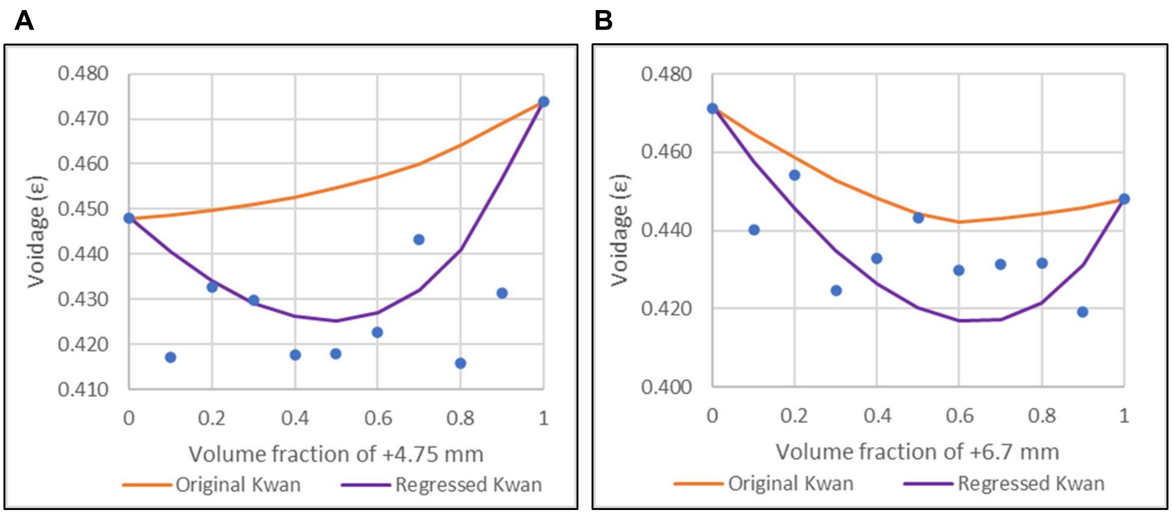

Figure 4-21: Kwan model voidage of (A) +4.75 mm and +6.70 mm mixture, (B) +6.7 mm and +9.50 mm mixture

4.2.2.3 Binary bed voidage improved model

Various packing models mentioned above were regressed for the coke particles but still yielded unsatisfactory fittings for the data. It was found that by regressing the original literature Kwan model parameters, the model can be improved to form the modified Kwan model; the original literature parameters (Equation 2-46 to Equation 2-48) were regressed for binary coke mixtures to obtain the new model parameters (Equation 4-4 to Equation 4-6). The difference in the models is prominent in the constants used, as highlighted in Table 4-6, and the average error percentages displayed in Table 4-7.

Table 4-6: Original literature Kwan equations vs modified Kwan equations

Model equation
Original literature Kwan model

$$\varepsilon_{m1}^* = (1+\varepsilon_i)\cdot x_i + (1+\varepsilon_j)\cdot x_j - (1-a_{KM})(1+\varepsilon_i)\cdot x_i\cdot(1-c_{KM}[3.8^{x_i}-1]) - 1 \quad \text{Equation 2-50}$$

$$\varepsilon_{m2}^* = (1+\varepsilon_i)\cdot x_i + (1+\varepsilon_j)\cdot x_j - (1-b_{KM})\cdot\varepsilon_j\cdot x_j\cdot(1-c_{KM}[2.6^{x_j}-1]) - 1 \quad \text{Equation 2-51}$$

$$\varepsilon_m = \max\{\varepsilon_{m1}^*, \varepsilon_{m2}^*\} \quad \text{Equation 2-52}$$

$$a_{KM} = 1-(1-s)^{5.0} - 1.9\cdot s\cdot(1-s)^{3.6} \quad \text{Equation 2-47}$$

$$b_{KM} = 1-(1-s)^{1.9} - 2.1\cdot s\cdot(1-s)^{10.5} - 0.2\cdot(1-s)^{7.6} \quad \text{Equation 2-48}$$

$$c_{KM} = 0.335\cdot\tanh(26.9\cdot s) \quad \text{Equation 2-49}$$

$$s = \frac{d_{p_i}}{d_{p_j}};\ i<j$$

Modified Kwan model

$$\varepsilon_{m1}^* = (1+\varepsilon_i)\cdot x_i + (1+\varepsilon_j)\cdot x_j - (1-a_{KM})(1+\varepsilon_i)\cdot x_i\cdot(1-c_{KM}[3.8^{x_i}-1]) - 1 \quad \text{Equation 4-1}$$

$$\varepsilon_{m2}^* = (1+\varepsilon_i)\cdot x_i + (1+\varepsilon_j)\cdot x_j - (1-b_{KM})\cdot\varepsilon_j\cdot x_j\cdot(1-c_{KM}[2.6^{x_j}-1]) - 1 \quad \text{Equation 4-2}$$

$$\varepsilon_m = \max\{\varepsilon_{m1}^*, \varepsilon_{m2}^*\} \quad \text{Equation 4-3}$$

$$a_{KM} = 1-(1-s)^{4.5} - 0.2\cdot s\cdot(1-s)^{0.6} \quad \text{Equation 4-4}$$

$$b_{KM} = 1-(1-s)^{0.7} - 2.1\cdot s\cdot(1-s)^{10.6} - 0.2\cdot(1-s)^{7.6} \quad \text{Equation 4-5}$$

$$c_{KM} = 0.356\cdot\tanh(27\cdot s) \quad \text{Equation 4-6}$$

$$s = \frac{d_{p_i}}{d_{p_j}};\ i<j$$

Table 4-7: Summary comparing original literature Kwan and modified Kwan model

Model	Description	Ave. difference	Min. difference	Max. difference	R^2
Original literature Kwan	Overprediction	3.8%	-4%	14%	0.713
Modified Kwan	Satisfactory	2.4%	-9%	9%	0.764

The parity plot of the modified Kwan model, Figure 4-22, shows a satisfactory correlation between the experimental and modelled values due to having a R^2-value of 0.764. The deviation between the experimental and predicted values is within a ±10% range, and the model thus has a satisfactory prediction outcome. The model-predicted compared to the experimental results are shown in Figure 4-23 to Figure 4-32. The densest packing averages between 0.5 and 0.6 volumetric percent of the smaller particle in the binary mixture can be observed for all the model-predicted results.

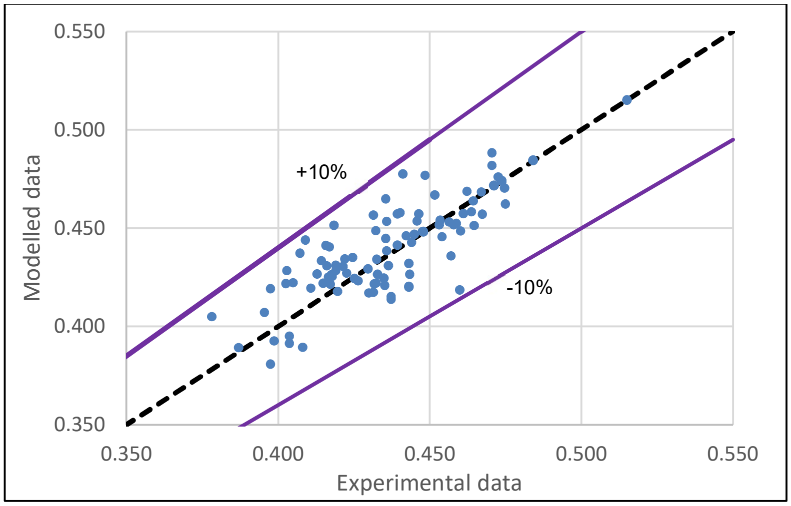

Figure 4-22: Parity plot of modified Kwan model

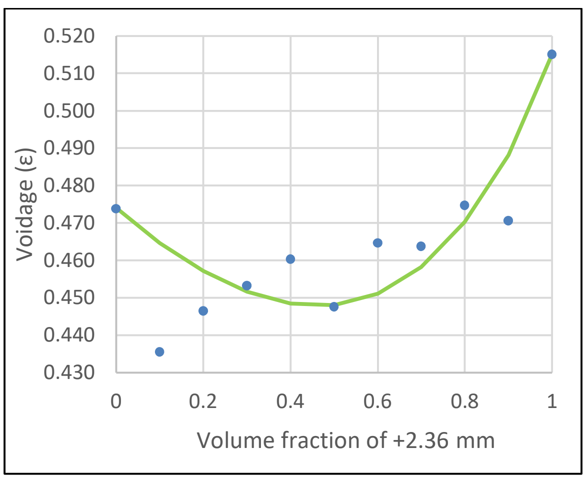

Figure 4-23: Modified Kwan model voidage of +2.36 mm and +4.75 mm mixture

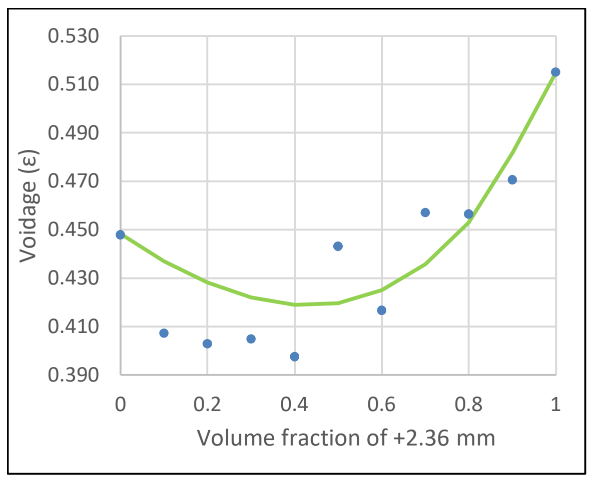

Figure 4-24: Modified Kwan model voidage of +2.36 mm and +6.70 mm mixture

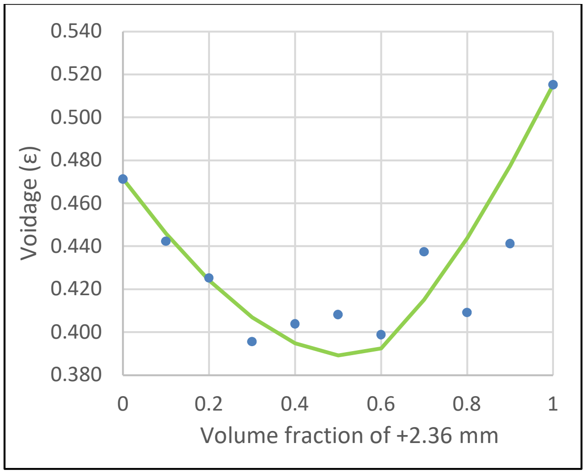

Figure 4-25: Modified Kwan model voidage of +2.36 mm and +9.50 mm mixture

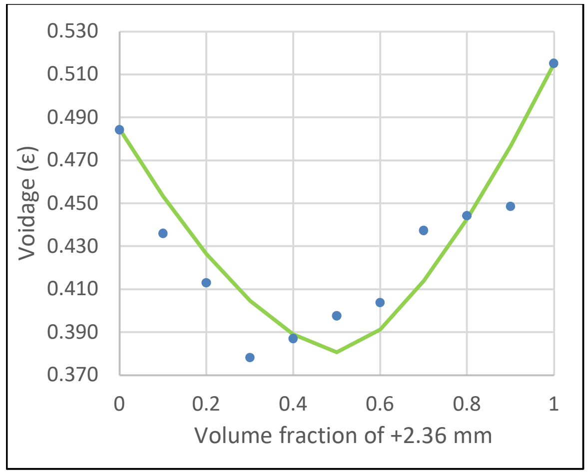

Figure 4-26: Modified Kwan model voidage of +2.36 mm and +11.20 mm mixture

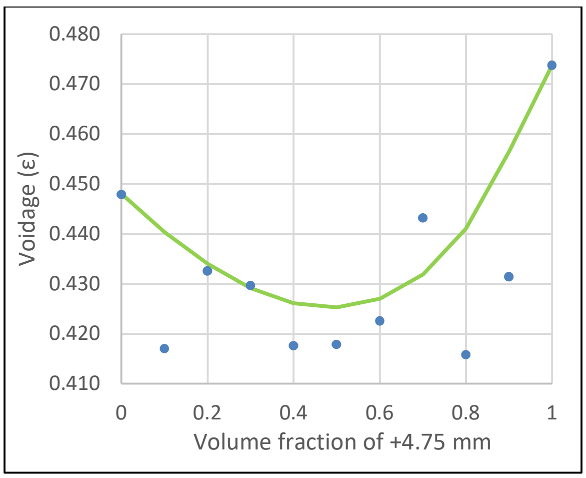

Figure 4-27: Modified Kwan model voidage of +4.75 mm and +6.70 mm mixture

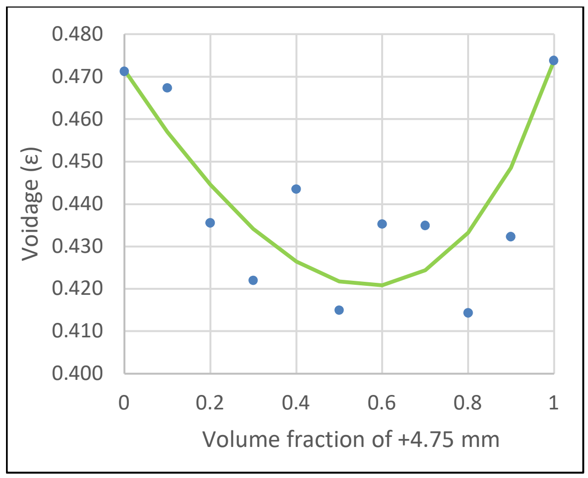

Figure 4-28: Modified Kwan model voidage of +4.75 mm and +9.50 mm mixture

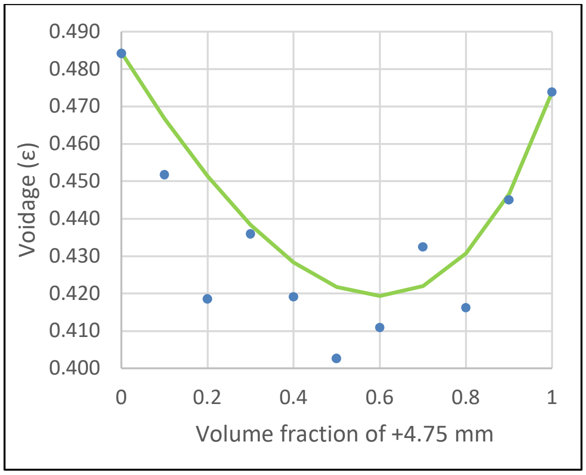

Figure 4-29: Modified Kwan model voidage of +4.75 mm and +11.20 mm mixture

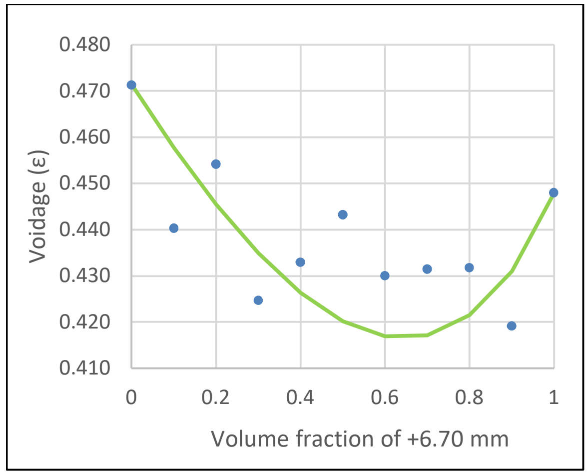

Figure 4-30: Modified Kwan model voidage of +6.70 mm and +9.50 mm mixture

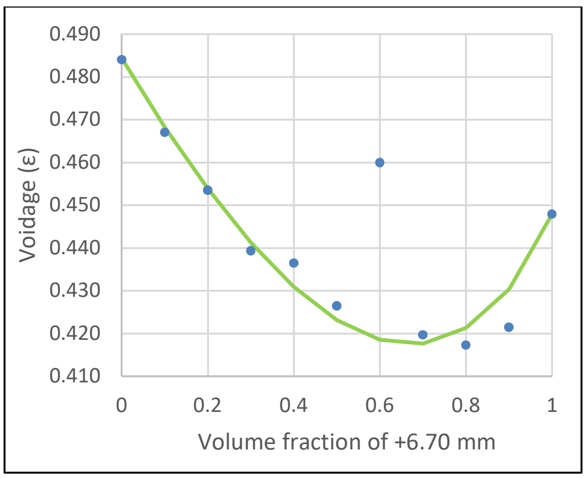

Figure 4-31: Modified Kwan model voidage of +6.70 mm and +11.20 mm mixture

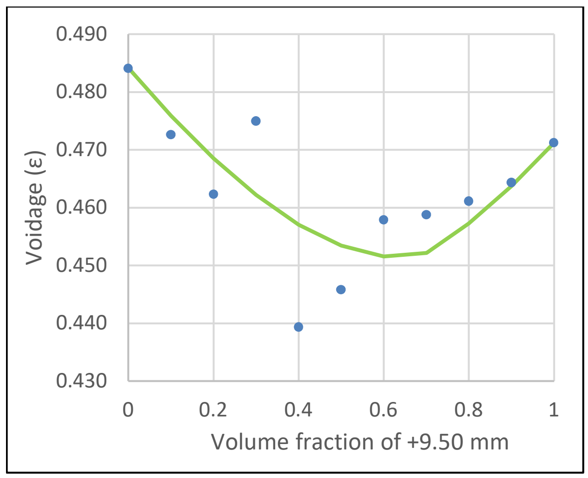

Figure 4-32: Modified Kwan model voidage of +9.50 mm and +11.20 mm mixture

The densest packing configuration modelled for every binary mixture is displayed in Table 4-8. This differs from the experimental data, which can be because of an experimental error (such as handling error, etc.) since the experimental data doesn't follow the usual parabolic curve or v-curve in some cases. If experimental errors are accounted for, the parabolic curve or v-curve would still be prominent in the experimental data. If the experimental error is accounted for, the experimental data and modelled data would have similar packing compositions for minimal voidage.

Table 4-8: Densest packing configuration for binary coke mixtures from modified Kwan model

d_i (mm)	x_i (%)	d_j (mm)	x_j (%)	Experimental voidage (ε_m)	Modelled voidage (ε_m)
+2.36	0.5	+4.75	0.5	0.448	0.448
+2.36	0.4	+6.70	0.6	0.398	0.419
+2.36	0.5	+9.50	0.5	0.408	0.390
+2.36	0.5	+11.20	0.5	0.398	0.381
+4.75	0.5	+6.70	0.5	0.418	0.426
+4.75	0.6	+9.50	0.4	0.435	0.421
+4.75	0.6	+11.20	0.4	0.411	0.420
+6.70	0.6	+9.50	0.4	0.430	0.417
+6.70	0.7	+11.20	0.3	0.420	0.418
+9.50	0.6	+11.20	0.4	0.458	0.452

The loosening effect parameters of the original literature Kwan model and the modified Kwan model follow the same trend as shown in Figure 4-33 A. For a diameter ratio $0 \leq s < 0.5$, the modified Kwan model has the largest loosening effect parameter, and for $0.5 < s \leq 1$, the original literature Kwan model has the largest. As the diameter ratio, *s* increases, the rate of the loosening effect for both models, it decreases first for the modified Kwan model, meaning as the size difference in a mixture between small and large particles increases the voidage increases by larger particles surrounding the smaller particles creating more voids that are unable to be filled by the smaller particles. The wall effect parameters of the original literature Kwan model and the modified Kwan model differ greatly, as shown in Figure 4-33 B, with the original literature Kwan model having the largest wall effect for any diameter ratio. As the diameter ratio, *s* increases, the rate of the wall effect decreases for the original literature Kwan model but increases for the modified Kwan model. This is due to smaller coke particles surrounding the larger coke particles forming small voids in the packed bed, and the coke particles being non-spherical and more porous than the quartz sand particles that were used in the original literature Kwan model. When the diameter ratio, *s,* is larger than 0.1, the wedging effect parameter stays constant for both models, displayed in Figure 4-33 C. The modified Kwan model has a slightly larger wedging effect parameter compared to the original literature Kwan model.

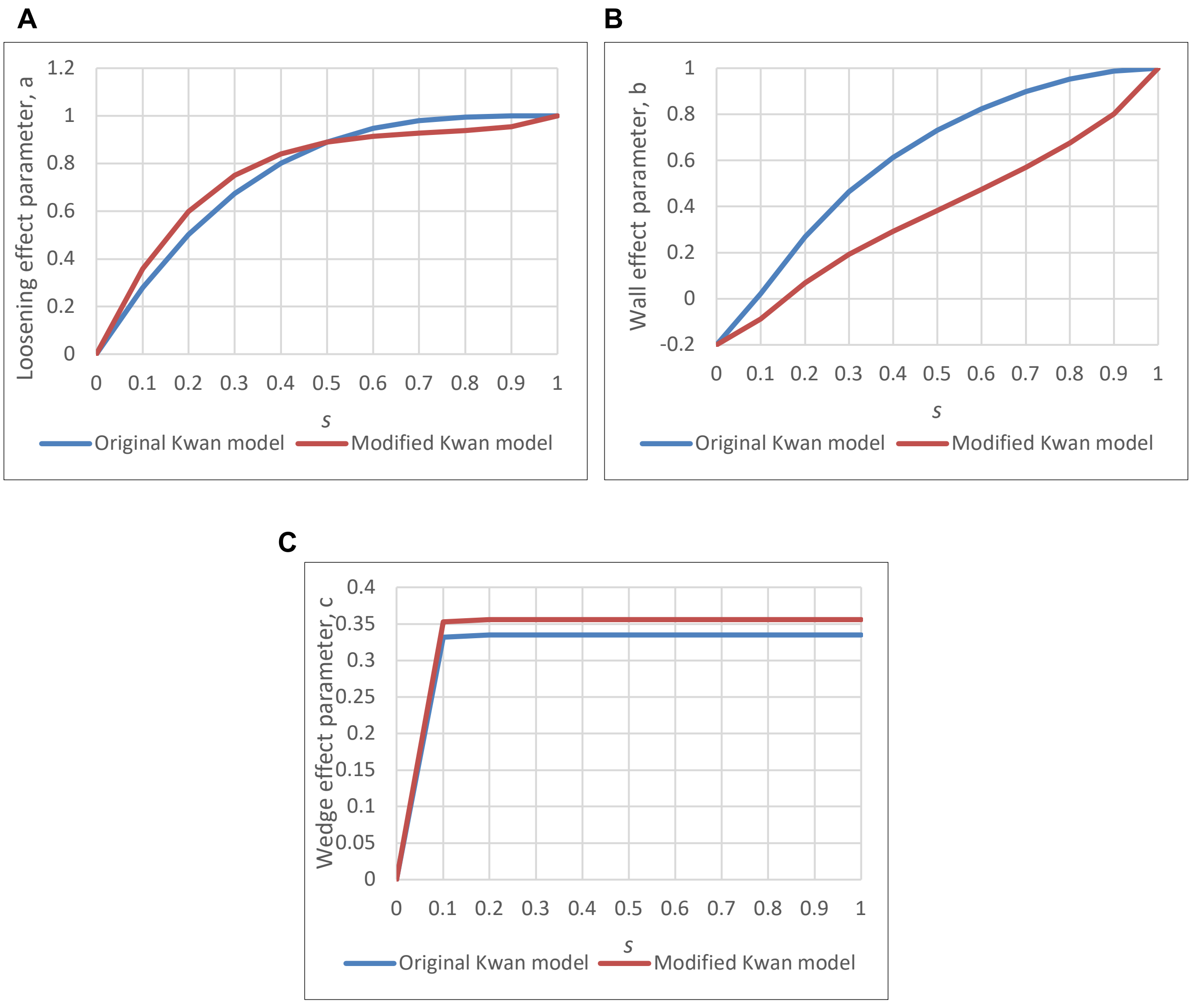

Figure 4-33: Packing effects between Original literature Kwan model and Modified Kwan model (A) loosening effect, (B) wall effect and (C) wedge effect

4.2.3 Ternary bed voidage results

The ternary plots were constructed using sample code found in MATLAB™ MathWorks (Sandrock & Afshari, 2016). Figure 4-34 to Figure 4-43 displays the voidage results of ternary coke mixtures as ternary diagrams, with contouring lines displaying different ternary mixtures in the same size range with the same voids. The densest packing configuration obtained for every ternary mixture from experimental results is displayed in Table 4-9 and indicated with a pink triangle, and the least compact configuration in Table 4-10 is indicated with a white triangle. During data acquisition, the average repeatability percentage is ±2.11%.

Table 4-9 shows that when two of the three particle ranges are close to each other (narrow particle distribution), one will dominate to fill the voids with the larger or smaller size range to create the densest packing. When a large or wide particle distribution is used, such as +4.75 mm, +6.70 mm and +11.20 mm mixture, it is observed that the densest packing is found when small particles fill the gap between medium and larger particles during packing.

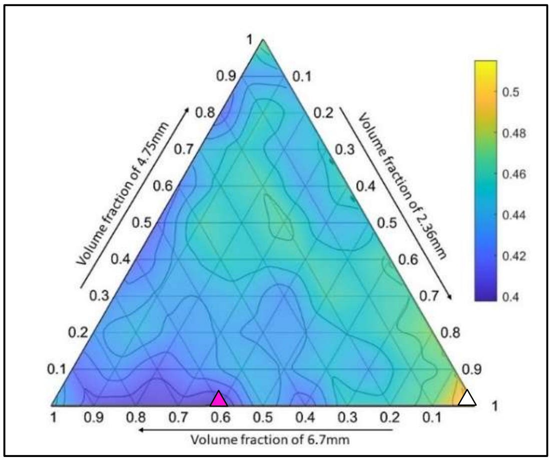

Figure 4-34: Voidage of +2.36 mm, +4.75 mm and +6.70 mm mixture

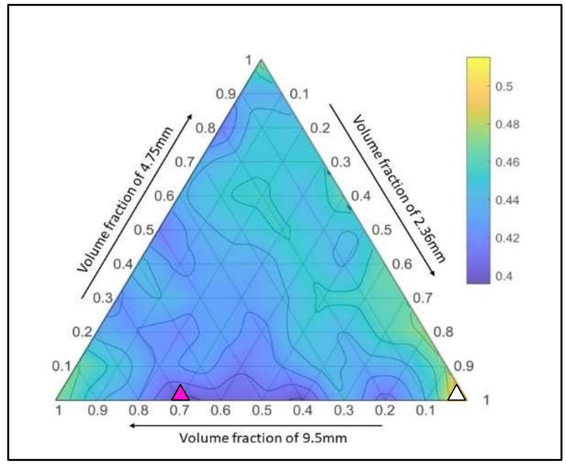

Figure 4-35: Voidage of +2.36 mm, +4.75 mm and +9.50 mm mixture

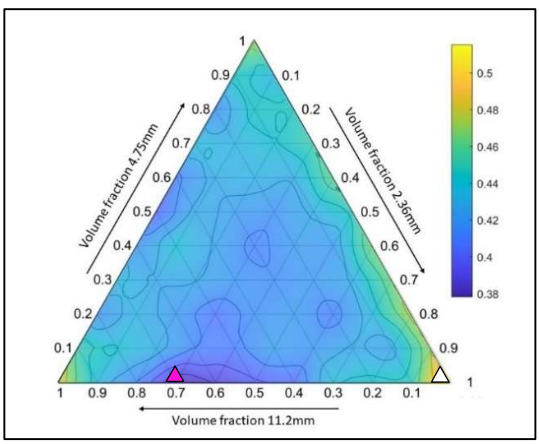

Figure 4-36: Voidage of +2.36 mm, +4.75 mm and +11.20 mm mixture

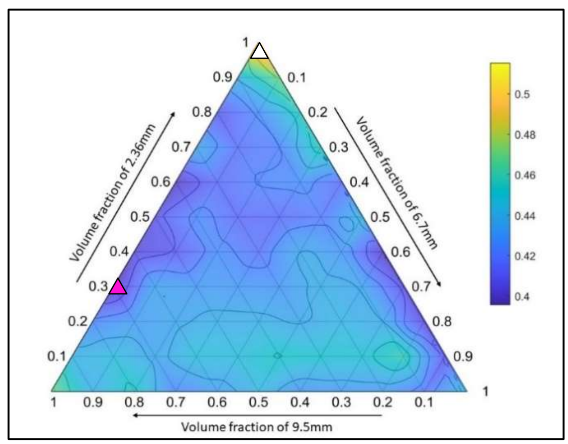

Figure 4-37: Voidage of +2.36 mm, +6.70 mm and +9.50 mm mixture

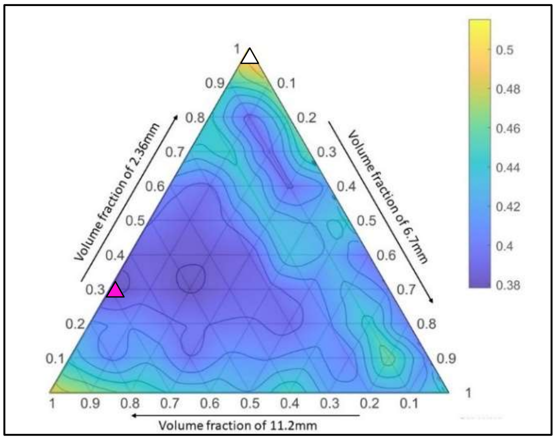

Figure 4-38: Voidage of +2.36 mm, +6.70 mm and +11.20 mm mixture

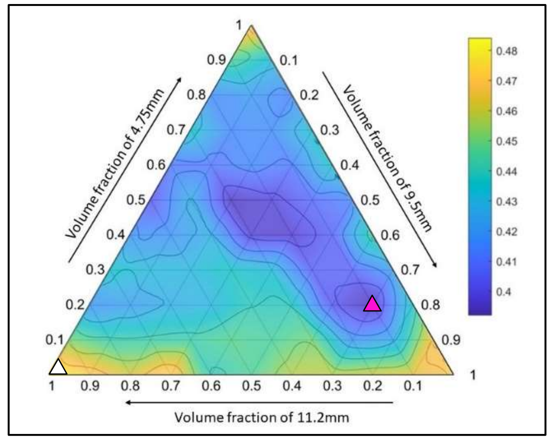

Figure 4-39: Voidage of +4.75 mm, +9.50 mm and +11.20 mm mixture

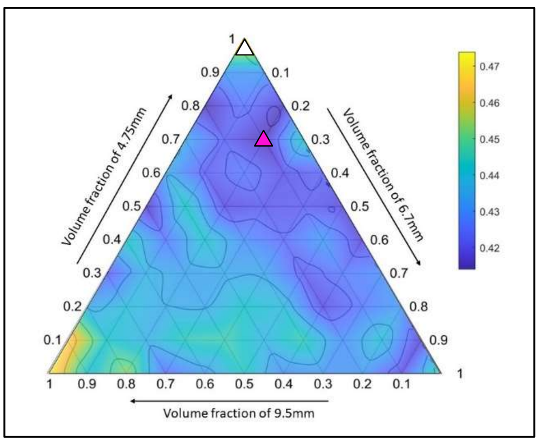

Figure 4-40: Voidage of +4.75 mm, +6.70 mm and +9.50 mm mixture

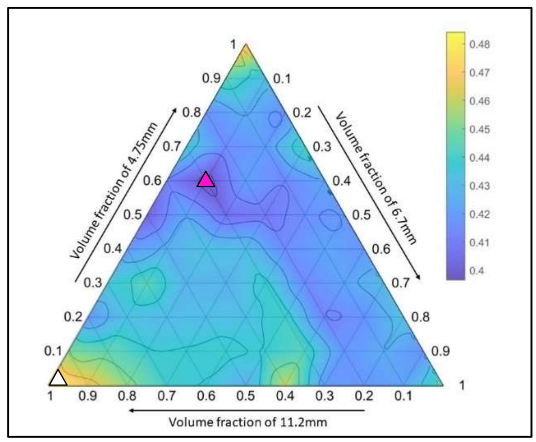

Figure 4-41: Voidage of +4.75 mm, +6.70 mm and +11.20 mm mixture

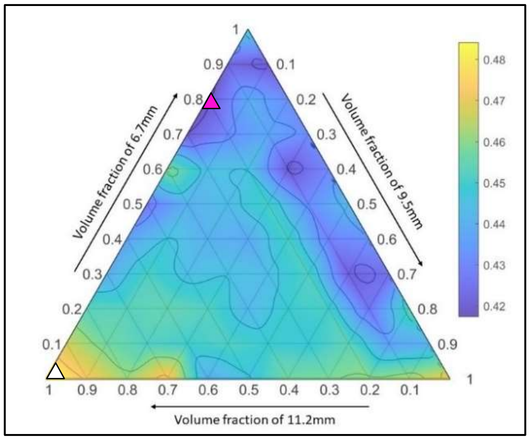

Figure 4-42: Voidage of +6.70 mm, +9.50 mm and +11.20 mm mixture

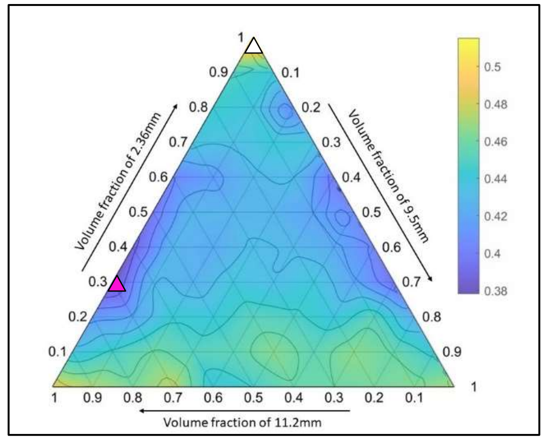

Figure 4-43: Voidage of +2.36 mm, +9.50 mm and +11.20 mm mixture

Table 4-9: Densest packing configuration for coke ternary mixtures

d_i (mm)	x_i (%)	d_j (mm)	x_j (%)	d_k (mm)	x_k (%)	Voidage (ε_m)
+2.36	0.4	+4.75	0	+6.70	0.6	0.398
+2.36	0.3	+4.75	0	+9.50	0.7	0.396
+2.36	0.3	+4.75	0	+11.2	0.7	0.378
+2.36	0.3	+6.70	0	+9.50	0.7	0.396
+2.36	0.3	+6.70	0	+11.20	0.7	0.378
+4.75	0.2	+9.50	0.7	+11.20	0.1	0.392
+4.75	0.7	+6.70	0.2	+9.50	0.1	0.414
+4.75	0.6	+6.70	0.1	+11.20	0.3	0.396
+6.70	0.8	+9.50	0	+11.20	0.2	0.417
+2.36	0.3	+9.50	0	+11.20	0.7	0.378

Table 4-10: Least compact packing configuration for coke ternary mixtures

d_i (mm)	x_i (%)	d_j (mm)	x_j (%)	d_k (mm)	x_k (%)	Voidage (ε_m)
+2.36	1	+4.75	0	+6.70	0	0.515
+2.36	1	+4.75	0	+9.50	0	0.515
+2.36	1	+4.75	0	+11.20	0	0.515
+2.36	1	+6.70	0	+9.50	0	0.515
+2.36	1	+6.70	0	+11.20	0	0.515
+4.75	0	+9.50	0	+11.20	1	0.484
+4.75	1	+6.70	0	+9.50	0	0.474
+4.75	0	+6.70	0	+11.20	1	0.484
+6.70	0	+9.50	0	+11.20	1	0.484
+2.36	1	+9.50	0	+11.20	0	0.515

4.2.3.1 Ternary bed voidage existing models

Voidage models to predict ternary mixtures from the literature will be discussed below and how these models will predict the voidage of coke particle mixtures with the particle size distribution as was discussed in Chapter 3.

Table 4-11 displays ternary voidage models' prediction capabilities of ternary mixtures of particles. The best-fitting model from the literature was the Simple Centroid Design model from Yu *et al.* (1987), with an average percentage difference of 11.5% and the highest R^2-value of 0.14, which, in essence, is not considered a good fit.

Table 4-11: Ternary voidage models from literature summary

Model	Model equation	Parity plot	Description	Ave. difference	Min. difference	Max. difference	R^2
Simple Centroid Design	Equation 2-52	Figure 4-44	Underprediction	11.5%	-26%	4%	0.140
D-optimal Design	Equation 2-56	Figure 4-45	Mixed prediction	29.2%	-74%	74%	0.037
Wong & Kwan	Equation 2-61	Figure 4-46	Overprediction	14.7%	-37%	-1%	0.049

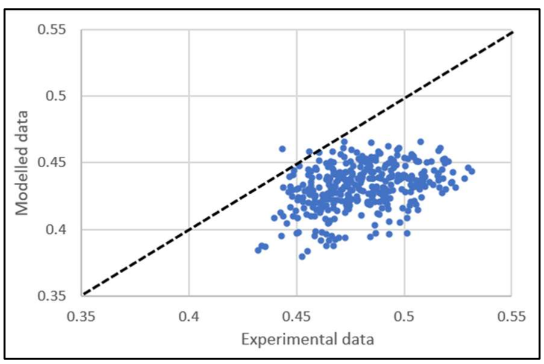

Figure 4-44: Parity plot of Simple Centroid Design

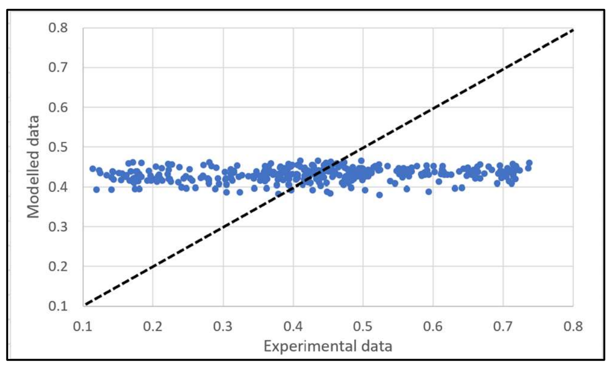

Figure 4-45: Parity plot of D-optimal Design

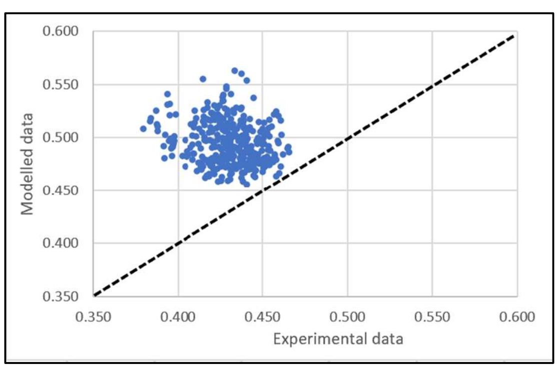

Figure 4-46: Parity plot of Wong & Kwan model

Table 4-12 displays the regressed bed voidage models for coke particle ternary mixtures using the models from literature found in Table 4-11, with each regressed model's parity plot available in Annexure B. All the regressed models showed improvement from the original literature models, but two models stood out; the regressed D-optimal Design model and the regressed Wong & Kwan model, with the D-optimal Design model being the best-fitting with an average difference of 2.3% and an R^2 value of 0.473.

Table 4-12: Regressed ternary voidage models from literature summary

Model	Model equation	Description	Ave. difference	Min. difference	Max. difference	R^2
Regressed Simple Centroid Design	Equation 2-52	Underprediction	7.2%	-19%	6%	0.229
Regressed D-optimal Design	Equation 2-56	Mixed prediction	2.3%	-12%	10%	0.473
Regressed Wong & Kwan	Equation 2-61	Mixed prediction	5.1%	-19%	16%	0.006

4.2.3.2 Regressed D-optimal Design model

Table 4-13 displays the change in constants to adapt the original literature model to the model regressed for the coke particles. The regressed D-optimal Design model has an average percentage difference of 2.3% compared to the original literature model, with an average percentage difference of 29.2%. The parity plot for the regressed model can be viewed in Figure 4-48; the deviation between the experimental and predicted values was within the ±10% range with minimal outliers; the model does not have a satisfactory prediction outcome due to a low R^2 value of 0.473.

Table 4-13: Original literature D-optimal Design model equations vs regressed D-optimal Design model equations

Model equation

Original literature Wong & Kwan model

$$\varepsilon_m = \sum_{i=1}^{3} \beta_{i\_DO} X_i + \sum_{i<j} \beta_{ij\_DO} X_i X_j + \sum_{i<j} v_{ij\_DO} X_i X_j (X_i - X_j) + \beta_{123\_DO} X_1 X_2 X_3 \quad \text{Equation 2-57}$$

$$\beta_{i\_DO} = \varepsilon_i \quad \text{Equation 2-58}$$

$$\beta_{ij\_DO} = \frac{\varepsilon_{ij} + \varepsilon_{ji} - (\varepsilon_i + \varepsilon_j)}{0.4032} \quad \text{Equation 2-59}$$

$$v_{ij\_DO} = \frac{\varepsilon_{ij} - \varepsilon_{ji} - 0.44(\varepsilon_i - \varepsilon_j)}{0.177408} \quad \text{Equation 2-60}$$

$$\beta_{123\_DO} = 27\varepsilon_{123} - \frac{3}{0.4032}(\varepsilon_{12} + \varepsilon_{13} + \varepsilon_{23} + \varepsilon_{21} + \varepsilon_{31} + \varepsilon_{32} - 2[\varepsilon_1 + \varepsilon_2 + \varepsilon_3]) - 9(\varepsilon_1 + \varepsilon_2 + \varepsilon_3) \quad \text{Equation 2-61}$$

$$i, j = 1, 2, 3; i < j$$

Modified Wong & Kwan model

$$\varepsilon_m = \sum_{i=1}^{3} \beta_{i\_DO} X_i + \sum_{i<j} \beta_{ij\_DO} X_i X_j + \sum_{i<j} \nu_{ij\_DO} X_i X_j (X_i - X_j) + \beta_{123\_DO} X_1 X_2 X_3 \quad \text{Equation 4-7}$$

$$\beta_{i\_DO} = \varepsilon_i \quad \text{Equation 4-8}$$

$$\beta_{ij\_DO} = \frac{\varepsilon_{ij} + \varepsilon_{ji} - (\varepsilon_i + \varepsilon_j)}{0.4131} \quad \text{Equation 4-9}$$

$$\nu_{ij\_DO} = \frac{\varepsilon_{ij} - \varepsilon_{ji} - 0.0017(\varepsilon_i - \varepsilon_j)}{0.373089} \quad \text{Equation 4-10}$$

$$\beta_{123\_DO} = 27.17\varepsilon_{123} - \frac{3.42}{0.4131}(\varepsilon_{12} + \varepsilon_{13} + \varepsilon_{23} + \varepsilon_{21} + \varepsilon_{31} + \varepsilon_{32} - 2.03[\varepsilon_1 + \varepsilon_2 + \varepsilon_3]) - 9.45(\varepsilon_1 + \varepsilon_2 + \varepsilon_3) \quad \text{Equation 4-11}$$

$$i, j = 1, 2, 3; i < j$$

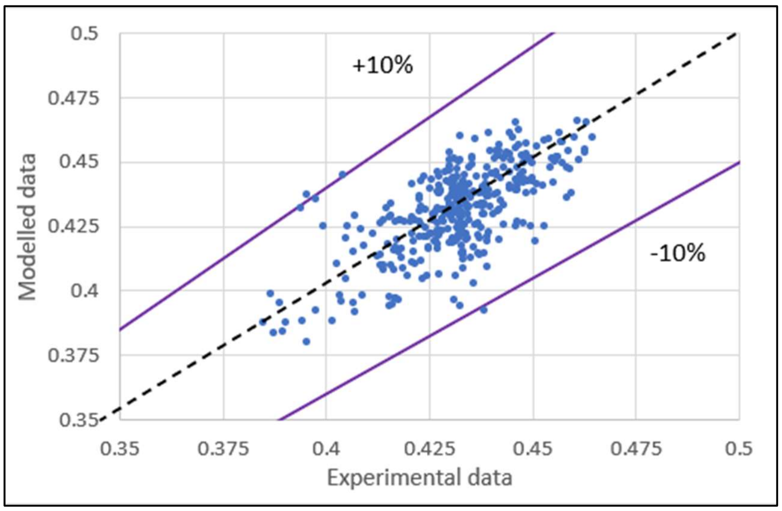

Figure 4-47: Parity plot of regressed D-optimal Design model

4.2.3.3 Ternary bed voidage improved Wong& Kwan model

The original literature Wong & Kwan model (Equation 2-61 to Equation 2-63) was regressed for ternary coke mixtures to obtain a new model called the modified Wong & Kwan model (Equation 4-12 to Equation 4-14). The constants equations (Equation 4-16 to Equation 4-18) were also regressed for coke particles and are highlighted in Table 4-14. The difference is further noticed in average error percentages and is shown in the parity plots of the two models.

The middle point voidage (ε_T), where there is a mixture of equal volume percentages of each size range, is calculated in the original literature Wong & Kwan model (Equation 2-68) on the basis that all particles are mono-sized, where the modified Wong Kwan model, the middle point voidage uses a reference point as seen in the Yu *et al.* (1987) models; as the coke particles are not mono-sized.

The modified Wong & Kwan model is an improvement from the original literature model and regressed model, as displayed in Table 4-15, with an average percentage difference of 2.9%.

Table 4-14: Original lieterature Wong & Kwan equations vs modified Wong & Kwan equations

Model equation	
Original literature Wong & Kwan model	
$\frac{1}{\varepsilon_{m1}^{*}} = \frac{1}{\varepsilon_T} - (1-b_{12})(1-\varepsilon_2)\left(\frac{x_2}{\varepsilon_2}\right)\left(1-c_{12}[2.6^{(x_2+x_3)}-1]\right) - (1-b_{13})(1-\varepsilon_3)\left(\frac{x_3}{\varepsilon_3}\right)\left(1-c_{13}[2.6^{(x_2+x_3)}-1]\right)$	Equation 2-62
$\frac{1}{\varepsilon_{m2}^{*}} = \frac{1}{\varepsilon_T} - (1-a_{12})\left(\frac{x_1}{\varepsilon_1}\right)(1-c_{12}[3.8^{x_1}-1]) - (1-b_{23})(1-\varepsilon_3)\left(\frac{x_3}{\varepsilon_3}\right)(1-c_{23}[2.6^{x_3}-1])$	Equation 2-63
$\frac{1}{\varepsilon_{m3}^{*}} = \frac{1}{\varepsilon_T} - (1-a_{13})\left(\frac{x_1}{\varepsilon_1}\right)(1-c_{13}[3.8^{x_1}-1]) - (1-a_{23})\left(\frac{x_2}{\varepsilon_2}\right)(1-c_{23}[3.8^{x_2}-1])$	Equation 2-64
$\varepsilon_m = \min\{\varepsilon_{m1}^{*}, \varepsilon_{m2}^{*}, \varepsilon_{m3}^{*}\}$	Equation 2-65
$a_{WK} = 1-(1-s)^{3.3} - 2.6 \cdot s \cdot (1-s)^{3.6}$	Equation 2-66
$b_{WK} = 1-(1-s)^{1.9} - 2 \cdot s \cdot (1-s)^{6}$	Equation 2-67
$c_{WK} = 0.322 \cdot \tanh(11.9 \cdot s)$	Equation 2-68
$\frac{1}{\varepsilon_T} = \frac{x_1}{\varepsilon_1} + \frac{x_2}{\varepsilon_2} + \frac{x_3}{\varepsilon_3};\ for\ mono-size\ particles$	Equation 2-69
$s = \frac{d_{p_i}}{d_{p_j}};\ i < j$	

Modified Wong & Kwan model	
$$\frac{1}{\varepsilon^*_{m1}} = \frac{1}{\varepsilon_T} - (1-b_{12})(1-\varepsilon_2)\left(\frac{x_2}{\varepsilon_2}\right)\left(1-c_{12}[1.6^{(x_2+x_3)}-1]\right) - (1-b_{13})(1-\varepsilon_3)\left(\frac{x_3}{\varepsilon_3}\right)\left(1-c_{13}[1.6^{(x_2+x_3)}-1]\right)$$	Equation 4-12
$$\frac{1}{\varepsilon^*_{m2}} = \frac{1}{\varepsilon_T} - (1-a_{12})\left(\frac{x_1}{\varepsilon_1}\right)(1-c_{12}[2.9^{x_1}-1]) - (1-b_{23})(1-\varepsilon_3)\left(\frac{x_3}{\varepsilon_3}\right)(1-c_{23}[1.6^{x_3}-1])$$	
$$\frac{1}{\varepsilon^*_{m3}} = \frac{1}{\varepsilon_T} - (1-a_{13})\left(\frac{x_1}{\varepsilon_1}\right)(1-c_{13}[2.9^{x_1}-1]) - (1-a_{23})\left(\frac{x_2}{\varepsilon_2}\right)(1-c_{23}[2.9^{x_2}-1])$$	Equation 4-13
$$\varepsilon_m = \min\{\varepsilon^*_{m1}, \varepsilon^*_{m2}, \varepsilon^*_{m3}\}$$	Equation 4-14
$$a_{WK} = 1-(1-s)^{4.7} - 1.6 \cdot s \cdot (1-s)^{6.1}$$	Equation 4-15
$$b_{WK} = 1-(1-s)^{2.7} - 2 \cdot s \cdot (1-s)^{6}$$	Equation 4-16
$$c_{WK} = 0.552 \cdot \tanh(14.1 \cdot s)$$	Equation 4-17
ε_T is given as a reference point below	Equation 4-18

x_1	x_2	x_3	Voidage
1/3	1/3	1/3	ε_T

$$s = \frac{d_{p_i}}{d_{p_j}};\ i < j$$

Table 4-15: Summary of the variations in the Wong & Kwan voidage model

Model	Description	Ave. difference	Min. difference	Max. difference	R^2
Original literature Wong & Kwan	Overprediction	17.70%	-37%	-1%	0.048
Regressed Wong & Kwan	Mixed prediction	5.1%	-19%	16%	0.006
Modified Wong & Kwan	Mixed prediction	2.9%	-12%	15%	0.268

The parity plot of the modified Wong-Kwan model, Figure 4-48, showed a mixed correlation between the experimental and modelled values for the bed voidage prediction of ternary mixtures. The modified Wong & Kwan model is not a satisfactory fit; although the deviation between the experimental and predicted values were within a ±10% range with minimal outliers, the R^2 value was too low.

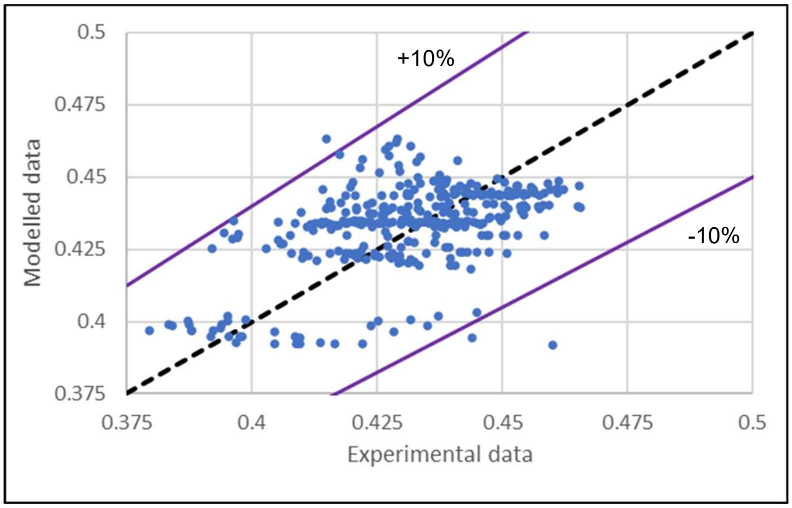

Figure 4-48: Parity plot of Modified Wong Kwan model

4.2.3.4 Best-fitting ternary voidage model for coke particles

Both the regressed D-optimal Design model and the modified Wong & Kwan model displayed low average percentage difference results to calculate the ternary voidage for coke particle systems, but the regressed D-optimal Design model was the best fitting. The regressed D-optimal Design model has the lowest average percentage difference and highest R^2 value, compared to the modified Wong & Kwan model with the second-best average percentage difference and second-highest R^2 value. The regressed D-optimal Design model was the best-fitting model for the coke particles; it does not predict the bed voidage of ternary coke mixtures to a satisfactory extent.

4.3 Pressure drop results

4.3.1 Mono-size particles pressure drop results

The pressure drop for each mono-size batch can be viewed in Figure 4-49; all the data follow the same exponential trend with an average repeatability percentage of 8.05%. The -4.75 + 2.36 mm size range has a higher pressure drop than the -13.20 + 11.20 mm size range; as the average particle diameter decreases, the pressure drop across the packed bed increases with similar findings found in Koekemoer (Koekemoer & Luckos, 2015).

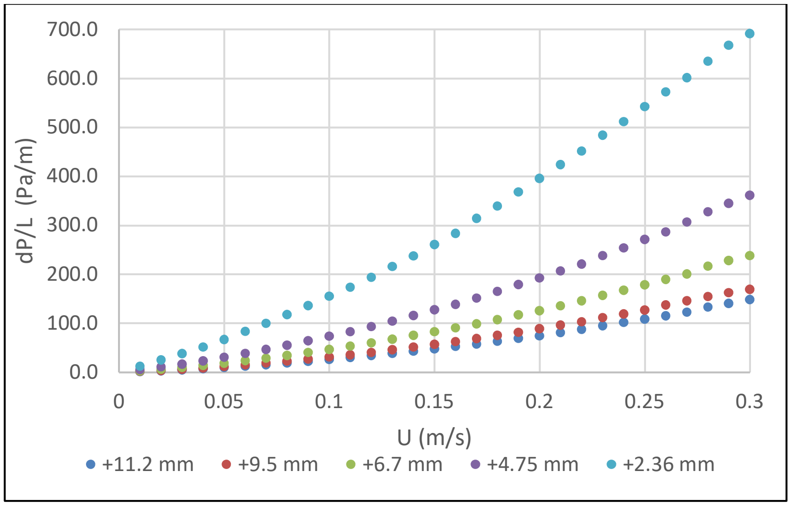

Figure 4-49: Mono-size batch pressure drop results

4.3.2 Binary mixtures pressure drop results

The pressure drop for each binary mixture can be viewed in Figure 4-50 to Figure 4-59. The pressure drop of binary mixtures follows the same exponential trend with an average repeatability percentage of 8.05%. The mono-size batch of the smaller particles has a higher pressure drop than the mono-size batch of larger particles, with similar findings found in Koekemoer (Koekemoer & Luckos, 2015).

There are some exceptions where the pressure drop of some binary mixtures is close to that of a mono-size batch. This is more relevant to particles with a close size range, such as the +9.50 mm and +11.20 mm mixture and +6.70 mm and +9.50 mm mixture, or with batches with a large size distribution, such as the +2.36 mm and +9.5 mm mixture and +4.75 mm and +11.20 mm mixture.

This is due to how the particles pack with each other and the voidage present in the packed bed. Similar-sized particles will stack to create larger voids than filling the gaps, and larger size distributions allow the smaller particles to fill gaps more easily, like how mono-size small particles stack together.

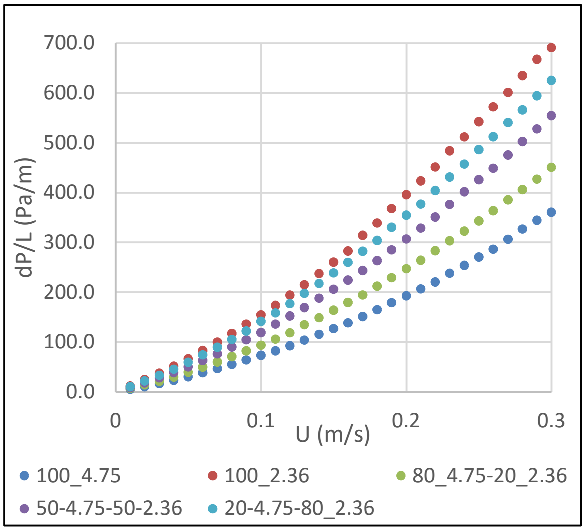

Figure 4-50: Pressure drop of +2.36 mm and +4.75 mm mixture

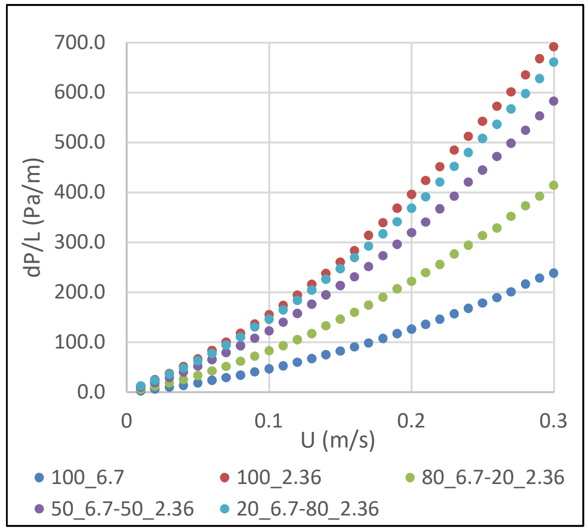

Figure 4-51: Pressure drop of +2.36 mm and +6.70 mm mixture

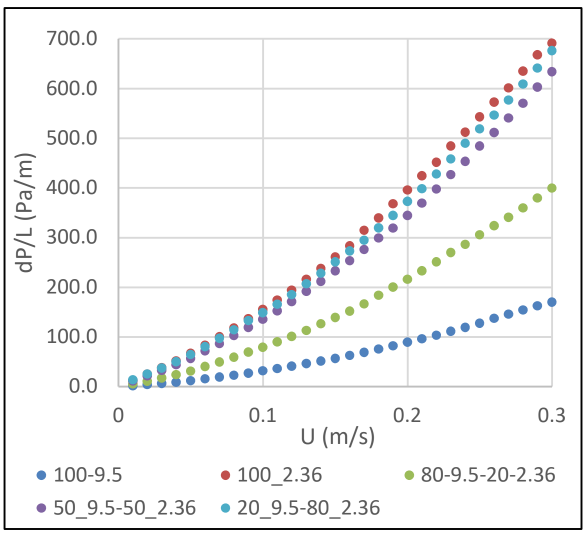

Figure 4-52: Pressure drop of +2.36 mm and +9.50 mm mixture

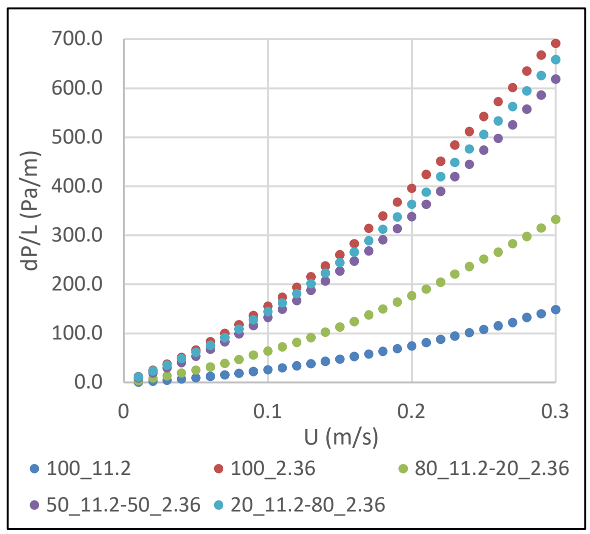

Figure 4-53: Pressure drop of +2.36 mm and +11.20 mm mixture

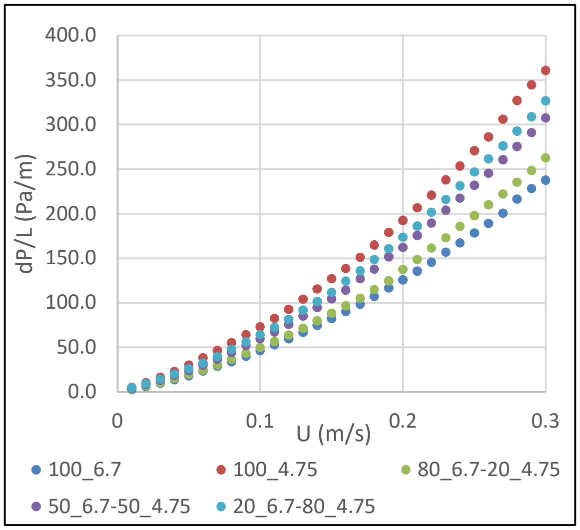

Figure 4-54: Pressure drop of +4.75 mm and +6.70 mm mixture

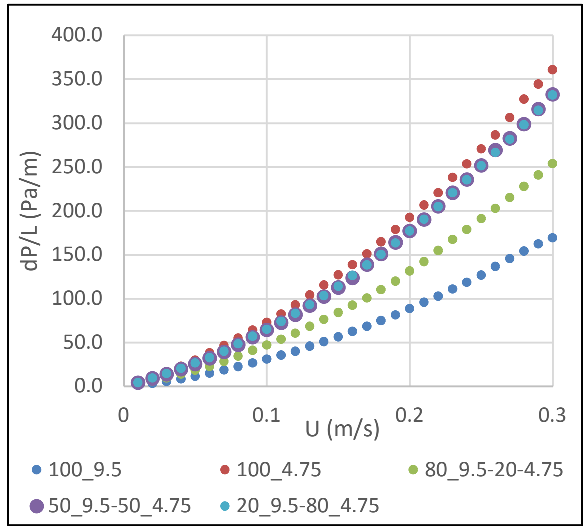

Figure 4-55: Pressure drop of +4.75 mm and +9.50 mm mixture

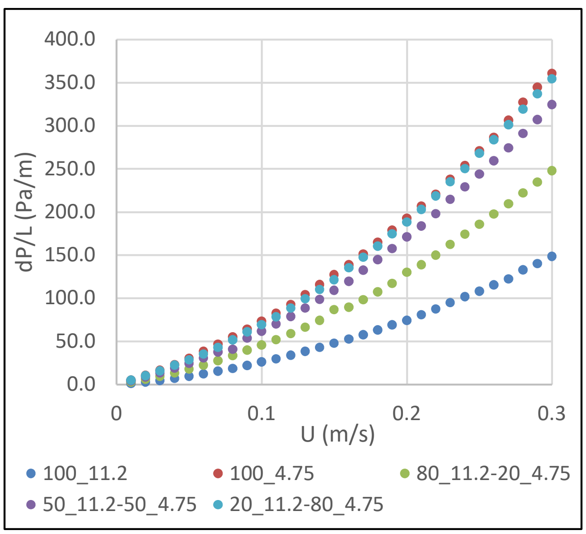

Figure 4-56: Pressure drop of +4.75 mm and +11.20 mm mixture

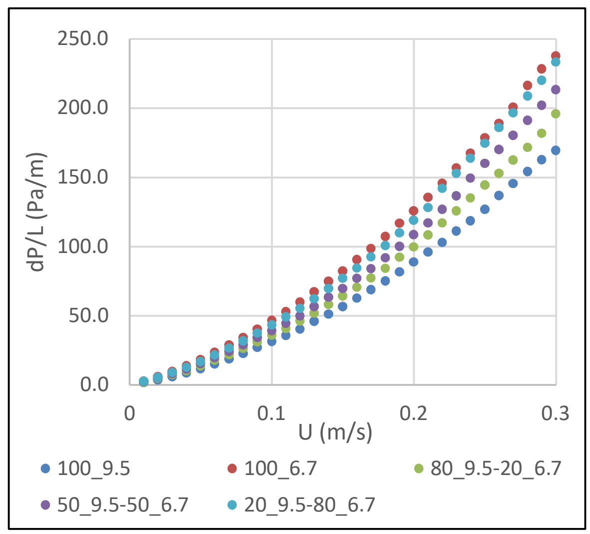

Figure 4-57: Pressure drop of +6.70 mm and +9.50 mm mixture

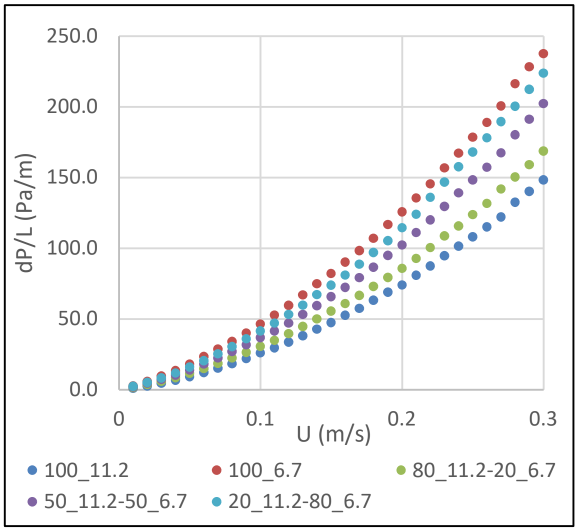

Figure 4-58: Pressure drop of +6.70 mm and +11.20 mm mixture

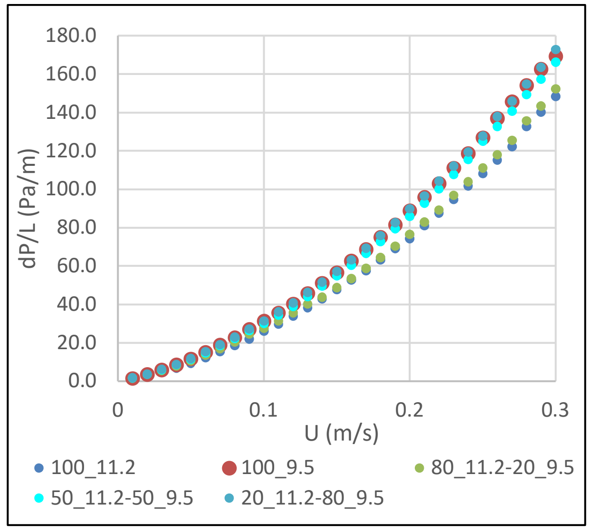

Figure 4-59: Pressure drop of +9.50 mm and +11.20 mm mixture

4.3.3 Ternary mixtures pressure drop results

4.3.3.1 Particle size effect on pressure drop in ternary mixtures with similar voidage

Figure 4-60 A and B display the pressure drop of different mixtures with a voidage of 0.438 but different mixture diameters. As the Sauter mean particle diameter of a mixture increases through #1 to #17, the pressure drop decreases. Some exceptions are visible, mixtures #13 to #17. This is due to how particles pack in different size distributions and how the flow is obstructed by the packing form in the bed, although the voidage is constant. From Figure 4-61 A and B, it can be observed that the packed bed mixture diameter influences pressure drop and is dependent on particle diameter.

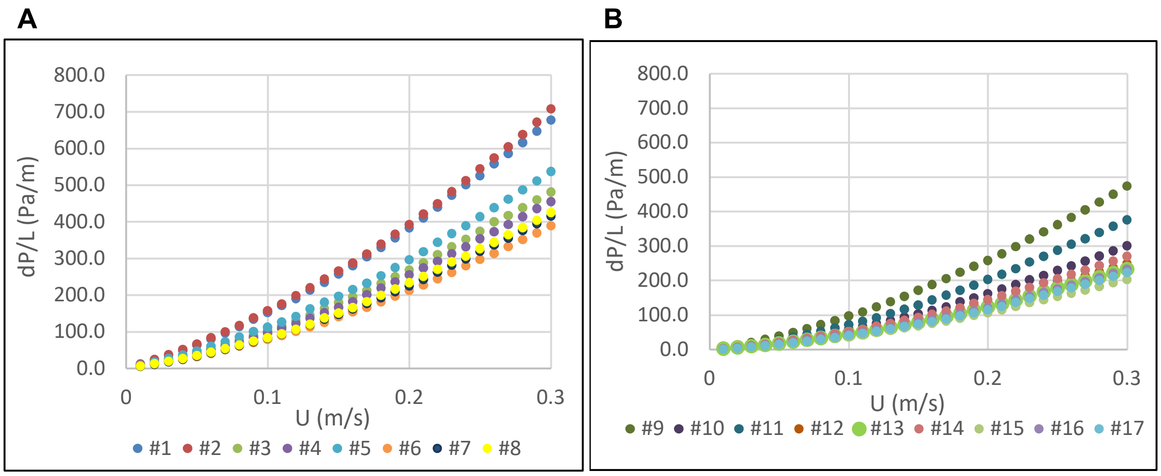

Mix	#1	#2	#3	#4	#5	#6	#7	#8	#9	#10	#11	#12	#13	#14	#15	#16	#17
dp_{SM} (mm)	3.99	4.14	4.94	5.33	5.37	6.14	6.18	6.51	6.87	7.58	7.68	8.00	8.07	8.40	9.20	9.26	9.77
+11.2	0	10	0	0	0	0	0	0	40	30	20	0	10	40	30	60	70
+9.50	10	10	0	0	20	0	10	30	30	0	60	40	20	0	30	0	0
+6.70	0	0	10	50	40	60	70	50	0	40	0	50	70	50	40	30	20
+4.75	10	0	60	20	0	30	0	0	0	30	0	10	0	10	0	10	10
+2.36	80	80	30	30	40	10	20	20	30	0	20	0	0	0	0	0	0

Figure 4-60: Pressure drop of volume percentage mixtures with voidage 0.438

4.3.3.2 Bed voidage effect on pressure drop in ternary mixtures with similar particle diameters

Figure 4-61 displays the pressure drop across packed beds with similar mean particle diameter (±4.5 mm) is plotted with varying voidage. The binary mixture #3 has the densest packing with a voidage of 0.417 and the largest mean diameter but does not have the highest pressure drop. This is due to how particles stack when compared to a ternary mixture where better stacking of particles can be observed. The difference between ternary #1 and #2 is the size distribution, with #1 having a wide size distribution (particle size ranges that are far apart) and #2 a narrow distribution (particle size ranges that are close to each other or follow up on each other), both having similar voidage and mean diameter. It is observed that #1 has a higher pressure drop across the packed bed. This is due to how relatively large, medium, and small particles stack and fill the gaps between each other compared to how particles with relatively close diameters can fill the gaps in a packed bed.

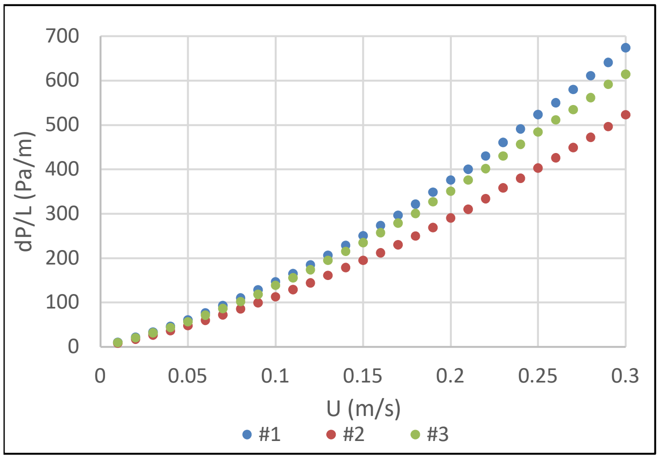

Mix	#1	#2	#3
Voidage	0.441	0.453	0.417
dp_{SM} (mm)	4.46	4.48	4.49
+11.20	0.1	0	0
+9.50	0.2	0	0
+6.70	0	0.1	0.4
+4.75	0	0.4	0
+2.36	0.7	0.5	0.6

Figure 4-61: Pressure drop of particles with diameter ±4.5mm

In Figure 4-62, the pressure drop across packed beds with similar mean particle diameter (±5.5 mm) is plotted with varying voidage. The binary mixture #1 has the densest packing with a voidage of 0.398 and the smallest mean diameter. It has the highest pressure drop due to how the particle stack with the largest particle size and the smallest particle size fills most gaps. This acts almost as a mono-size +2.36 mm batch. The difference between ternary #2 and #3 is the composition of the same particle sizes and thus the same size distribution, with #3 having a wider volumetric distribution than mixture #2. It is observed that #3 has a higher pressure drop across the packed bed. This is due to a wider volumetric distribution where more particles can interact with each other compared to an uneven divide in volumetric distribution. Furthermore, the rate at which the pressure increases as the velocity increases is greater for a smaller Sauter mean diameter particle packed bed than for a larger Sauter mean diameter particle packed bed.

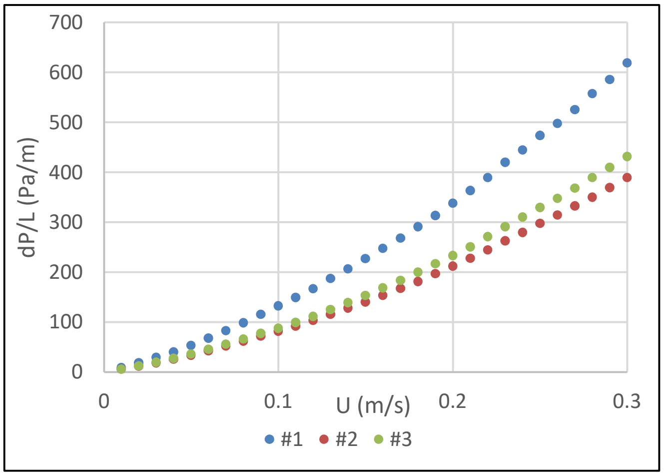

Mix	#1	#2	#3
Voidage	0.398	0.458	0.456
dp_{SM} (mm)	5.43	5.52	5.53
+11.20	0.5	0	0
+9.50	0	0	0
+6.70	0	0.1	0.4
+4.75	0	0.8	0.4
+2.36	0.5	0.1	0.2

Figure 4-62: Pressure drop of particles with diameter ±5.5mm

Figure 4-63 displays the pressure drop across packed beds with similar mean particle diameter (±8.4 mm) and is plotted with varying voidage. The binary mixture #3 has the highest packing density with a voidage of 0.443 and the largest mean diameter. It does have the lowest pressure drop; this is due to how particles stack when the particle sizes are close to each other. Ternary mixtures #1 and #2 are different particle sizes but have similar volumetric and size distributions. It can be concluded from the data that pressure drop depends more on mean diameter than voidage.

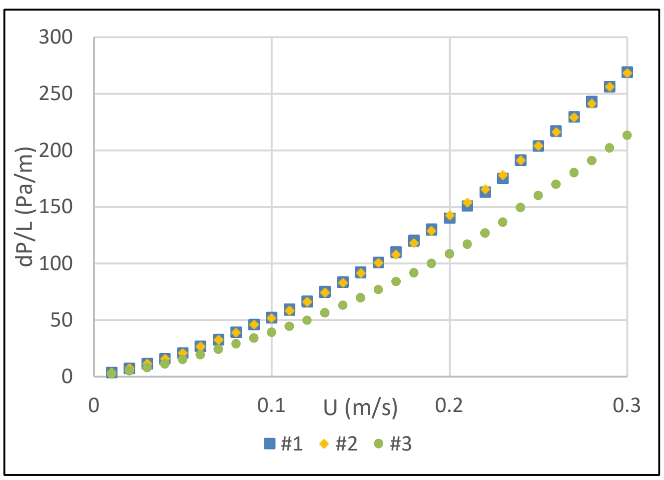

Mix	#1	#2	#3
Voidage	0.432	0.406	0.443
dp_{SM} (mm)	8.28	8.40	8.49
+11.2	0.5	0.2	0
+9.50	0	0.5	0.5
+6.70	0.3	0	0.5
+4.75	0.2	0.3	0
+2.36	0	0	0

Figure 4-63: Pressure drop of particles with diameter ±8.4mm

4.3.4 Existing pressure drop models

Table 4-16 gives a summary of how pressure drop models found in literature performed to predict pressure drop across a packed bed of coke particles. It was found that the Ergun model was best fitting with the lowest average percentage difference, although the Montillet model has a higher R^2 value. The Ergun model is also mostly used in pressure drop calculations.

Table 4-16: Summary of pressure drop models found in the literature

Model	Model equation	Parity plot	Description	Ave. difference	Min. difference	Max. difference	R^2
Reichelt	Equation 2-76	Figure 4-64	Overprediction	95.5%	34%	100%	0.404
Wu	Equation 2-79	Figure 4-65	Overprediction	39.5%	-3%	77%	0.888
KTA	Equation 2-82	Figure 4-66	Overprediction	35.4%	1%	69%	0.921
Montillet	Equation 2-83	Figure 4-67	Underprediction	54.6%	-171%	2%	0.954
Ergun	Equation 2-84	Figure 4-69	Mixed prediction	20.6%	-410%	182%	0.929

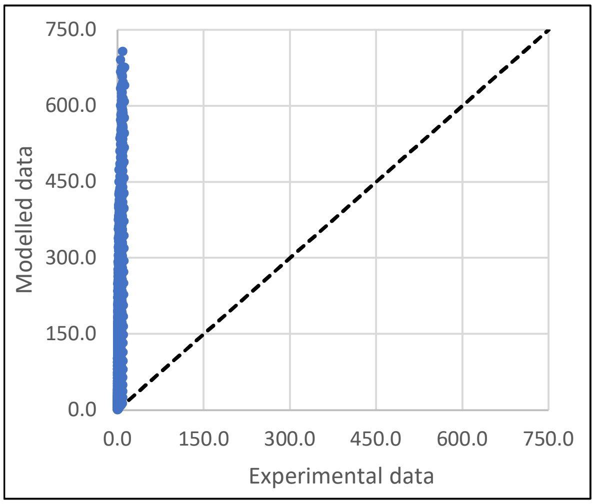

Figure 4-64: Parity plot of Reichelt model

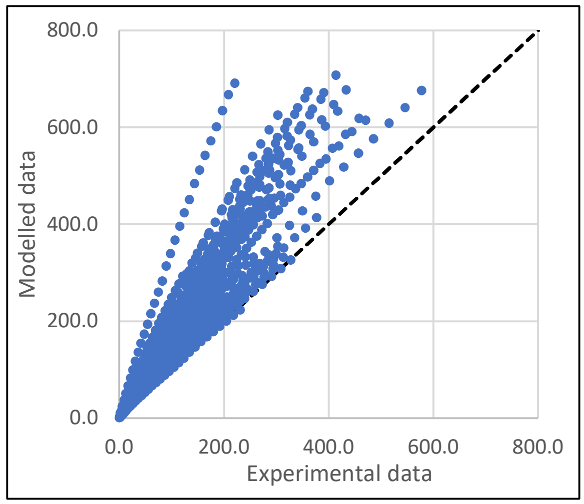

Figure 4-65: Parity plot of Wu model

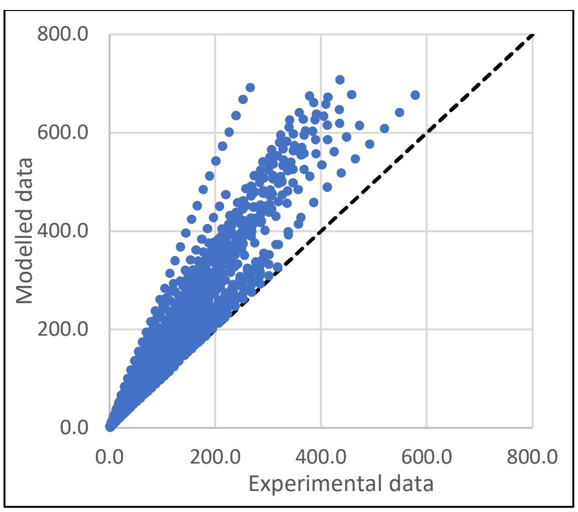

Figure 4-66: Parity plot of KTA model

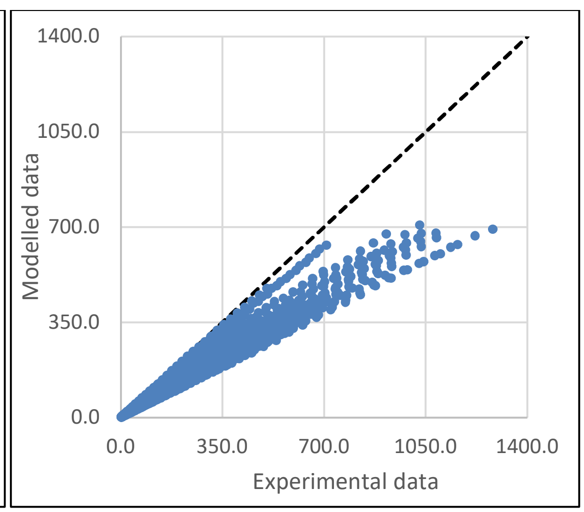

Figure 4-67: Parity plot of Montillet model

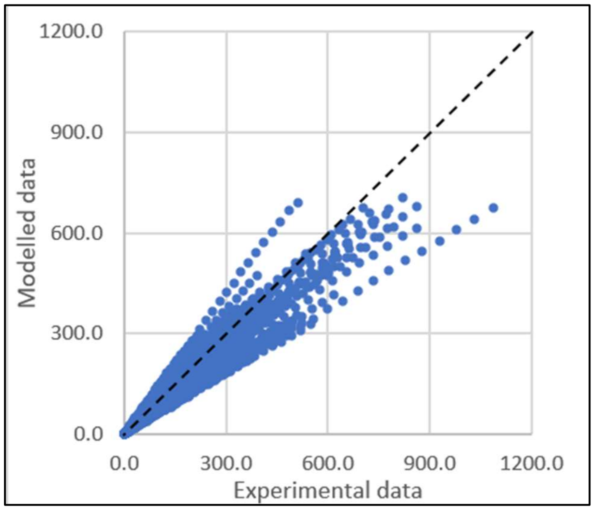

Figure 4-68: Parity plot of Ergun model

Table 4-17 displays how the models in Table 4-16 adapts to coke particles when regressed. All the models' parity plots in the table can be viewed in Annexure C. All the models have improved, i.e., the biggest improvements are seen in the KTA, Montillet and Ergun models. The Montillet model is the best-fitting pressure drop model when regressed, with an average percentage difference of 12.8%. Although the Montillet model being the best-fitting model of all the regressed models it is still not a satisfactory fit for the coke particles.

Table 4-17: Summary of coke particles regressed literature models

Model	Model equation	Description	Ave. difference	Min. difference	Max. difference	R^2
Reichelt	Equation 2-76	Mixed prediction	44.4%	-174%	89%	0.750
Wu	Equation 2-79	Mixed prediction	18.2%	-96%	51%	0.897
KTA	Equation 2-82	Mixed prediction	15.8%	-75%	44%	0.922
Montillet	Equation 2-83	Mixed prediction	12.8%	-46%	49%	0.957
Ergun	Equation 2-84	Mixed prediction	15.1%	-55%	46%	0.929

4.3.4.1 Modified Ergun pressure drop model results

Studies have modified the Ergun model, Equation 2-85 to adapt to their particles through regression. The modified Ergun model constants were regressed for the coke particles used in this study; the result of each model is displayed in Table 4-18.

Table 4-18: Ergun model constants

Model	A_E	B_E	Source
Ergun	150	1.75	(Koekemoer & Luckos, 2015)
Koekemoer char	160.4	2.8	(Koekemoer & Luckos, 2015)
Koekemoer coal	77.4	2.8	(Koekemoer & Luckos, 2015)
Tian	213	8.8	(Tian *et al.*, 2016)
Carman	180	2.87	(Tian *et al.*, 2016)
Modified Ergun	124.4	1.49	(From study)

Table 4-19 displays a summary of different studies regressing the Ergun model. Koekemoer (Koekemoer & Luckos, 2015) used coal particles which is similar particle to the coke particles used in this study, due to coke originated from coal and the particle sizes used in the study by Koekemoer& Luckos (2015) (-26.5 mm +4.75 mm) being similar to the particle sizes used in this study (-13.2 mm +2.36mm). Koekemoer constants still was not an optimal fit for the coke particles with an average percentage difference of 28.3%. The parity plot of the modified Ergun model showed a mixed spread between the experimental and modelled values. The coke particles regressed Ergun model is an improvement from the original literature Ergun model, but is not a fit for the coke particles, due to it having a lower average percentage difference.

Table 4-19: Summary of Ergun regressed models

Model	Parity plot	Description	Ave. difference	Min. difference	Max. difference	R^2
Original literature Ergun	Figure 4-68	Mixed prediction	20.6%	-86%	36%	0.929
Koekemoer char	Figure 4-69	Underprediction	52.2%	-138%	27%	0.927
Koekemoer coal	Figure 4-70	Underprediction	28.3%	-109%	61%	0.915
Tian	Figure 4-71	Underprediction	254%	-548%	-10%	0.912
Carman	Figure 4-72	Underprediction	62.2%	-150%	19%	0.928
Modified Ergun	Figure 4-73	Mixed prediction	15.1%	-55%	46%	0.929

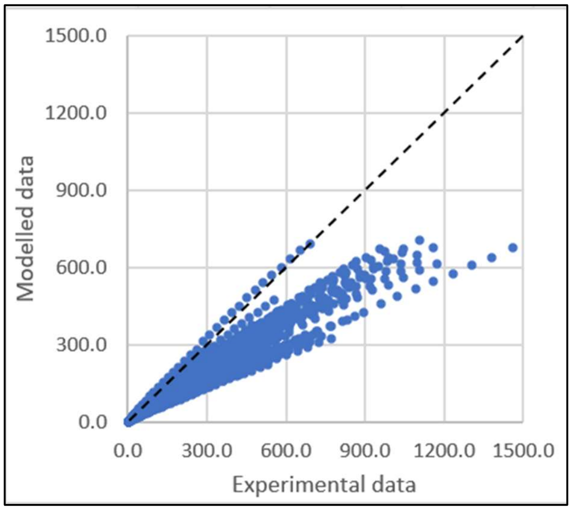

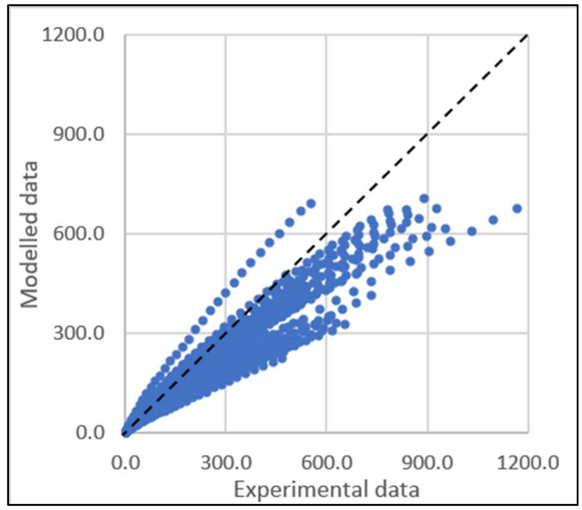

Figure 4-69: Parity plot of Koekemoer constants with Ergun model for char particles

Figure 4-70: Parity plot of Koekemoer constants with Ergun model for coal particles

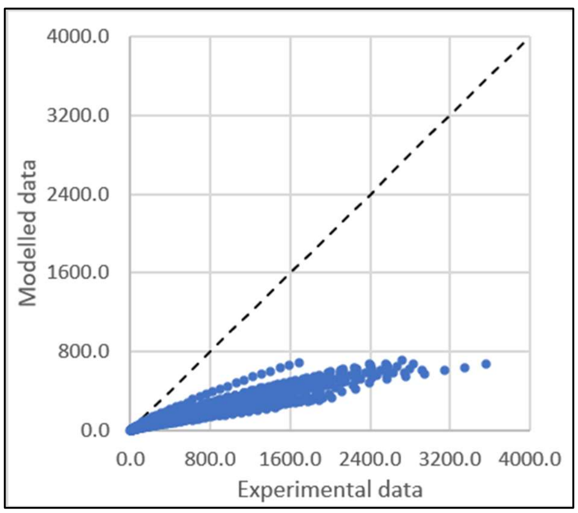

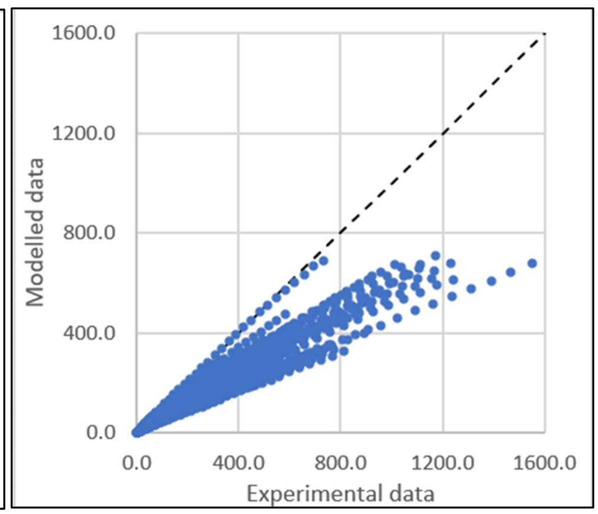

Figure 4-71: Parity plot of Tian constants with Ergun model

Figure 4-72: Parity plot of Carman constants with Ergun model

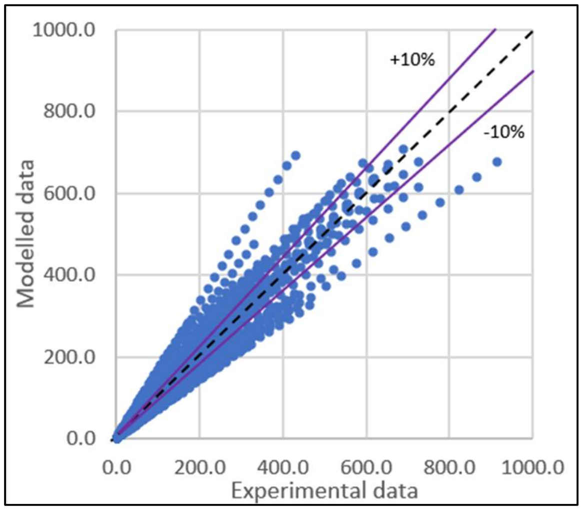

Figure 4-73: Parity plot of Modified Ergun model

4.3.4.2 Statistical models

Table 4-20 gives a summary of the developed statistical models for pressure drop across a packed bed of coke particles, and Table 4-21 gives the regressed constants for the statistical models. Compared to the models from the literature (Table 4-16 and Table 4-19), the statistical models are better fitting models for the coke particles, with lower average percentage differences and greater R^2 values.

From Table 4-20 it is observed that the root mean square error value differs significantly for each model compared to the average percentage difference and R^2 value, with the standard polynomial model having the smallest root mean square error and average error as well as the highest R^2 value, indicating that it is the best model to fit the pressure drop data for coke particles.

Table 4-20: Summary of statistical models

Model	Model equation	Parity plot	Description	Ave. difference	Min. difference	Max. difference	RMSE	R^2
Pade polynomial	Equation 2-86	Figure 4-74	Satisfactory	7.20%	-16%	61%	8.86	0.9961
Quad-K polynomial	Equation 2-87	Figure 4-75	Satisfactory	7.28%	-18%	61%	8.65	0.9963
Standard polynomial	Equation 2-88	Figure 4-77	Satisfactory	7.15%	-19%	61%	8.51	0.9964

Table 4-21: Statistical model constants

Constant	Pade polynomial	Quad-K polynomial	Standard polynomial
β_1	43.51	732.44	742.95
β_2	52.31	935.49	933.59
β_3	57.32	1323.89	1326.66
β_4	270.56	1931.21	1930.72
β_{11}	0.0592	-	-
β_{22}	0.0554	-	-
β_{33}	0.0437	-	-
β_{44}	0.1360	-	-
β_{55}	0.0419	-	-
β_{23}	125.07	2500.58	232.25
β_{24}	337.74	4160.31	1273.63
β_{25}	480.97	9416.57	4879.23
β_{34}	305.03	3688.21	531.13
β_{35}	358.05	8078.07	3198.70
β_{45}	691.45	6752.85	1350.40
β_{123}	-	-	24.48
β_{124}	-	-	706.03
β_{125}	-	-	-1653.60
β_{134}	-	-	2246.19
β_{135}	-	-	833.53
β_{145}	-	-	1386.77
β_{234}	-	-	-122.88
β_{235}	-	-	-192.13
β_{245}	-	-	4563.96
β_{345}	-	-	-3857.26
θ	1.441	1.441	1.441

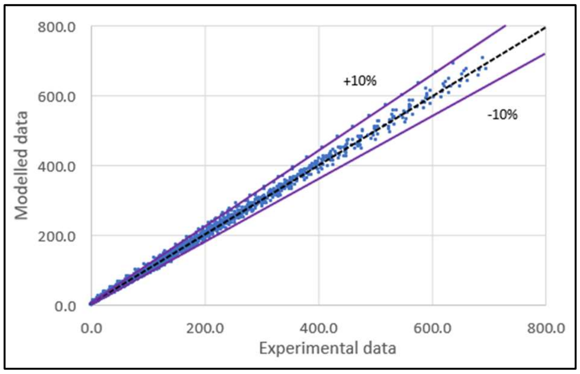

Figure 4-74: Parity plot of Pade polynomial

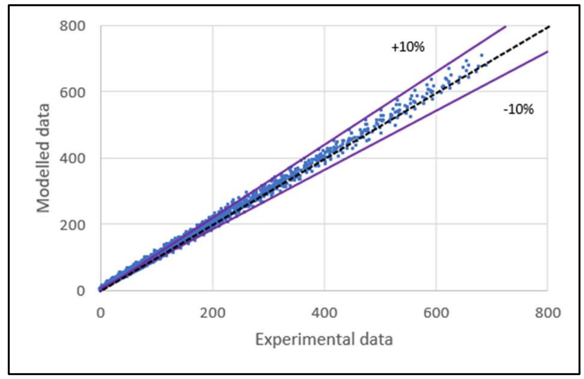

Figure 4-75: Parity plot of Quad-K polynomial

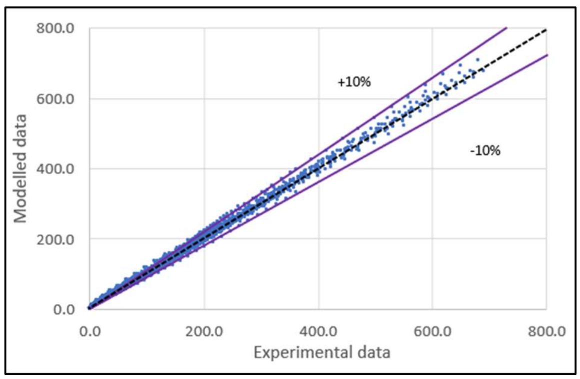

Figure 4-76: Parity plot of Standard polynomial

CHAPTER 5 CONCLUSION AND RECOMMENDATIONS

5.1 Conclusion

Present bed voidage models that rely only on particle size to pipe diameter or particle size to particle diameter ratio are insufficient to model particle packing. The models can be improved by including mono-size batch and binary mixtures experimentally determined voids as a parameter to increase the accuracy. The modified Kwan model for binary mixtures and the regressed D-optimal Design model for ternary mixtures was the best-fitting voidage models for the coke particles but still needed regression to fit the coke particles. The results indicate that the densest packing range is not dependent on average particle size for mono-, binary-, and ternary mixtures. It is observed that when two of the three particle ranges have a narrow particle distribution, one will dominate to fill the voids with the larger or smaller size range to create the densest packing. When a large or wide particle distribution is used, the densest packing is found when small particles fill the gap between medium and larger particles during packing. The main parameter that influences bed voidage is the particle size distribution of the bed.

Most pressure drop models are developed based on the friction factor, where some are modified to include bed voidage through the modified Reynolds number. No existing model accurately predicted the pressure drop for coke particles, so statistical models were considered. It was found that the standard polynomial statistical method was the most accurate for predicting pressure drop across a packed bed of coke particles. Comparing the most used literature pressure drop model, the Ergun model, to the statistical models, it was found that the pressure drop to fluid velocity correlation for the Ergun model is given as $\Delta P \propto U^2$ compared to the correlation for the statistical models given as $\Delta P \propto U^{1.441}$. The results indicate that as the average particle diameter decreases for mono-sized batches, the pressure drop across the packed bed increases; similar results were observed for binary-; and ternary mixtures, that as the Sauter mean particle diameter of a packed bed increases the pressure drop decreases. It is observed that a wide size distribution has a higher pressure drop across the packed bed compared to a narrow size distribution with similar bed voidage and mean particle diameter. This is due to how relatively large, medium, and small particles stack and fill the gaps between each other compared to how particles with relatively close diameters can fill the gaps in a packed bed. It was found that particle size distribution had the most significant influence on pressure drop in mixtures compared to sphericity and bed voidage; similar results were reported in the literature.

5.2 Recommendation

Bed voidage models from literature rely mostly on the particle diameter or particle-to-particle diameter as parameters to construct the models; a shape factor such as sphericity should be included to investigate the impact of particle shape on the packing models.

From using statistical models to predict pressure drop, it would be beneficial to integrate particle parameters to the model like sphericity, voidage and average particle diameter into the statistical pressure drop model to fill the breach to basic flow models derived from friction factors.

Further research should be done to see the accuracy of the statistical model if only using reference points, such as bure batch and binary mixtures data, for model regression instead of doing all experiments.

The influence of pipe diameter to particle diameter should be further researched to investigate the influence on the pressure drop across the packed bed; since most studies are done on a small scale ranging from $3 < D/d_p < 14$, including this study with a range of $9 < D/d_p < 44$, large scale operation should be further investigated.

Research should be done to define sphericity further and obtain a new method to define and measure sphericity; this can help to improve bed voidage and pressure drop models further.

BIBLIOGRAPHY

(KTA), N.S.S.C. Management, S.O.N.W. 1986. Reactor Core Design for High-Temperature Gas-Cooled Reactors Part 3: Loss of Pressure through Friction in Pebble Bed Cores.

Abbas, M.N. 2011. Modeling of porosity equation for water flow through packed bed of monosize spherical packing. *Journal of engineering and development*, 15(4):205-226.

Amiri, L., Ghoreishi-Madiseh, S.A., Hassani, F.P. & Sasmito, A.P. 2019. Estimating pressure drop and Ergun/Forchheimer parameters of flow through packed bed of spheres with large particle diameters. *Powder Technology*, 356:310-324.

Babich, A., Senk, D. & Gudenau, H. 2009. Effect of coke reactivity and nut coke on blast furnace operation. *Ironmaking & Steelmaking*, 36(3):222-229.

Bo-Ming, Y. & Jian-Hua, L. 2004. A geometry model for tortuosity of flow path in porous media. *Chinese Physics Letters*, 21(8):1569.

Botlhoko, S., Campbell, Q., le Roux, M. & Nakhaei, F. 2021. Application of RhoVol information for coal washability analysis. (*In*. Proceedings of the Coal Processing Conference 2021 organised by: Secunda.

Brunner, K.M., Perez, H.D., Peguin, R.P., Duncan, J.C., Harrison, L.D., Bartholomew, C.H. & Hecker, W.C. 2015. Effects of particle size and shape on the performance of a trickle fixed-bed recycle reactor for Fischer–Tropsch synthesis. *Industrial & Engineering Chemistry Research*, 54(11):2902-2909.

Carter, M.R. & Gregorich, E.G. 2007. Soil sampling and methods of analysis: CRC press.

Coetzee, J. 1971. The future development of the iron and steel industry in South Africa. *Journal of the Southern African Institute of Mining and Metallurgy*, 71(8):167-170.

DeBeers. 2013. RhoVol Leafdlet.

Deng, Y., Dewil, R., Appels, L., Zhang, H., Li, S. & Baeyens, J. 2021. The need to accurately define and measure the properties of particles. *Standards*, 1(1):19-38.

Di Maio, F.P. & Di Renzo, A. 2016. Direct modeling of voidage at layer inversion in binary liquid-fluidized bed. *Chemical Engineering Journal*, 284:668-678.

Du Plessis, J.P. 1994. Analytical quantification of coefficients in the Ergun equation for fluid friction in a packed bed. *Transport in porous media*, 16(2):189-207.

Duffy, N.T. & Eaton, J.A. 2013. Investigation of factors affecting channelling in fixed-bed solid fuel combustion using CFD. *Combustion and flame*, 160(10):2204-2220.

Dullien, F.A. 1997. Structural properties of packings of particles. Handbook of Powder Science & Technology. Springer. p. 53-95).

Ðuriš, M., Arsenijević, Z., Jaćimovski, D. & Radoičić, T.K. 2016. Optimal pixel resolution for sand particles size and shape analysis. *Powder Technology*, 302:177-186.

El-Husseiny, A., Vanorio, T. & Mavko, G. 2019. Predicting porosity of binary mixtures made out of irregular nonspherical particles: Application to natural sediments. *Advanced Powder Technology*, 30(8):1558-1566.

Epstein, N., Leclair, B. & Pruden, B. 1981. Liquid fluidization of binary particle mixtures—I: Overall bed expansion. *Chemical Engineering Science*, 36(11):1803-1809.

Everitt, B.S. & Skrondal, A. 2010. The Cambridge dictionary of statistics.

Fogler, H.S. & Gürmen, M. 1999. Elements of Chemical Reaction Engineering. 2005. *There is no corresponding record for this reference.[Google Scholar]*:741-760.

Furnas, C. 1931. Grading aggregates-I.-Mathematical relations for beds of broken solids of maximum density. *Industrial & Engineering Chemistry*, 23(9):1052-1058.

Furnas, C.C. 1929. Flow of gases through beds of broken solids. Vol. 307: US Government Printing Office.

Geyer, P. & Halifa, Z. 2014. Blast furnace tapping practice at arcelor mittal South Africa, vanderbijlpark works. (*In*. The South African Institute of Mining and Metallurgy, Furnace Tapping Conference, Muldersdrift, South Africa organised by.

Gonick, L. & Smith, W. 1993. The cartoon guide to statistics: HarperCollins Publishers, Inc.

Gräbner, M. 2014. Industrial coal gasification technologies covering baseline and high-ash coal: John Wiley & Sons.

Hartman, M., Trnka, O. & Svoboda, K. 2000. Fluidization characteristics of dolomite and calcined dolomite particles. *Chemical engineering science*, 55(24):6269-6274.

Hassan, Y.A. & Kang, C. 2012. Pressure drop in a pebble bed reactor under high Reynolds number. *Nuclear technology*, 180(2):159-173.

Haughey, D. & Beveridge, G. 1969. Structural properties of packed beds—a review. *The Canadian Journal of Chemical Engineering*, 47(2):130-140.

Helmy, I.M. & Abdel Azim, A.M. 2012. Efficacy of ImageJ in the assessment of apoptosis. *Diagnostic Pathology*, 7(1):15.

Jia, Y., Li, Y. & Hlavka, D. 2009. Flow through packed beds. *Universityof-Rochester, New York*.

Johns, J. 2010. Environmental Impact Assessment for the Proposed Re-Commissioning of a Coke Oven Battery at ArcelorMittal South Africa, Newcastle Works. *Draft Scoping Report*.

Jones, R., den Hoed, P. & Erwee, M. Comparing Electrical and Carbon Combustion Based Energy Technologies for the Production of High Carbon Ferromanganese: A Literature Review.

Kenney, J.F. 1939. Mathematics of statistics: D. Van Nostrand.

Keyser, M., Conradie, M., Coertzen, M. & Van Dyk, J. 2006. Effect of coal particle size distribution on packed bed pressure drop and gas flow distribution. *Fuel*, 85(10-11):1439-1445.

Koekemoer, A. & Luckos, A. 2015. Effect of material type and particle size distribution on pressure drop in packed beds of large particles: Extending the Ergun equation. *Fuel*, 158:232-238.

Kowalczuk, P.B. & Drzymala, J. 2016. Physical meaning of the Sauter mean diameter of spherical particulate matter. *Particulate Science and Technology*, 34(6):645-647.

Kuang, S., Li, Z. & Yu, A. 2018. Review on modeling and simulation of blast furnace. *steel research international*, 89(1):1700071.

Kwan, A.K.H., Chan, K.W. & Wong, V. 2013. A 3-parameter particle packing model incorporating the wedging effect. *Powder technology*, 237:172-179.

Li, Z., Kobayashi, N., Nishimura, A. & Hasatani, M. 2005. A Method to Predict the Minimum Fluidization Velocity of Binary Mixtures Based on Particle Packing Properties. *Chemical Engineering Communications*, 192:918-932.

Liu, Q., Jia, D. & Miao, J. 2020. Study of the linear and nonlinear packing model based on mixing of quartz sand. *Powder Technology*, 366:382-394.

Luckos, A. & Bunt, J.R. 2011. Pressure-drop predictions in a fixed-bed coal gasifier. *Fuel*, 90(3):917-921.

Matsuhashi, S., Kurosawa, H., Natsui, S., Kon, T., Ueda, S., Inoue, R. & Ariyama, T. 2012. Evaluation of coke mixed charging based on packed bed structure and gas permeability changes in blast furnace by DEM-CFD model. *ISIJ international*, 52(11):1990-1999.

Montillet, A. 2004. Flow through a finite packed bed of spheres: a note on the limit of applicability of the Forchheimer-type equation. *J. Fluids Eng.*, 126(1):139-143.

Morgan, T., Bossert, JP, Harris, JF & La Grange, C. 1951. Investigations relating to the production of metallurgical coke from South African coals. *Journal of the Southern African Institute of Mining and Metallurgy*, 51(7):219-238.

Nemec, D. & Levec, J. 2005. Flow through packed bed reactors: 1. Single-phase flow. *Chemical Engineering Science*, 60(24):6947-6957.

Nhiwatiwa, J. & Cromarty, R. 2022. Evaluation of Coke Resistivity for the Manganese Alloy Market. *Materials*, 15(8):2897.

Ozahi, E., Gundogdu, M.Y. & Carpinlioglu, M.Ö. 2008. A modification on Ergun's correlation for use in cylindrical packed beds with non-spherical particles. *Advanced Powder Technology*, 19(4):369-381.

Peacey, J.G. & Davenport, W.G. 2016. The iron blast furnace: theory and practice: Elsevier.

Rase, H.F. 2013. Fixed-bed reactor design and diagnostics: gas-phase reactions: Butterworth-Heinemann.

Rhodes, M.J. 2008. Introduction to particle technology: John Wiley & Sons.

Sandrock, C. & Afshari, S. 2016. alchemyst/ternplot: DOI version (Version v1.1.0): Zenodo.

Sohn, H.Y. & Moreland, C. 1968. The effect of particle size distribution on packing density. *The Canadian Journal of Chemical Engineering*, 46(3):162-167.

Standish, N. & Yu, A. 1987a. Limitation of the simplex-centroid design for the porosity calculation of ternary mixtures. *Powder technology*, 53(1):69-72.

Standish, N. & Yu, A. 1987b. Porosity calculations of ternary mixtures of particles. *Powder Technology*, 49(3):249-253.

Subramanian, P. & Arunachalam, V. 1980. A simple device for the determination of sphericity factor. *Industrial & Engineering Chemistry Fundamentals*, 19(4):436-437.

Takashimizu, Y. & Iiyoshi, M. 2016. New parameter of roundness R: circularity corrected by aspect ratio. *Progress in Earth and Planetary Science*, 3(1):2.

Tian, F.-y., Huang, L.-f., Fan, L.-w., Qian, H.-l., Gu, J.-x., Yu, Z.-t., Hu, Y.-c., Ge, J. & Cen, K.-f. 2016. Pressure drop in a packed bed with sintered ore particles as applied to sinter coolers with a novel vertically arranged design for waste heat recovery. *Journal of Zhejiang University-SCIENCE A*, 2(17):89-100.

Trahan, J., Graziani, A., Goswami, D.Y., Stefanakos, E., Jotshi, C. & Goel, N. 2014. Evaluation of pressure drop and particle sphericity for an air-rock bed thermal energy storage system. *Energy Procedia*, 57:633-642.

Van Niekerk, W. & Dippenaar, R. 1991. Blast-furnace coke: a coal-blending model. *Journal of the Southern African Institute of Mining and Metallurgy*, 91(2):53-61.

Wang, D. & Fan, L.-S. 2013. Particle characterization and behavior relevant to fluidized bed combustion and gasification systems. Fluidized bed technologies for near-zero emission combustion and gasification. Elsevier. p. 42-76).

Westman, A.E.R. 1936. The packing of particles: empirical equations for intermediate diameter ratios. *Journal of the American Ceramic Society*, 19(1-12):127-129.

Wills, B.A. & Finch, J. 2015. Wills' mineral processing technology: an introduction to the practical aspects of ore treatment and mineral recovery: Butterworth-Heinemann.

Wong, V. & Kwan, A.K.H. 2014. A 3-parameter model for packing density prediction of ternary mixes of spherical particles. *Powder Technology*, 268:357-367.

Wu, J., Yu, B. & Yun, M. 2008. A resistance model for flow through porous media. *Transport in Porous Media*, 71(3):331-343.

Yang, W.-C. 2003. Handbook of fluidization and fluid-particle systems: CRC press.

Yang, Y., Goodfellow, J., Goh, Y., Nasserzadeh, V. & Swithenbank, J. 2001. Investigation of channel formation due to random packing in a burning waste bed. *Process Safety and Environmental Protection*, 79(5):267-277.

Yu, A.-B., Zou, R. & Standish, N. 1996. Modifying the linear packing model for predicting the porosity of nonspherical particle mixtures. *Industrial & engineering chemistry research*, 35(10):3730-3741.

Yu, A.B., Standish, N. & McLean, A. 1993. Porosity calculation of binary mixtures of nonspherical particles. *Journal of the American Ceramic Society*, 76(11):2813-2816.

Zhou, H., Zhou, M., Cheng, M., Guo, W. & Cen, K. 2017. Experimental study and X-ray microtomography based CFD simulation for the characterization of pressure drop in sinter bed. *Applied Thermal Engineering*, 112:811-819.

ANNEXURE A

Table 5-1: RhoVol average data of complete analysis

Particle size range	Mass (mg)	Volume (mg/mm3)	Density (SG)	Minimum Circle Diameter (mm)	Minimum Square Sieve Size (mm)	Roller Gap Size (mm)	Compactness	Elongation	Flatness
+2.36 mm	38.20	28.70	1.35	4.28	3.58	2.54	0.68	1.43	1.79
+4.75 mm	142.40	120.06	1.22	6.73	5.73	4.52	0.73	1.37	1.51
+6.7 mm	257.15	237.96	1.08	8.48	7.26	5.72	0.74	1.33	1.44
+9.5 mm	528.39	645.91	0.82	11.94	10.23	7.98	0.74	1.33	1.48
+11.2 mm	740.89	919.42	0.80	13.06	11.23	8.81	0.73	1.38	1.47

Table 5-2: ImageJ average data of complete analysis

Particle size range	Area (mm^2)	Perimeter (mm)	Circularity
+2.36 mm	19.739	18.926	0.6857
+4.75 mm	54.315	31.015	0.7072
+6.7 mm	51.973	29.982	0.7231
+9.5 mm	116.91	45.012	0.7242
+11.2 mm	167.5	54.086	0.7119

Table 5-3 : Sample of ImageJ analysis results for - mm +2.36 mm

Sample nr.	Compactness	Circularity
1	0.691	0.7247
2	0.677	0.5074
3	0.764	0.7656
4	0.544	0.7604
5	0.715	0.6688
6	0.803	0.7297
7	0.807	0.7479
8	0.754	0.8281
9	0.731	0.5462
10	0.776	0.6461
11	0.717	0.7062
12	0.793	0.7849
13	0.594	0.847
14	0.771	0.772
15	0.79	0.7927
16	0.689	0.8022
17	0.721	0.6241

18	0.727	0.5796
19	0.757	0.6937
20	0.693	0.6451
21	0.488	0.7905
22	0.634	0.6691
23	0.761	0.7143
24	0.624	0.7239
25	0.739	0.6989
26	0.667	0.7938
27	0.665	0.7594
28	0.668	0.7575
29	0.596	0.7157
30	0.592	0.7412
31	0.513	0.7461
32	0.772	0.7079
33	0.615	0.5698
34	0.609	0.8184
35	0.387	0.7601
36	0.738	0.6021
37	0.632	0.6878
38	0.667	0.7629
39	0.807	0.638
40	0.848	0.8202
41	0.586	0.7762
42	0.681	0.7331
43	0.667	0.7499
44	0.537	0.7133
45	0.642	0.7884
46	0.541	0.7513
47	0.658	0.6413
48	0.706	0.8321
49	0.838	0.668
50	0.751	0.6825
51	0.774	0.4854
52	0.725	0.5874
53	0.652	0.524
54	0.643	0.6481
55	0.493	0.6313
56	0.563	0.6763
57	0.547	0.7337
58	0.649	0.6901
59	0.726	0.7663
60	0.578	0.613
61	0.699	0.8177

62	0.88	0.6508
63	0.831	0.6742
64	0.707	0.8067
65	0.621	0.7765
66	0.843	0.7045
67	0.76	0.8088
68	0.689	0.5678
69	0.696	0.5948
70	0.669	0.7288
71	0.847	0.5156
72	0.822	0.7299
73	0.665	0.8315
74	0.735	0.5979
75	0.675	0.6899
76	0.643	0.6157
77	0.701	0.7174
78	0.625	0.6627
79	0.535	0.7329
80	0.76	0.7489
81	0.455	0.6075
82	0.708	0.7717
83	0.838	0.7732
84	0.742	0.6768
85	0.742	0.7006
86	0.728	0.7145
87	0.776	0.7794
88	0.789	0.6622
89	0.797	0.5045
90	0.621	0.639
91	0.707	0.7714
92	0.798	0.7195
93	0.626	0.7215
94	0.717	0.6018
95	0.607	0.6561
96	0.616	0.6874
97	0.606	0.6897
98	0.59	0.8362
99	0.646	0.684
100	0.582	0.73
101	0.612	0.3424
102	0.647	0.7617
103	0.57	0.3605
104	0.765	0.6682
105	0.652	0.5655

106	0.781	0.6062
107	0.757	0.7675
108	0.417	0.7038
109	0.573	0.7203
110	0.817	0.7401
111	0.722	0.7695
112	0.753	0.4487
113	0.632	0.7215
114	0.78	0.5175
115	0.801	0.5768
116	0.626	0.6632
117	0.799	0.8068
118	0.761	0.782
119	0.74	0.5174
120	0.645	0.8102
121	0.641	0.2432
122	0.708	0.5874
123	0.585	0.4238
124	0.611	-
125	0.467	-
126	0.604	-
127	0.717	-
128	0.77	-
129	0.73	-
130	0.826	-
131	0.63	-
132	0.768	-
133	0.825	-
134	0.725	-
135	0.831	-
136	0.655	-
137	0.731	-
138	0.722	-
139	0.716	-
140	0.558	-
141	0.594	-
142	0.784	-
143	0.719	-
144	0.719	-
145	0.67	-
146	0.706	-
147	0.752	-
148	0.559	-
149	0.759	-

150	0.455	-
151	0.622	-
152	0.794	-
153	0.786	-
154	0.703	-
155	0.607	-
156	0.574	-
157	0.745	-
158	0.524	-
159	0.738	-
160	0.671	-
161	0.74	-
162	0.662	-
163	0.655	-
164	0.543	-
165	0.7	-
166	0.717	-
167	0.757	-
168	0.664	-
169	0.472	-
170	0.719	-
171	0.727	-
172	0.704	-
173	0.74	-
174	0.811	-
175	0.639	-
176	0.596	-
177	0.657	-
178	0.348	-
179	0.637	-
180	0.64	-
181	0.689	-
182	0.673	-
183	0.548	-
184	0.849	-
185	0.775	-
186	0.696	-
187	0.587	-
188	0.65	-
189	0.835	-
190	0.668	-
191	0.771	-
192	0.467	-
193	0.665	-

194	0.772	-
195	0.647	-
196	0.722	-
197	0.727	-
198	0.613	-
199	0.614	-
200	0.413	-
201	0.633	-
202	0.637	-
203	0.819	-
204	0.595	-
205	0.871	-
206	0.702	-
207	0.464	-
208	0.67	-
209	0.498	-
210	0.484	-
211	0.61	-
212	0.835	-
213	0.6	-
214	0.669	-
215	0.529	-
216	0.826	-
217	0.782	-
218	0.874	-
219	0.647	-
220	0.593	-
221	0.547	-
222	0.467	-
223	0.766	-
224	0.579	-
225	0.575	-
226	0.607	-
227	0.593	-
228	0.589	-
229	0.582	-
230	0.752	-
231	0.711	-
232	0.771	-
233	0.819	-
234	0.818	-
235	0.74	-
236	0.778	-
237	0.715	-

238	0.832	-
239	0.662	-
240	0.821	-
241	0.759	-
242	0.454	-
243	0.709	-
244	0.683	-
245	0.71	-
Average	0.680	0.686
Standard deviation	0.102	0.108
Error (%)	15.01	15.69
Error	0.102	0.108

ANNEXURE B

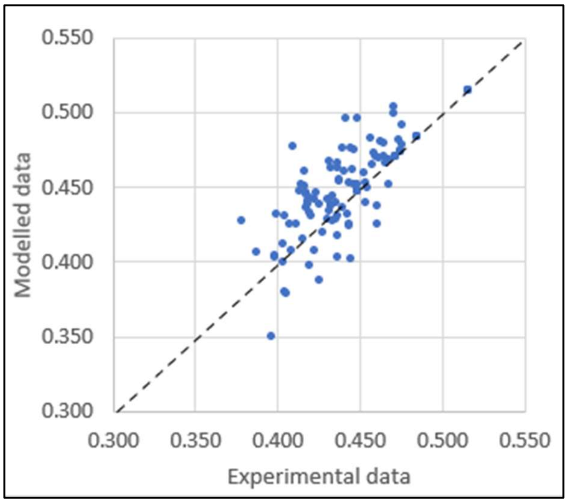

Figure 5-1: Parity plot of regressed El-Husseiny model

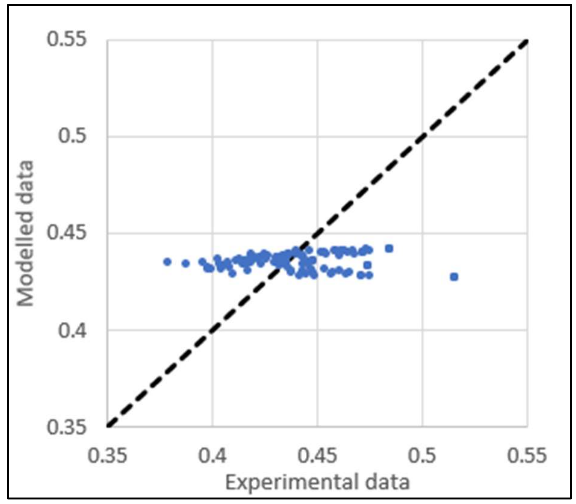

Figure 5-2: Parity plot of regressed Abbas model

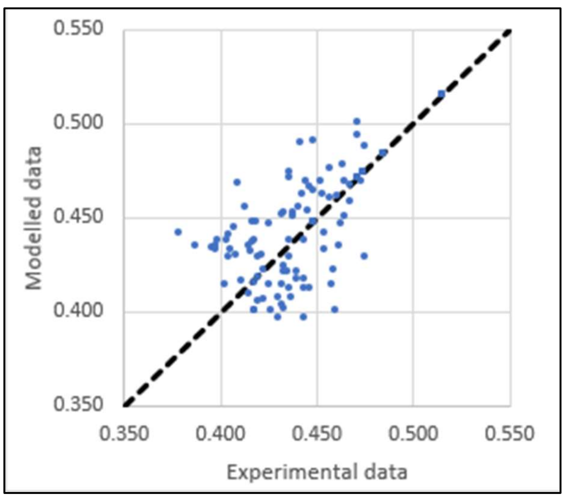

Figure 5-3: Parity plot of regressed Toufar model

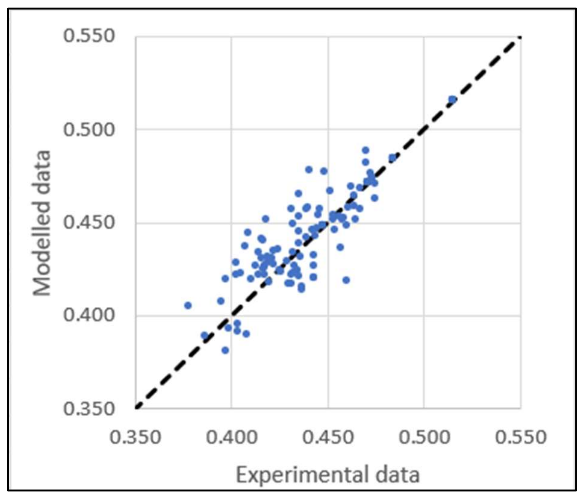

Figure 5-4: Parity plot of regressed Kwan model

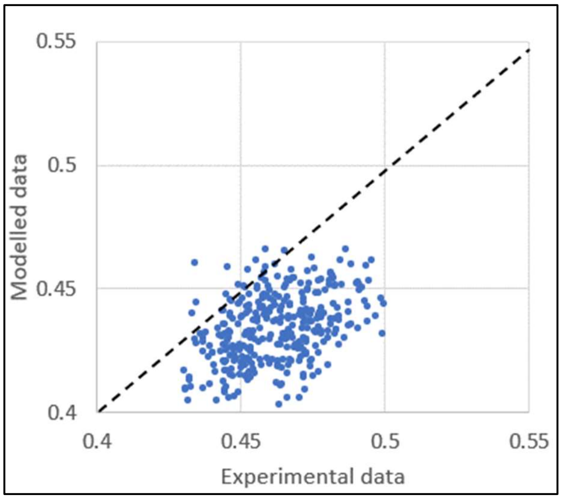

Figure 5-5: Parity plot of regressed Simple Centroid Design model

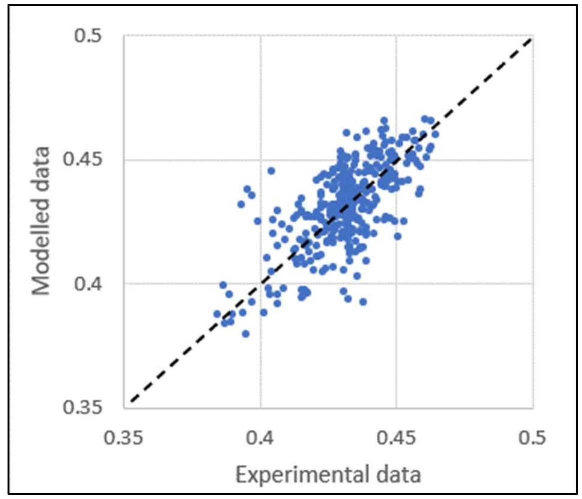

Figure 5-6: Parity plot of regressed D-optimal Design model

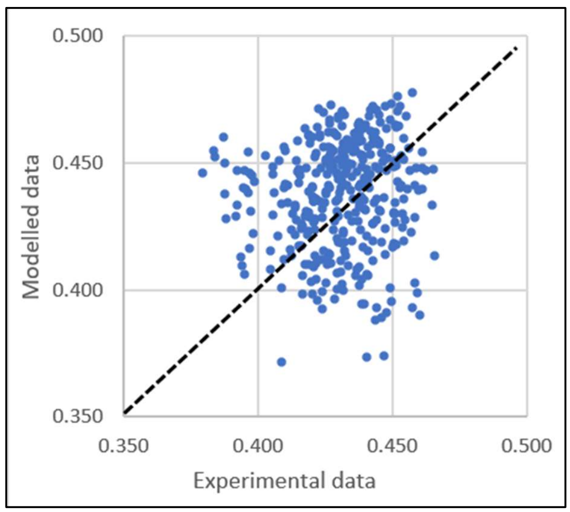

Figure 5-7: Parity plot of regressed Wong & Kwan model

ANNEXURE C

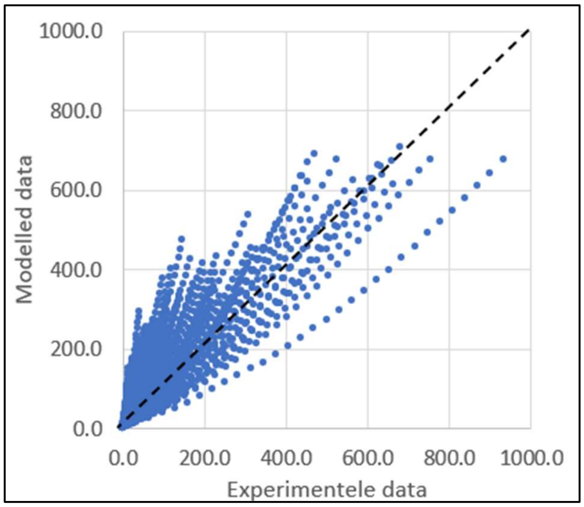

Figure 5-8: Parity plot of regressed Reichelt model

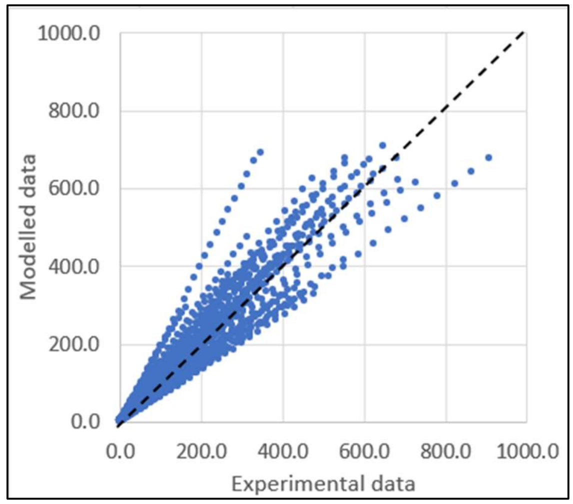

Figure 5-9: Parity plot of regressed Wu model

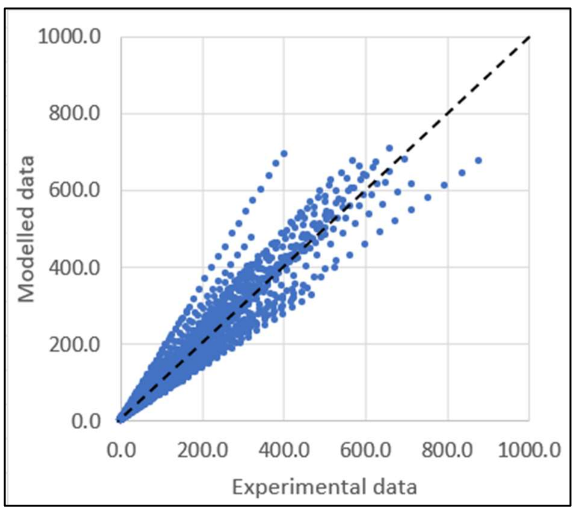

Figure 5-10: Parity plot of regressed KTA model

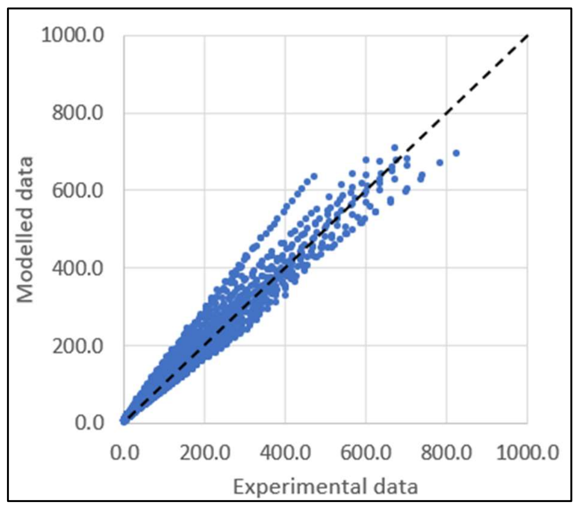

Figure 5-11: Parity plot of regressed Montillet model